Titre: Title:	Optimization of Power-Cycle Arrangements for Supercritical Water Cooled Reactors (SCWRS)
Auteur: Author:	Laure Lizon-a-Lugrin
Date:	2011
Type:	Mémoire ou thèse / Dissertation or Thesis
Référence: Citation:	Lizon-a-Lugrin, L. (2011). Optimization of Power-Cycle Arrangements for Supercritical Water Cooled Reactors (SCWRS) [Mémoire de maîtrise, École Polytechnique de Montréal]. PolyPublie. https://publications.polymtl.ca/520/

URL de PolyPublie: PolyPublie URL:	https://publications.polymtl.ca/520/
Directeurs de recherche: Advisors:	Alberto Teyssedou, & Igor Pioro
Programme: Program:	Génie énergétique

UNIVERSITÉ DE MONTRÉAL

OPTIMIZATION OF POWER-CYCLE ARRANGEMENTS FOR SUPERCRITICAL WATER COOLED REACTORS (SCWRS)

LAURE LIZON-A-LUGRIN

DÉPARTEMENT DE GÉNIE PHYSIQUE

ÉCOLE POLYTECHNIQUE DE MONTRÉAL

MÉMOIRE PRÉSENTÉ EN VUE DE L'OBTENTION

DU DIPLÔME DE MAÎTRISE ÈS SCIENCES APPLIQUÉES

(GÉNIE ÉNERGÉTIQUE)

MARS 2011

UNIVERSITÉ DE MONTRÉAL

ÉCOLE POLYTECHNIQUE DE MONTRÉAL

Ce mémoire intitulé:

OPTIMIZATION OF POWER-CYCLE ARRANGEMENTS FOR SUPERCRITICAL WATER COOLED REACTORS (SCWRS)

présenté par : LIZON-A-LUGRIN Laure

en vue de l'obtention du diplôme de : Maîtrise ès sciences appliquées

a été dûment accepté par le jury d'examen constitué de :

M. TAPUCU Altan, D.Sc.A., président

M. TEYSSEDOU Alberto, Ph.D., membre et directeur de recherche

M. PIORO Igor, Ph.D., membre et codirecteur de recherche

M. AUBÉ François, Ph.D., membre

DEDICATION

To My Beloved Parents

ACKNOWLEDGEMENTS

I wish to sincerely thank my research director Professor Alberto Teyssedou for giving me the opportunity to work on this subject and providing me support all along this work. I am sincerely grateful for his advices, his help and the time he spend on my project. I am keeping the memories of someone who loves science and moreover his ability of sharing it.

I would like to thank my co-director Professor Igor Pioro for giving me all the information I needed during my master. I am thankful for his advices and his support.

I would like to thank all the members of the Institute of Nuclear Energy and especially teachers from École Polytechnique de Montréal for the quality of the courses given.

I also wish to thank my colleagues for their help and advices but also for their friendship and their good mood.

I am certainly grateful to my parents, my friends and my family for helping and supporting me during this project as well as my French engineering school for offering me the opportunity to do this exchange and live this great experience.

Finally, I am sincerely grateful to Sophie Charalambous for proofreading this thesis.

RÉSUMÉ

La croissance démographique et l'augmentation du niveau de vie moyen de la population entraînent une forte augmentation de la demande énergétique mondiale. Par ailleurs, soucieux de préserver l'environnement, la majorité des pays se tournent vers de nouvelles technologies et de nouveaux procédés pour la conversion d'énergie. C'est dans ce contexte qu'est né le Forum International Génération IV. Les pays membres de ce consortium ont pour objectif de développer la IV^{e} génération de réacteurs nucléaires prévue aux horizons 2030. Les principales caractéristiques retenues sont : durabilité, compétitivité économique, sureté, fiabilité et résistance à la prolifération. Afin de répondre à ces nouvelles exigences six concepts de réacteurs nucléaires ont été retenus par les pays membres et sont actuellement en développement. Ainsi, le Canada a décidé de travailler sur le réacteur nucléaire refroidi à l'eau supercritique (SCWR – SuperCritical Water-cooled Reactor). Les travaux sur ce réacteur en sont encore à leur début, cependant il est dores et déjà attendu que la pression d'utilisation du fluide sera de l'ordre de 25 MPa et la température de sortie d'environ 625°C. Outre l'augmentation du rendement thermodynamique du cycle due à une température élevée du fluide, l'utilisation d'un fluide supercritique s'affranchit des changements de phase, ce qui permet de supprimer générateur et séparateur de vapeur. Il est également possible d'utiliser un cycle direct ; le fluide chauffé par le cœur du réacteur nucléaire est alors directement envoyé à la turbine sans passer par un cycle intermédiaire. Dans ce cadre, plusieurs cycles thermodynamiques appropriés aux spécificités de ce réacteur seront présentés ainsi que leur optimisation. Pour ce faire, un logiciel développé à l'Institut de Génie Nucléaire basé sur les algorithmes génétiques a été couplé aux modèles thermodynamiques du cycle en question. Cette méthode a été privilégiée étant donné la complexité que représente l'optimisation d'un cycle thermodynamique ; il s'agit en effet d'un problème multi-objectif. Le but de cette optimisation est d'accroitre le rendement thermodynamique du cycle ainsi que la puissance produite, deux fonctions en compétition. L'enjeu de cette optimisation est de trouver les solutions optimales au fonctionnement de la centrale tout en satisfaisant les contraintes physiques associées au problème. Les résultats obtenus offrent de nombreuses combinaisons de soutirage permettant d'atteindre des rendements de l'ordre de 50 % avec une puissance nette de 1200 MW. Il est à noter que dans la majorité des cas, seulement une partie des variables de décision contrôlent l'ensemble des solutions, ce qui est un facteur important dans la conception du cycle thermodynamique. Par ailleurs, des calculs de dimensionnement de la tuyauterie ainsi que des

profils de températures ont été établis afin d’apporter une idée de la faisabilité de tels systèmes dans des conditions de température et de pression aussi extrêmes.

ABSTRACT

The world energy demand is continuously rising due to the increase of both the world population and the standard of life quality. Further, to assure both a healthy world economy as well as adequate social standards, in a relatively short term, new energy-conversion technologies are mandatory. Within this framework, a Generation IV International Forum (GIF) was established by the participation of 10 countries to collaborate for developing nuclear power reactors that will replace the present technology by 2030. The main goals of these nuclear-power reactors are: economic competitiveness, sustainability, safety, reliability and resistance to proliferation. As a member of the GIF, Canada has decided to orient its efforts towards the design of a CANDU-type Super Critical Water-cooled Reactor (SCWR). Such a system must run at a coolant outlet temperature of about 625°C and at a pressure of 25 MPa. It is obvious that at such conditions the overall efficiency of this kind of Nuclear Power Plant (NPP) will compete with actual supercritical water-power boilers. In addition, from a heat-transfer viewpoint, the use of a supercritical fluid allows the limitation imposed by Critical Heat Flux (CHF) conditions, which characterize actual technologies, to be removed. Furthermore, it will be also possible to use direct thermodynamic cycles where the supercritical fluid expands right away in a turbine without the necessity of using intermediate steam generators and/or separators. This work presents several thermodynamic cycles that could be appropriate to run SCWR power plants. Improving both thermal efficiency and mechanical power constitutes a multi-objective optimization problem and requires specific tools. To this aim, an efficient and robust evolutionary algorithm, based on genetic algorithm, is used and coupled to an appropriate power plant thermodynamic simulation model. The results provide numerous combinations to achieve a thermal efficiency higher than 50% with a mechanical power of 1200 MW. It is observed that in most cases the landscape of Pareto's front is mostly controlled only by few key parameters. These results may be very useful for future plant design engineers. Furthermore, some calculations for pipe sizing and temperature variation between coolant and fuel have been carried out to provide an idea on their order of magnitude.

CONDENSÉ EN FRANÇAIS

La croissance démographique et l'augmentation du niveau de vie moyen de la population entraînent une forte augmentation de la demande énergétique mondiale. C'est dans un souci de conservation et de protection de l'environnement que les pays établissent aujourd'hui une nouvelle politique énergétique. Ainsi le scénario central du « World Energy Outlook 2010 » publié par l'Agence Internationale de l'Énergie prend en compte les différents engagements politiques annoncés par les États en matière de réduction des émissions de gaz à effet de serre et l'élimination progressive des subventions attribuées aux systèmes énergétiques utilisant des combustibles fossiles. Basée sur ces hypothèses, la demande mondiale en énergie primaire devrait croître de 36 % d'ici 2035 et les combustibles fossiles tels que le pétrole, charbon et gaz naturel resteront les sources d'énergie prédominantes en 2035. Toutefois, étant donnée la forte augmentation des prix du pétrole associée aux politiques de promotion des énergies nouvelles, la part du pétrole dans la demande en énergie primaire devrait chuter à 28 % alors qu'elle s'établissait à 33 % en 2008. En effet, la part des énergies nouvelles telles que le solaire, l'éolien, l'hydraulique ou encore la biomasse devrait tripler. En ce qui concerne la demande mondiale en électricité, une augmentation de 2.2% par an entre 2008 et 2035 est prévue. Il est attendue que 80 % de cette augmentation est attribuable aux pays non membre de l'OCDE ; ainsi, en Chine, la demande devrait tripler d'ici 2035. En termes de politiques énergétiques actuelles, il s'agit d'investir dans des technologies à faibles émissions de CO_2 et d'assurer une certaine autonomie énergétique. La part des combustibles fossiles dans la production d'électricité devraient ainsi passer de 68% à 55% en 2035, laissant ainsi place au nucléaire et aux énergies renouvelables.

Ainsi, le marché de l'énergie électrique subit une période de forte transformation, c'est dans ce contexte que dix pays se sont unis pour former le Forum International Génération IV. Les membres de ce consortium ont pour objectif de développer la 4^{eme} génération de réacteurs nucléaires prévue aux horizons 2030. Ces technologies présentent de nombreux progrès technologiques comparés aux systèmes actuels. Par ailleurs, quatre critères majeurs doivent être respectés par ces systèmes à savoir : durabilité, compétitivité économique, sureté-fiabilité et résistance à la prolifération. Pour répondre à ces nouvelles exigences, six concepts de réacteurs nucléaires ont été retenus par les pays membres et sont actuellement en cours de développement. Parmi ces technologies, le Canada a décidé de travailler sur le réacteur nucléaire refroidis à l'eau supercritique (SCWR – SuperCritical Water-cooled Reactor). Les travaux sur ce réacteur en sont

encore à leur début, cependant il est déjà attendu que la pression d'utilisation du fluide sera de l'ordre de 25 MPa et la température à la sortie du réacteur d'environ 625°C. Outre, l'augmentation du rendement thermodynamique du cycle due à une température élevée du fluide, l'utilisation d'un fluide supercritique s'affranchit des changements de phase, ce qui permet de supprimer l'utilisation de générateur et séparateur de vapeur. Il est ainsi possible d'utiliser un cycle direct, c'est à dire que le fluide chauffé par le cœur du réacteur est directement envoyé à la turbine sans passer par un cycle intermédiaire.

Les caractéristiques du SCWR

L'utilisation de l'eau à l'état supercritique dans des centrales thermiques remonte aux années 1950-1960. Ces centrales fonctionnent au charbon et atteignent des puissances de l'ordre de 1300 MW avec des conditions de pression d'environ 24MPa et des températures de 540°C. Ces conditions d'opérations extrêmes poussent les matériaux de l'époque à leurs limites. C'est ainsi que les centrales avec double resurchauffe sont privilégiées car elles permettent de respecter le degré d'humidité nécessaire en sortie de turbine basse pression sans avoir recours à des températures aussi extrêmes. Toutefois, depuis une vingtaine d'années les progrès réalisés dans le domaine des matériaux et dans le design des turbines remettent à l'ordre du jour les centrales utilisant un fluide à l'état supercritique. Les rendements obtenus dépassent largement les 40% en travaillant avec des pressions de l'ordre de 25 MPa et des températures avoisinant les 600°C.

C'est ainsi que le SCWR devrait atteindre un rendement thermodynamique de l'ordre de 45 à 50% alors que les centrales actuelles permettent seulement un rendement entre 33 et 35%. Les performances accrues de ce réacteur sont dues aux propriétés thermodynamiques de l'eau à l'état supercritique. Cet état est atteint lorsque la pression et la température sont supérieures à celles définies au point critique à savoir 22.064 MPa et 373.95°C dans le cas de l'eau. Une fois cette frontière franchie, il n'y a alors plus de distinction possible entre les phases liquides et gazeuses du fluide. L'enthalpie obtenue est alors considérable ; ainsi, en sortie de réacteur, la différence d'enthalpie entre les conditions attendues pour le SCWR et celles d'un CANDU actuel, par exemple, est de l'ordre de 2160 kJ/kg. Étant donné que l'enthalpie agit directement sur la valeur de la puissance et du rendement d'une centrale, il est clair que le SCWR offre un avantage certain. Par ailleurs, d'autres propriétés physiques telles que la densité ou la chaleur massique

subissent des variations importantes à la frontière du point critique. Des études sont en cours pour connaitre plus en détail le comportement de l'eau à cet état relativement complexe.

Ainsi, dans la littérature plusieurs cycles thermodynamiques pour le SCWR ont été proposés. Dans le cadre de ce travail, seuls les cycles directs (i.e., sans générateur de vapeur) ont été considérés à des fins d'optimisation.

Procédure d'optimisation

L'optimisation d'une centrale, qu'elle soit nucléaire ou thermique, requière des outils complexes et adaptés au problème. Il s'agit ici d'augmenter à la fois la valeur du rendement thermodynamique et la puissance de la centrale. Or ces deux fonctions ont des comportements antagonistes ; en effet, lorsque le rendement augmente c'est la puissance mécaniques des turbines qui diminue et vice versa. Il s'agit ainsi d'un problème d'optimisation multi-objectif qui ne peut être satisfait par une solution unique mais par une série de compromis entre ces deux fonctions. Pour traiter ce problème d'optimisation, un logiciel basé sur les algorithmes génétiques, développé à l'Institut de Génie Nucléaire de l'École Polytechnique, a été utilisé. L'optimiseur BEST (Boundary Exploration Searching Technique) est développé en VBA* (Visual Basic for Application) et est caractérisé par sa robustesse et sa rapidité de convergence vers le front optimal de Pareto. Le front de Pareto représente la frontière des solutions optimales au problème de maximisation des deux fonctions-objectif, ici le rendement thermodynamique et la puissance nette de la centrale, tout en satisfaisant un certain nombre de contraintes liées au respect de la physique et notamment aux deux principes de la thermodynamique. Cet optimiseur est couplé via l'outil « Dynamic Data Exchange *» à un simulateur écrit sous Matlab qui calcule les propriétés thermodynamique en chaque point du cycle selon des modèles thermodynamiques et thermiques propres à chaque composant du système. Les propriétés thermodynamiques sont calculées en utilisant la librairie X-Steam, également codée sous Matlab, qui reprend les équations données par IAPWS-97.

L'optimiseur part ainsi d'une population initiale aléatoire de variables qui vont alors être évaluées par le simulateur pour déterminer les fonctions objectifs correspondantes. L'espace des solutions obtenues est alors subdivisé en couloirs d'observations pour chaque fonction ; il s'agit ainsi de chercher dans chaque couloir la meilleure solution. Les solutions ainsi repérées servent alors de

* Marque de commerce de Microsoft

parents à la génération suivante de variables. En effet, le principe des algorithmes génétiques est basé sur la sélection naturelle, croisant ainsi les meilleurs éléments de la population précédente et leur faisant subir des mutations ; il est alors possible d'améliorer les solutions obtenues jusqu'à la convergence vers le front de Pareto.

Cette méthode a été validée à plusieurs reprises et notamment en la confrontant à une méthode d'optimisation largement utilisée dans le domaine énergétique qu'est la méthode du pincement associée à une étude exergétique. Ce travail a été réalisé sur une centrale thermique à haute performance existante. Elle est constituée de trois turbines, sept échangeurs de chaleur, un dégazeur, une chaudière et condenseur ; à noter également la présence d'une resurchauffe. Le cycle a pu être reproduit avec une précision de l'ordre du centième, ce qui permet de comparer les deux modes d'optimisation avec une erreur relativement restreinte. Cette optimisation a été réalisée en utilisant les fractions de soutirages, au nombre de sept, comme variables de décisions. Les fonctions-objectif du problème sont évidemment le rendement thermodynamique et la puissance mécanique nette du cycle. Le front de Pareto obtenu offre plus de 89 solutions permettant à l'utilisateur de privilégier la fonction-objectif désirée. Cependant, en plus du grand nombre de solutions obtenues, la valeur optimale acquise par la méthode du pincement se trouve sous le front de Pareto par 0.2 point en pourcentage pour ce qui est du rendement thermodynamique. Ceci montre qu'il est alors possible d'accroitre le rendement et la puissance de la centrale en faisant varier les fractions de soutirages avec un meilleur résultat que celui obtenu par la méthode du pincement associé à l'analyse exergétique.

Simulation-optimisation de cycles thermodynamiques adaptés au SCWR

Plusieurs cycles thermodynamiques appropriées au SCWR ont été simulés et optimisés dans ce travail. Dans un premier temps, quatre cycles basiques ont été étudiés. Ils permettent d'avoir une idée des conditions d'utilisation de ce futur réacteur et de montrer l'intérêt d'une optimisation du cycle durant la phase de conception. Il s'agit de quatre cycles dimensionnés pour une capacité de 1200 MW. La simulation de ces cycles ne tient pas compte des irréversibilités dans les turbines, ni des pertes de pressions. Néanmoins, il est intéressant de constater la possibilité d'optimiser ces cycles en utilisant les pressions dans les turbines, notamment aux extractions comme variables de

décisions. Les deux premiers cycles n'utilisent pas le procédé de régénération et ne présentent pas de grande possibilité au niveau de l'optimisation ; en revanche, ils ont montré que le rendement avait tendance à augmenter avec la valeur de la pression en sortie de turbine au détriment de la puissance nette. Les deux autres cycles offrent une plus grande marge de manœuvre pour l'optimisation grâce à la présence des échangeurs de chaleurs pour permettre l'utilisation du principe de régénération de la chaleur ; les variables de décision sont alors les pressions et les fractions de soutirage. Les fronts de Pareto obtenus dans ces deux cas sont très intéressants et montrent que seule une partie des variables de décisions contrôle la tendance du front. En effet, dans certaines zones, c'est la pression qui en augmentant va accroitre le rendement au détriment de la puissance ou vice versa, alors que la zone suivante peut être contrôlée par la fraction de soutirage. Le dernier cycle est pourtant simplement composé de deux turbines, deux réchauds, un dégazeur et présente une resurchauffe. Néanmoins, le front de Pareto présente quatre régions distinctes contrôlées par des variables différentes ; on peut ainsi imaginer la complexité que représente l'optimisation d'une centrale réelle.

Le prolongement logique de ce travail est donc de simuler et d'optimiser des cycles plus élaborés. Il s'agit de deux cycles similaires comportant tout deux : trois turbines, neuf réchauds (échangeurs de chaleur) et un dégazeur. La différence entres ces deux options est le fait que le second cycle présente une resurchauffe. Les variables de décisions dans cette optimisation sont les pressions aux extractions et en sortie de turbines, il s'agit toujours d'augmenter à la fois le rendement thermodynamique et la puissance du cycle. Pour cette étude, les rendements isentropiques de pompes et des turbines ont été incorporés à la simulation et les réchauds respectent les caractéristiques données par l'auteur concernant les différences de température entre les lignes de courants. Par ailleurs, il faut savoir que dans l'industrie, les turbines sont supposées respecter un certain ratio de pression entre leurs étages successifs. Nous avons voulu étudier les résultats obtenus lors d'une optimisation respectant ces conditions de définition des pressions. Deux cas d'optimisation ont donc été testés : les variables de décision sont sélectionnées aléatoirement dans les bornes indiquées dans l'optimiseur dans le premier cas alors que dans le second, les pressions sont définies en fonction d'un ratio de pression pour chaque corps de turbine. Au niveau des résultats, le front de Pareto pour le cycle avec une resurchauffe est supérieur à celui sans resurchauffe ce qui est en accord avec les principes de bases des cycles thermodynamiques. Ces deux fronts présentent également entre trois et quatre zones distinctes

qui sont contrôlées par des variables différentes. Pour ce qui est de l'optimisation où les pressions sont définies en respectant un ratio, le front de Pareto n'est composé que de cinq ou six points mais s'étend sur une plage suffisamment grande pour offrir à l'exploitant de la centrale le choix de favoriser le rendement ou la puissance, ou même une position intermédiaire.

Finalement un projet russe de centrale supercritique au charbon a été adaptée aux conditions attendues pour le SCWR, c'est-à-dire 25 MPa et 625°C en sortie de réacteur. Deux options ont été proposées et étudiées, à savoir une boucle de 1200 MW versus deux boucles de 600 MW en parallèle. Le cycle original a également été simulé à des fins de validation, la simulation respecte les rendements isentropiques des pompes et des turbines, les écarts de températures des lignes de courant au niveau des réchauds, ainsi que les pertes de pressions dans la tuyauterie. Pour les deux cas, les variables de décision utilisées sont les pressions. Les fronts de Pareto obtenus sont similaires et sont légèrement au dessus des valeurs de références. Il est possible de distinguer deux régions distinctes sur ces fronts : par exemple, dans les deux cas, la première région, constituant majoritairement le front de Pareto, est principalement contrôlée par la pression en sortie de la turbine haute pression. Ainsi une augmentation de la pression à cet endroit entraîne une augmentation du rendement, au détriment de la puissance. Ces deux solutions sont alors équivalentes en termes de rendement et de puissance ; par conséquent, il faudrait associer une fonction liée au coût pour différentier les deux options. En effet, dans le cas de deux boucles de 600 MW fonctionnant en parallèle, il faut doubler tous les équipements mécaniques. Toutefois, il est certain qu'ils seront de dimensions réduites en comparaison à l'équipement nécessaire dans le cas d'une boucle unique de 1200 MW.

Plusieurs cycles ont été considérés, simulés et optimisés durant ce travail. Dans le but de vérifier la faisabilité d'une telle centrale nucléaire, aux contraintes de pression et température aussi importantes, des calculs basiques de dimensionnement des tuyaux et des variations de température au sein du caloporteur ont ainsi été réalisés.

Dimensionnement des composants mécaniques

Le fait d'ajouter une resurchauffe au cycle thermodynamique accroît le rendement thermodynamique de façon significative ; néanmoins, cette modification nécessite une révision de la conception du cœur du réacteur. À la fin des années 1960, deux réacteurs expérimentaux ont

été développés en Russie avec une resurchauffe de vapeur au sein du réacteur. Ces deux réacteurs fonctionnaient à une pression de l'ordre de 10–12 MPa et une température d'environ 320°C à l'entrée du premier passage ; en sortie de resurchauffe la température avoisinait les 510°C pour une pression de 10 MPa. Le rendement thermodynamique était de l'ordre de 37–38 %, ce qui est comparable, voire supérieur, à celui des centrales nucléaires actuelles. Dans les deux unités, les canaux dédiés à la resurchauffe de vapeur ne sont pas placés de la même façon au sein du cœur du réacteur. En effet, dans le premier cas, ils sont placés en couronne et en alternance avec les canaux où a lieu l'évaporation du fluide lors du premier passage du caloporteur dans le réacteur ; pour la seconde unité, les canaux de resurchauffe sont placés au centre du cœur toujours en alternance avec ceux consacrés à l'évaporation. Il s'avère que la distribution du flux neutronique dans le second cas et plus uniforme que pour la première version. Ce retour d'expérience est encourageant et très instructif quant à la conception du futur SCWR.

Ainsi, une proposition de circuit hydraulique pour le SCWR de type CANDU est présentée dans ce mémoire. L'idée est d'utiliser des canaux bidirectionnels entre la partie où le fluide est à l'état supercritique et la partie où la vapeur est surchauffée : il est alors possible d'équilibrer la température moyenne à chaque extrémité du réacteur. Un point marquant dans ce chapitre est la différence significative de puissance nécessaire pour la phase de resurchauffe en comparaison avec la partie supercritique. Pour satisfaire une puissance constante sur le plan radial du réacteur, les calculs donnent un produit de la section du canal par la vitesse du fluide 37.5 fois plus important pour la resurchauffe que pour la partie supercritique. Par conséquent, une étude thermo-hydraulique couplée à une étude neutronique doit être menée pour approfondir cette question.

Étant données les fortes contraintes thermiques et mécaniques subies par la tuyauterie, le dimensionnement de l'épaisseur des tubes de pression, des collecteurs d'entrée et de sortie ainsi que des tuyaux d'alimentation a été réalisé. Les équations des codes ASME pour les tubes sous pression ont été utilisés : ainsi, il s'avère que les matériaux les plus adéquats seraient l'Inconel-625 ou encore l'Hastelloy. Néanmoins, des études approfondies sur ces matériaux et notamment leur résistance à la corrosion sont actuellement en cours et sont indispensables au dimensionnement final de ces éléments. Toutefois, ces calculs d'épaisseur offrent un ordre de grandeur satisfaisant dans la cadre de cette étude de faisabilité.

La question de la température au centre de la pastille du combustible a également été étudiée tout comme la distribution de température entre le caloporteur et le modérateur. Pour effectuer ces calculs, les équations de transfert de chaleur ont été établies séparément pour les deux études. Les résultats obtenus indiquent une température au centre du combustible inférieure à sa température de fusion. Il en va de même pour les températures supportées par la gaine. Toutefois, ces températures semblent très élevées et des calculs plus approfondis sont nécessaire pour valider le design de ces composants. Ces calculs ont été menés pour un tube de pression isolé du modérateur par une couche en céramique : il s'agit du concept retenu à ce jour.

Ainsi, ce travail montre l'intérêt et les possibilités offertes par cette méthode d'optimisation durant la phase de conception des cycles thermodynamiques. Les résultats ont indiqué des fronts de Pareto divisés en plusieurs régions distinctes et contrôlées par des variables de décision différentes. Le dimensionnement des composants mécaniques tels que les échangeurs de chaleur dépendra ainsi de la solution finalement retenue. En effet, les débits massiques au niveau des soutirages ne sont pas les mêmes pour tous les points du front de Pareto ; il n'est alors pas possible de passer d'une configuration à une autre en cours d'exploitation. Le choix des conditions d'opération correspondant aux variables de décision doit être judicieusement effectué au moment de la conception de l'ensemble de la centrale. Il faut ainsi déterminer un point satisfaisant au mieux le compromis entre le rendement thermodynamique et la puissance dépendamment des conditions d'opération de la future centrale. Il reste par ailleurs beaucoup de travail quant à l'étude du comportement neutronique du cœur, notamment pour la partie liée à la resurchauffe de vapeur. Des études sur les effets liées aux variations des propriétés thermo-physiques de l'eau à l'état supercritique comme la densité sont également en cours.

TABLE OF CONTENTS

LIST OF TABLES

LIST OF FIGURES

LIST OF SYMBOLS AND ABREVIATIONS

A	cross-sectional area (m^2)
c	the sum of the mechanical allowances
C_p	specific heat capacity at constant pressure ($J \cdot kg^{-1} \cdot K^{-1}$)
d	inside diameter of pipe (mm)
D	external diameter of pipe (mm)
f	Darcy friction factor
G	water flow rate per unit area ($kg \cdot m^{-2} \cdot s$)
h_i	enthalpy at state i ($J \cdot kg^{-1}$)
h	heat transfer coefficient ($W \cdot m^{-2} \cdot K^{-1}$)
H_i	feedwater Heater number i
k	thermal conductivity ($W \cdot m^{-1} \cdot K^{-1}$)
L	pipes length (m)
$\dot{m}$	mass-flow rate ($kg \cdot s^{-1}$)
P	pressure (Pa)
ϕ_l	linear heat flux ($W \cdot m^{-1}$)
$\dot{Q}$	heat transfer rate (W)
R, r	radius (m)
S	stress value for material from Table A-1 in ASME code (MPa)
s	entropy ($J \cdot kg^{-1} \cdot K^{-1}$)
t_w	pressure design thickness
T, t	temperature (°C)
v	specific volume ($m^3 \cdot kg^{-1}$)
V	velocity ($m \cdot s^{-1}$)

$\dot{W}$	power (W)
x	steam quality (%)
Y	coefficient from Table 304.1.1 in ASME reference
y	steam content (%)
ΔP	Pressure drop (Pa)
η	thermal efficiency (%)
η_s	isentropic efficiency (%)
ρ	density ($kg \cdot m^{-3}$)
#	state
AECL	Atomic Energy of Canada Limited
ASME	American Society of Mechanical Engineers
BEST	Boundary Exploration Searching Technique
BNPP	Beloyarsk Nuclear Power Plant
BWR	Boiling Water Reactor
CANDU	CANada Deuterium Uranium
CHF	Critical Heat Flux
CO_2	Carbon dioxide
cond	condensate
Cr	Chromium
cw	cooling water
D_2O	heavy water
DCS	Drain-Cooler Approach
DDE*	Dynamic Data Exchange

* Trademark of Microsoft

fw	feedwater
GC	Gas Cooler heat exchangers
GFR	Gas-cooled Fast Reactor
GIF	Generation IV International Forum
HP	High Pressure
IAEA	International Atomic Energy Agency
IAPWS-97	International Association for the Properties of Water and Steam
IEA	International Energy Agency
IP	Intermediate Pressure
LFR	Lead-cooled Fast Reactor
LP	Low Pressure
MHI	Mitsubishi Heavy Industries
MSR	Molten Salt Reactor
NA	Not Available
NPP	Nuclear Power Plant
OCDE	Organisation pour la Coopération et le Développement Economique
OECD	Organisation for Economic Co-operation and Development
PWR	Pressurized Water Reactor
pc	pseudocritical
SCW	SuperCritical Water
SCWR	SuperCritical Water-cooled Reactor
st	steam
SFR	Sodium-cooled Fast Reactor
TTD	Terminal Temperature Differences

USA	United States of America
VBA*	Visual Basic for Application
VHTR	Very High-Temperature gas cooled Reactor
YSZ	Yttria Stabilized Zirconia

* Trademark of Microsoft

INTRODUCTION

The world energy demand is continuously rising due to the increase of both the world population and the standard of living. The International Energy Agency published in the “World Energy Outlook 2010” the projection of the energy demand for three different scenarios [1]. The main scenario presented is called “the New Policies Scenario” which takes into account the broad policy commitments announced by countries around the world, including greenhouse gas emissions reduction and the decrease of fossil-fuelled energy subsidies. With this scenario, world primary energy demand increases by 36 % between 2008 and 2035, which corresponds to 4 400 million tons of oil equivalent. This projected rate of 1.2 % per year on average is lower than the rate of 2 % of the previous 27-year period.

Every fuel source shows a global increase, but fossil fuels account for over one-half of the increase in the total primary energy demand. Rising fossil-fuel price helps to prevent demand growth, thus oil which remains the main fuel in primary energy drops to 28 % while it stood at 33 % in 2008. In the case of coal, demand rises through to around 2020 and afterward declines. The most important increase concerns the demand of natural gas, which is more suitable for the environment and for practical attributes. The nuclear power part increases from 6 % in 2008 to 8 % in 2035. The part of modern renewable energy in total primary energy demand doubles to reach 14 %. Countries from the non-OECD are responsible for 93 % of the projected increase in demand of world primary energy. China’s demand is rising by 75 % between 2008 and 2035, and thus will account for 22 % of world demand. The second most important country contributing to the increase in global demand is India with 18 % of the rise.

Government policies encouraged low-carbon technologies to enhance energy security and to curb emissions of CO_2. This results into main changes in the electricity production. In “the New Policy Scenario” fossil fuels, such as coal and natural gas, remain dominant but demand drops to 55 % in 2035 whereas their share of total generation was 68 % in 2008. These changes are mainly due to nuclear and renewable sources expansion which is the main new low-carbon technology. Investment in renewable energy reached an all-time high in 2008 and stayed at similar levels in 2009 despite the global financial crisis. In the same way nuclear power is undergoing a renaissance. China, India and Russia have planned major expansions of nuclear capacity. Several

other countries are actively considering building new nuclear power stations as their existing installations are starting to be aged.

First nuclear power programs started in the mid 1960s and in the early 1970s in the United States and in Europe respectively [2]. The development of nuclear power was brought in following concerns about fossil fuel depletion and the desire of countries to reduce their energy dependency. This interest for nuclear power slows down with public opposition following nuclear accidents such as Three-Mile Island Unit-2 in 1979 and Chernobyl in 1986. Between 1970 and 1990 about 399 reactors were built, while between 1990 and 2008 the capacity increased only by 14.4 %. According to the International Atomic Energy Agency (IAEA), for the year 2010, 437 nuclear power reactors are in operation worldwide and 56 units are under construction, this being the largest number since 1992 [3]. They constitute 371 GW of installed electricity generating capacity. About one half of these units are installed in the USA, France and Japan. Moreover the share of nuclear power in global generation increased from 7.8 % in 1980 to 15.5 % in 2005 [4].

Within this framework of energy production revolution and the recovery of interest for nuclear power, ten countries decided to collaborate for the development of the fourth generation of nuclear reactors [5]. To guide the activities of research and development a consortium was created in 2000: “the Generation IV International Forum” (GIF), whose active members are required to ratify a Framework agreement. This fourth generation of nuclear power reactors are expected to be in commercial operation by 2030. These systems are also intended to deliver significant improvements compared to current advanced systems. GIF members underlined four major goals for this new generation of nuclear reactors which are: sustainability, safety and reliability, economic competitiveness and resistance to proliferation [6].

To satisfy these requirements, six nuclear power reactor concepts were selected by active GIF members. Among these technologies three concepts are considered as thermal reactors and the rest are classified as fast reactors. Fast reactors means, that fast neutron with energies higher than 1MeV are used to avoid absorption cross section resonances. The selected technologies are the following:

- Very High-Temperature gas cooled Reactor (VHTR);

This reactor concept utilizes a graphite-moderated core with a once-through uranium fuel cycle. The high temperature at the reactor outlet, around 1000°C, enables other applications such as hydrogen production or heat process to be achieved.

- Gas-cooled Fast Reactor (GFR);

This reactor design is a helium-cooled system using a direct Brayton cycle gas turbine and enable high thermal efficiency.

- Sodium-cooled Fast Reactor (SFR);

In this concept the coolant is liquid-sodium and the fuel is a metallic alloy of uranium and plutonium.

- Lead-cooled Fast Reactor (LFR);

This reactor is cooled by liquid metal such as lead or lead/bismuth eutectic mixture. The envisaged fuel is metal or nitride-based containing fertile uranium and transuranics in a closed fuel cycle.

- Molten Salt Reactor (MSR);

In this type, the primary coolant is a molten salt mixture, which runs at high temperatures but atmospheric pressure for higher thermal efficiency. The nuclear fuel is dissolved in the molten fluoride salt as uranium tetrafluoride (UF_4). The core is composed by graphite which also serves as the moderator.

- Super-Critical Water-cooled Reactor (SCWR);

This reactor uses supercritical water as the working fluid and could operate at much higher temperatures than both current Pressurized Water Reactor (PWR) and Boiling Water Reactor (BWR). Since Canada is interested in this technology, this concept is largely described in Chapter 1.

Among these technologies, Canada has oriented its efforts towards the design of a SCWR. In the literature several steam-cycle arrangements used in existing thermal power plants have been

extensively discussed. In particular, the authors present a comparison of different thermodynamic cycles that could be appropriate to run SuperCritical Water-cooled Nuclear Power Plants (SCWR NPPs) [7-12]. However, none of the proposed cycles have been optimized yet. It is obvious that from an engineering viewpoint this constitutes a key issue. Thus, the present work is intended to fulfill this gap by including the optimization of different SCWR NPP cycles by using genetic algorithms.

To perform these calculations, models of mechanical equipments such as: turbines, pumps, condensers, reactors and heat exchangers for the simulation of the global thermal cycle are written and solved using Matlab. The description in details of these components has been achieved by Hounkonnou [13], in this work, similar but more simple models will be used.

The optimization of power plants constitutes multi-objective optimization problem where several objective functions must be satisfied simultaneously. Traditional optimization techniques such as linear programming or gradient method are not sufficient to solve this kind of multi-objective problem. Further, when two or more objectives are concerned, the solution is not necessarily unique. In this work, an efficient and robust evolutionary algorithm based on genetic algorithm is used. This tool, developed at the Nuclear Energy Institute of “École Polytechnique de Montréal”, has already been tested and validated using several benchmark cases[14, 15]. The optimization strategy and the validation of the optimizer against numerical benchmark are presented in this work. The first work of simulation-optimization presented here is performed on four simplified thermodynamic cycles given in [10]. In May 2010, this study has been presented at the Canadian Nuclear Society (CNS) conference [16].

The second step was to develop and optimize more realistic cycles. Thus two cycles (a no-reheat and a single-reheat) from Naidin *et al*. [8, 9] have been simulated and optimized. Finally, two alternative solutions of SCWR power cycles adapted from the project of a supercritical fossil-fuelled power plant are put forward [17]. The results of this study have been presented at the international conference of Nuclear Energy for New Europe in September 2010 [18].

CHAPTER 1 THE SUPERCRITICAL WATER-COOLED REACTOR

The SuperCritical Water-cooled Reactor (SCWR) is one of the six concepts selected by GIF members. Canada shows interest in this technology and works on the development of a CANDU-SCWR. The main goals of this technology are to increase the thermal efficiency of Nuclear Power Plants (NPPs), to decrease electricity energy costs and the possibility of hydrogen production. This reactor operates above the thermodynamic critical point, thus the coolant should be light water at 25 MPa with an inlet temperature around 350°C and an outlet temperature about 625°C [19]. Several design options using pressure tubes or pressure vessels are currently under investigation.

1.1 Supercritical thermal power plants: review

The water under supercritical conditions, as a working fluid, is used by conventional power industries since the 50’s and 60’s [20]. Most of the turbines used by these units were designed for main and reheat temperature around 353–545°C. The use of steam under supercritical pressure allows a high capacity for fossil-fired power plants; some of them can reach 1300 MW. In the United States, nine units of 1300 MW were commissioned with operating conditions of 24.1 MPa and 538/538°C (main/reheat temperatures). Some ultra supercritical units have also been built with pressure above 30 MPa. One of these famous units is the 125-MW Philo Unit 6 with water parameters of 31 MPa and 621°C for the main steam and 565/538°C for the two reheats steam temperature [21].

The high conditions of pressure and temperature require the use of austenitic steels, however, it turned out that these materials were ill-welded with common Cr-steels and vulnerable to unsteady thermal stresses. Hence, systems with high steam temperature conditions were dropped and replaced by a double reheat cycle. The use of a reheat allows acceptable moisture in the last stage of the low-pressure turbine.

The modern steam turbines used another approach to improve the efficiency with newly designed fossil-fuel power units; this was possible because of two main factors. The first one is the improvement in materials development; new heat-resistant steels allow steam turbines to reach high steam temperature. The second factor is the new advanced approaches that have been

developed for the design of turbines allowing a decrease in exit energy losses and an increase in turbines' efficiency.

Mitsubishi has developed a 600°C class steam turbine with a cross-compound using high pressure and intermediate pressure as primary shaft and two-low pressure turbines as secondary shaft. Two of these kind of 1000-MW units are: Matsuura No.2 (1997) Unit and Misumi No.1 Unit (1998), steam conditions are respectively 24.1 MPa, 593°C/593°C and 24.5 MPa, 600°C/600°C [22]. A well-known unit in Germany is the 2x800-MW Schwarze Pumpe with steam conditions of 26.8 MPa and 545/565°C (main/reheat temperatures) [23]. This plant was completed in 1998 with a net efficiency of 41.1 %; the design efficiency was 40.5 %. Another well-known German unit is the 907-MWe Boxberg power plant with a turbine designed by Siemens [24]. This unit went on line in June 2000, with main stream conditions of 26.6 MPa, 545°C and 5.8 MPa, 581°C for reheat. The net efficiency of this unit is 42.7 %, where the projected efficiency was 41.7 %. In december 2000 Tachibana-wan No.2, which was built by MHI, started commercial operation [25]. It is a 1050 MW unit with steam conditions of 25.1 MPa, 600°C/610°C. The performance test result of Tachibana-wan No.2 confirmed that the efficiency of the turbine was greater than the design value. With a gross efficiency of 49 % this steam turbine is considered as the most efficient worldwide [26].

1.2 Supercritical water-cooled nuclear reactor concepts: cycle configurations

Canada is currently working on the development of a SuperCritical Water-cooled Reactor (SCWR). This system will use water under supercritical conditions as the principal coolant and will run at much higher operating conditions as compared to current nuclear power plants. Thereby, the thermal efficiency of this kind of power plant will largely compete with actual supercritical steam power boilers which are about 45–50%.

In addition, the high coolant temperature will not only generate electricity, but will also have other energy applications such as: hydrogen production, sea water desalinisation or petroleum extraction [27]. From a thermodynamic cycle viewpoint, the use of a supercritical fluid allows sufficient heat transfer without reaching phase change. Therefore, risks associated to the possibility of triggering critical heat flux conditions, in principle, are largely reduced or eliminated. Further, the use of steam generators and steam separators can be completely avoided in SCWR. Thus, it is also possible to use direct thermodynamic cycles where the supercritical

fluid expands right away in the turbine without requiring the use of intermediate steam generators. The Figure 1-1 presents a schematic view of the SCWR. Although it is not the CANDU version, where the reactor is not formed by horizontal channels, it illustrates quite well the envisaged concept of a direct cycle.

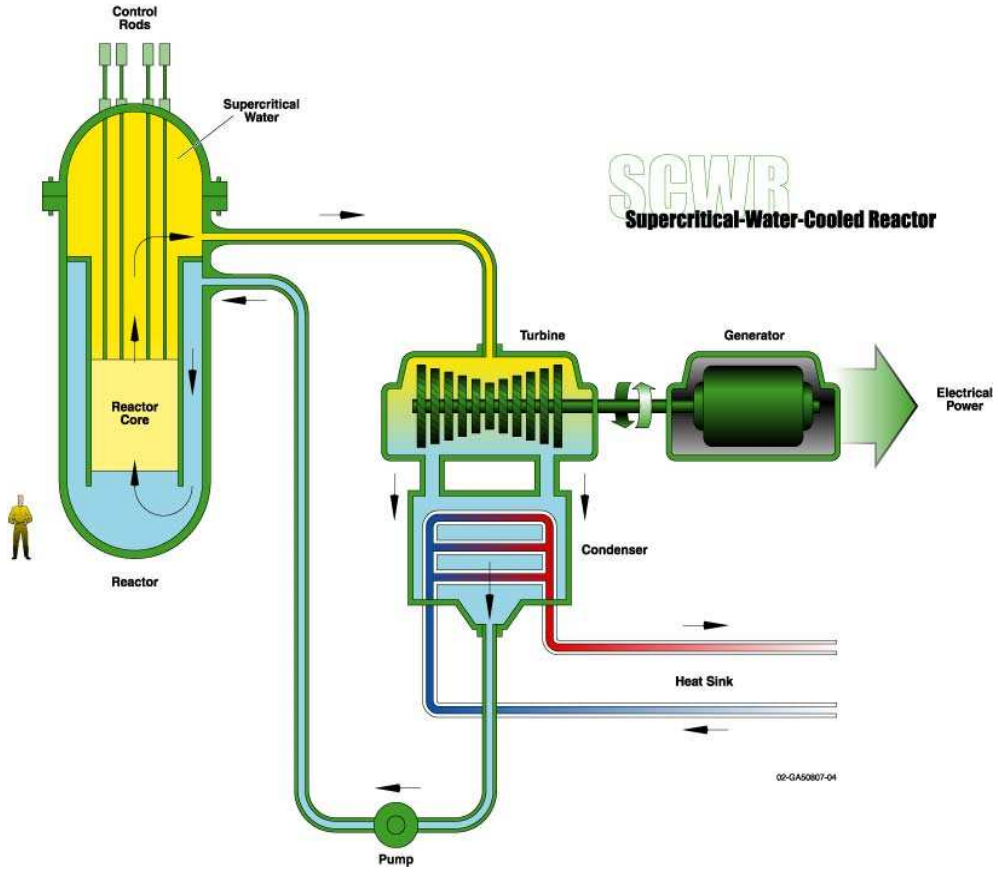

Figure 1-1: Schema of the SCWR concept (taken from [5]).

During this study several thermodynamic cycles are simulated and optimized. The following sections present the main characteristics of these cycles.

1.2.1 Supercritical water-cooled nuclear power plants: simplified thermodynamic cycles

The first step of this work is to simulate and optimize four simplified thermodynamic cycles given in Naidin *et al.* [10, 28]. These power-cycles, shown in Figure 1-2 and Figure 1-3, are proposed as the most suitable ones to be implemented in the next generation of SuperCritical Water Nuclear Power Plants (SCW NPPs). Operation conditions taken from the same reference

correspond to topologies that are variants of Rankine's type cycles working under supercritical water flow conditions of 25 MPa and 625°C. These four cycles are designed to produce a net mechanical power of 1200 MW.

The first cycle shown on Figure 1-2 (a) consists of two turbines and one steam-reheat. The thermal efficiency for this design has been estimated around 48.1 % with a mass flow rate of 613 kg/s.

The second cycle on Figure 1-2 (b) consists of a double reheat cycle with three turbines. With this configuration the thermal efficiency is around 49.3 % and the mass flow rate reaches 554 kg/s. The additional reheat increases the thermal efficiency as well as the capital cost of the equipment. It is also interesting to observe that thermal efficiency for the thermal cycles (b) has increased while the mass flow rate is lower than the previous configuration (a).

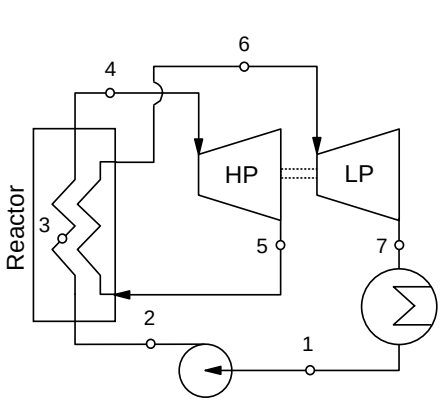

State	$T(^oC)$	$P\,(MPa)$	$h(kJ/kg)$
1	38.3	0.00677	160.8
2	39.1	25.0	186.0
3	350.0	25.0	1624.0
4	625.0	25.0	3567.0
5	345.0	4.9	3060.0
6	625.0	4.9	3725.0
7	38.3	0.00677	2275.0
Efficiency (%)			48.1
Mass flow rate (kg/s)			613.0

(a)

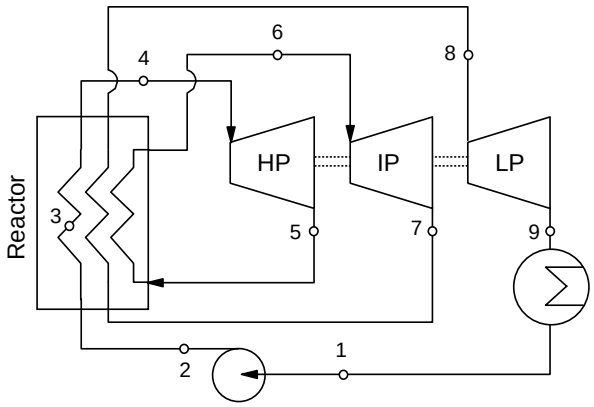

State	$T(^oC)$	$P\,(MPa)$	$h(kJ/kg)$
1	38.3	0.00677	160.8
2	39.1	25.0	186.0
3	350.0	25.0	1624.0
4	625.0	25.0	3567.0
5	410.0	7.6	3180.0
6	625.0	7.6	3705.0
7	418.0	2.3	3280.0
8	625.0	2.3	3745.0
9	38.3	0.00677	2390.0
Efficiency (%)			49.3
Mass flow rate (kg/s)			554.0

(b)

Figure 1-2: (a) Single-reheat cycle, (b) Double-reheat cycle [10, 28].

In addition, Figure 1-3 (a) and (b) shows two regenerative Rankine cycles which permit the thermal efficiency to be increased by using the latent heat of a fraction of steam extracted from the turbines to reheat the feedwater before it enters into the reactor core. It must be pointed out that the fractions of extracted fluid do not produce useful work but allow the overall efficiency to be increased.

The Figure 1-3 (a) presents a very simple regenerative single-reheat cycle with an open heat exchanger for the regeneration process. The steam is extracted from the high-pressure turbine to heat the feedwater through the deaerator. For this configuration the thermal efficiency is around 49.9 %. The mass flow rate required to reach 1200 MW is around 1030 kg/s, which is quite high regarding previous cycle configurations.

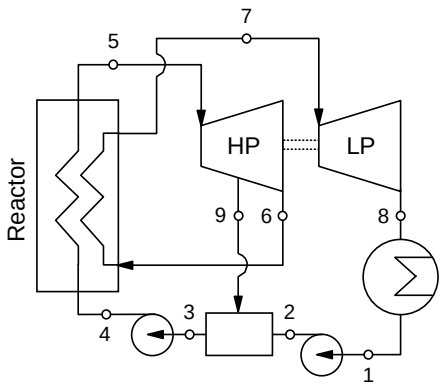

State	$T(^{o}C)$	$P(MPa)$	$h(kJ/kg)$
1	38.3	0.00677	160.8
2	38.8	14.9	175.0
3	340.0	14.9	1605.0
4	350.0	25.0	1624.0
5	625.0	25.0	3567.0
6	345.0	4.9	3060.0
7	625.0	4.9	3725.0
8	38.3	0.00677	2275.0
9	525.0	14.9	3385.0
Efficiency (%)			49.9
Mass flow rate (kg/s)			1030.0

(a)

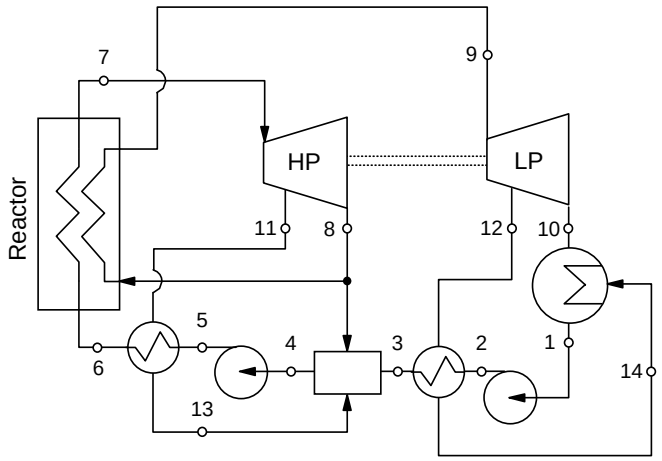

State	$T(^{o}C)$	$P(MPa)$	$h(kJ/kg)$	State	$T(^{o}C)$	$P(MPa)$	$h(kJ/kg)$
1	38.3	0.00677	160.8	8	350.0	5.0	3065.0
2	38.5	5.0	166.0	9	625.0	5.0	3725.0
3	200.0	5.0	850.0	10	38.3	0.00677	2270.0
4	265.0	5.0	1155.0	11	540.0	16.2	3415.0
5	270.0	25.0	1180.0	12	450.0	1.6	3314.0
6	350.0	25.0	1624.0	13	275.0	16.2	1210.0
7	625.0	25.0	3567.0	14	45.0	1.6	185.0
Efficiency (%)			52.7				
Mass flow rate (kg/s)			937.0				

(b)

Figure 1-3: (a) Single-reheat cycle with heat regeneration through single deaerator, (b) Single-reheat cycle with heat regeneration through single deaerator and two feedwater heaters [10, 28].

The last cycle (Figure 1-3(b)) presented in this section involves three feedwater heaters: one low-pressure heater, one deaerator and one high pressure heater. This arrangement allows a thermal efficiency of 52.7 % for a total mass flow rate of 937 kg/s. This configuration offers the possibility to substantially increase the thermal efficiency.

These very simple thermodynamic cycles constitute an excellent starting point for future designs of SCW NPPs. The relevance of using water under supercritical conditions is well demonstrated by the values of thermal efficiencies achieved. In the following sections more complex cycles with and without fluid reheat are studied and presented in detail. They have been proposed by Naidin *et al.* [7-9, 12].

1.2.2 No-reheat cycle

The no-reheat cycle is a direct regenerative cycle and consists of two turbines, one for high pressure (HP) and one for intermediate and low pressure (IP/LP) [8]. The scheme of the cycle is illustrated in Figure 1-4. Since the specific volume of the steam at the ehxaust of the HP turbine is quite low, two IP/LP turbines are required.

The regeneration process takes place in five low-pressure feedwater heaters (H1-5), one deaerator, three high-pressure feedwater heaters (H6-8) and one topping desuperheater (H9). The cycle also includes one condenser, associated pumps and the nuclear source of energy. This cycle is designed for a nuclear power plant output of 1200 MW and the thermal efficiency is approximately 51 %. The conditions of operation given by the author [8] are presented in the Table 1-1.

Table 1-1: Reference values of a nuclear power plant without reheat [8].

State #	$\dot{m}$ **(kg/s)**	**Temperature (°C)**	**Pressure (MPa)**
1	1190	625	25
3		410	6.6
11		38.4	0.00677
12		38.4	0.00677
13	1190	350	25.8

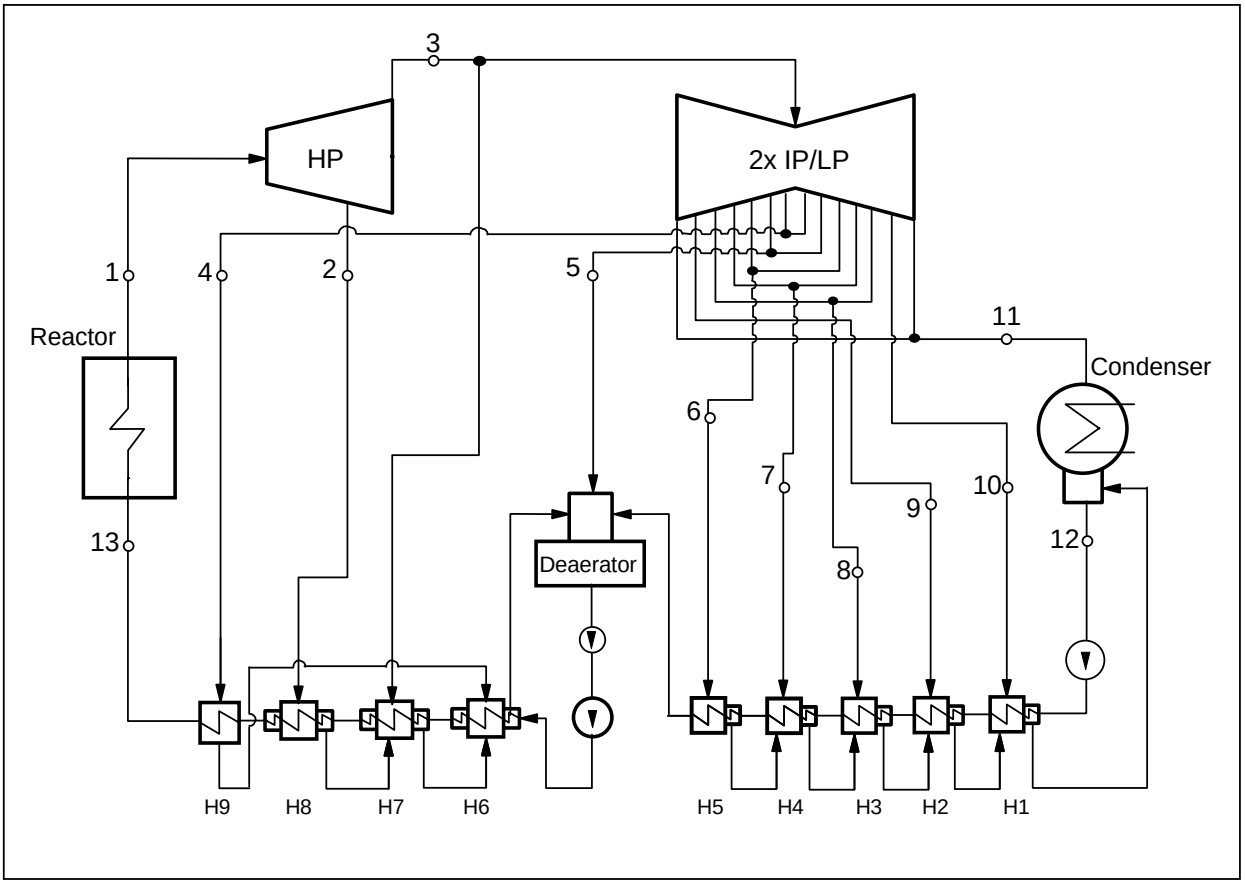

Figure 1-4: No-reheat cycle layout [8].

1.2.3 Single-reheat cycle

This cycle is very similar to the previous one but it has a direct single-reheat regenerative configuration [9]. The reheat requires the addition of the IP turbine. The scheme of this second option given by Naidin *et al*. [9] is presented in Figure 1-5 and some data are given in Table 1-2.The turbine-generator arrangement is a cross-compound: the HP and IP turbines are in tandem, i.e., coupled to the same mechanical shaft. The volume of the steam at the exhaust of the IP turbine is quite high; therefore, two LP turbines are required. However, these turbines are attached to a separate shaft.

With the actual configuration designed to obtain 1200 MW_{th}, the thermal efficiency was determined to be approximately 52 %. The addition of one reheat allows the improvement of the thermal efficiency; however this option presents some complexity in the reactor core due to the necessity of steam-reheat nuclear fuelled channels.

Table 1-2: Reference values of the Single-reheat power plant [9].

State #	$\dot{m}$ (kg/s)	Temperature (°C)	Pressure (MPa)
1	960	625	25
3	780	400	6.1
4	780	625	5.7
12		38.4	0.00677
13		38.4	0.00677
14	960	350	25.8

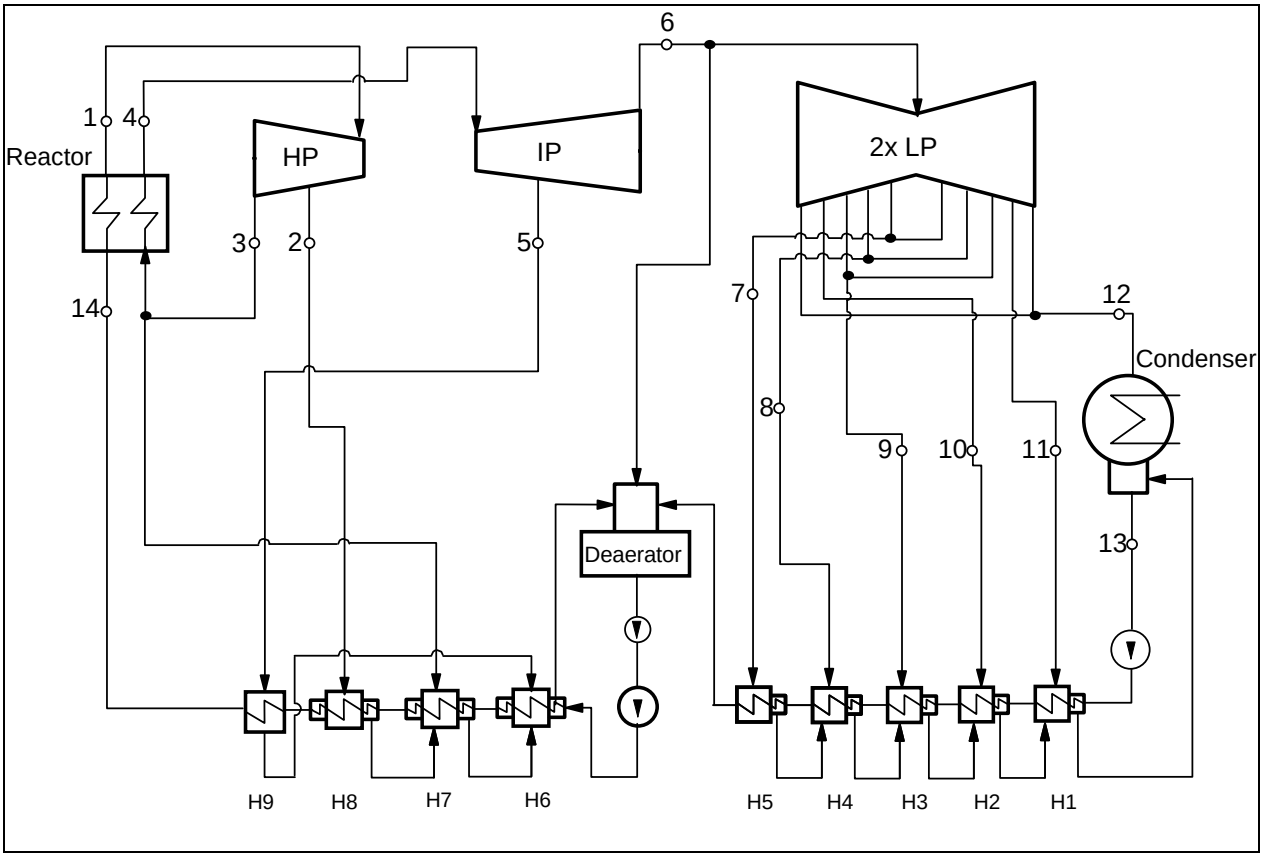

Figure 1-5: Single-reheat cycle [9].

1.2.4 Adaptation of a supercritical water fossil-fuelled power plant project to 1200-MW SCW NPP

In a second stage of this work, two possible cycle configurations for 1200-MW SCWR NPPs are developed based on a Russian 660-MW fossil-fuelled power plant project that is intended to run under supercritical water conditions [17]. It will be constructed near the Tom'-Usinsk site, which already has nine coal-power units, with a total capacity of 1272 MW. The commissioning of this power plant is expected to take place around 2011–2012. The schematic of the original system is shown in Figure1-6 and Table 1-3 summarizes the reference thermodynamic states as function of the corresponding numbers shown in the figure.

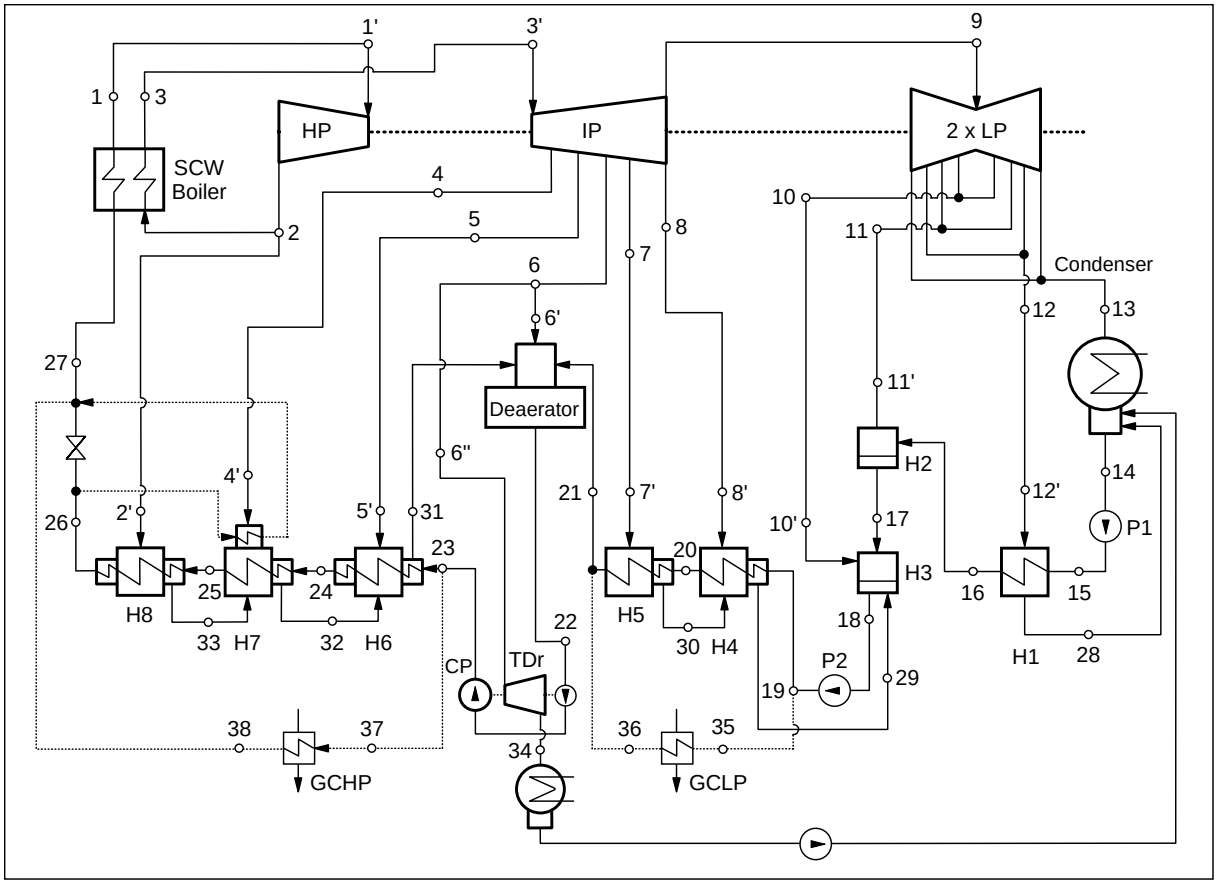

Figure 1-6: 669 MWe Tom'-Usinsk Russian supercritical water fossil fuelled plant [17].

The cycle consists of three turbines running in tandem within a supercritical water reheat-thermodynamic cycle. Supercritical water conditions are: 600°C and 30 MPa and the actual plant efficiency is close to 51 %. This power plant regenerates waste heat from gas streams through

two gas cooler heat exchangers (GCHP and GCLP in the figure). It also includes six closed feedwater heaters, one deaerator and two open feedwater heaters for the regeneration process.

Table 1-3: Reference values of the fossil fuelled power plant [17].

State #	$\dot{m}$ (kg/s)	T (°C)	P (MPa)	h (kJ/kg)	y (%)	State #	$\dot{m}$ (kg/s)	T (°C)	P (MPa)	h (kJ/kg)
1	475.9	600	30	3447		14	313.2	24.1	0.003	100.9
1'	475.9	597	29	3447		15	313.2	24.1	0.49	101.7
2	475.9	375.4	7.5	3079.4		16	313.2	53	0.39	222.3
2'	38.8	372.9	7.2	3079.4		17	326.9	76.1	0.04	318.6
3	437.1	620	7.3	3695.7		18	367.6	98.8	0.097	414.1
3'	437.1	619.7	7.2	3695.7		19	367.6	99	1.37	415.7
4	20.8	541.1	4.6	3534.5		20	321.8	131.9	1.27	555.2
4'	20.8	540.3	4.4	3534.5		21	367.6	147.4	1.18	621.3
5	29.1	457.9	2.7	3366.2		22	475.9	180.34	1.01	764.5
5'	29.1	457.2	2.6	3366.2		23	475.9	187.1	34.3	811.8
6	51.1	330.2	1.1	3113.7		24	440.8	231.6	34	1006.1
6'	19.6	329.3	1	3113.7		25	440.8	NA	33.7	1107.4
6''	31.5	328.8	0.97	3113.7		26	440.8	289.8	33.3	1277
7	9.1	235.3	0.5	2930.3		27	475.9	295	33.2	1302.5
7'	9.1	234.7	0.471	2930.3		28	17.3	56	0.017	234.5
8	18.2	191.9	0.333	2847.4		29	27.4	109	0.31	457.2
8'	18.2	191.3	0.314	2847.4		30	9.1	141.9	0.47	597.5
9	308.8	191.6	0.32	2847.4		31	88.7	197.1	2.6	839.9
10	13.4	NA	0.104	2655.7	0.93	32	59.6	241.6	4.4	1045.4
10'	13.4	NA	0.097	2655.7	0.79	33	38.8	264	7.2	1154.3
11	13.6	NA	0.043	2530.9	4.68	34	31.5	NA	0.006	2405.3
11'	13.6	NA	0.04	2530.9	4.56	35	45.8	99	1.37	415.7
12	17.3	NA	0.018	2422.9	7.67	36	45.8	147.4	1.18	621.3
12'	17.3	NA	0.0167	2422.9	7.55	37	35.1	187.1	34.3	811.8
13	264.4	NA	0.003	2267.6	11.35	38	35.1	295	33.2	1302.5

NA– Not Available

Note that this cycle is studied in more detail in chapter 4. Major thermal components are modeled and the whole system is optimized using an evolutionary algorithm.

CHAPTER 2 POWER PLANT MODELLING

As discussed in the previous section, the thermodynamic cycles considered for use in the future supercritical water-cooled power plants are based on Rankine cycle. Therefore, this section includes a brief analysis of this well known cycle followed by the modelling approach used for the simulation of each power plant.

2.1 The ideal Rankine cycle

The cycle presented here is an elemental on that consists of a heat source (i.e., a boiler), a turbine, a condenser and a pump. Figure 2-1 shows the required thermal as well as and the T-s diagram for this simple steam power plant operating on the Rankine cycle.

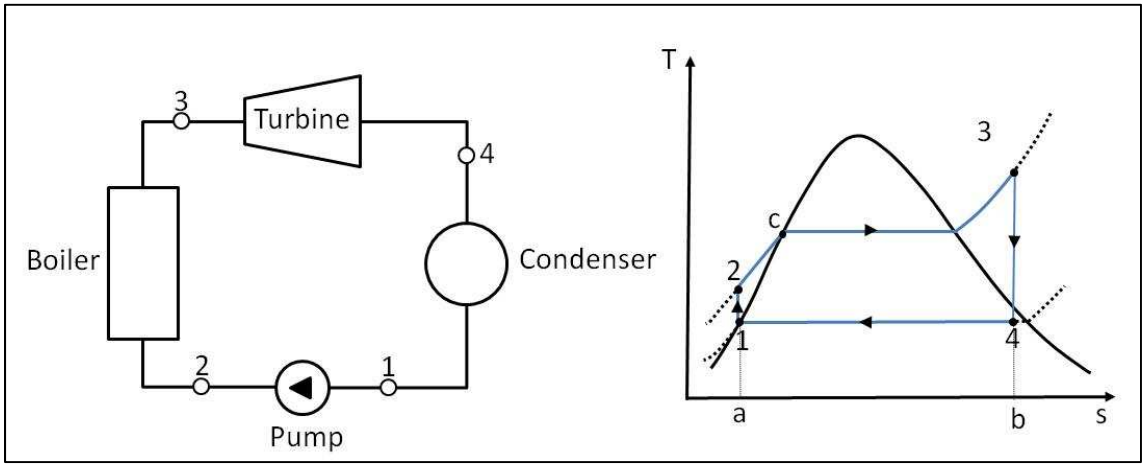

Figure 2-1: The ideal Rankine cycle.

At state 1, water enters into the pump as saturated liquid and is compressed isentropically until state 2 which corresponds to the operating pressure of the boiler. The fluid leaves the boiler at state 3 as superheated steam. Then, steam expands into the turbine isentropically up to state 4, where the liquid-vapour mixture in general has a high quality. Finally, it enters into the condenser to be condensed at constant pressure and reaches the saturated liquid state 1.

The net mechanical power of this cycle is given by the work produced by the turbine minus the work consumed by the pump, expressed as:

$$\dot{W}_{net} = \dot{W}_{turb} - \dot{W}_{pump} = \dot{m}\,(h_3 - h_4) - \dot{m}\,(h_2 - h_1) \tag{2-1}$$

The thermal efficiency is given by the ratio of this mechanical power to the total consumed energy, thus:

$$\dot{Q}_{in} = \dot{m}\,(h_3 - h_2) \tag{2-2}$$

$$\eta = \frac{\dot{W}_{net}}{\dot{Q}_{in}} \tag{2-3}$$

The operating parameters such as temperature and pressure are directly related to the overall performances of the cycle. Thus, according to equation (2-3), improving the overall thermal efficiency requires increasing the net mechanical work and decreasing the total consumed energy. The thermal efficiency of the Rankine cycle can also be obtained in terms of average temperatures during heat interaction process. Indeed, the heat transfer into the working fluid per unit of mass through the boiler is given by the total area: 3-b-a-2-c-3 and it can be written as:

$$\frac{\dot{Q}_{in}}{\dot{m}} = \int_1^4 T\,ds = area\ 3 - \mathrm{b} - \mathrm{a} - 2 - \mathrm{c} - 3 \tag{2-4}$$

The integral can be replaced by an average temperature of heat addition: $\bar{T}_{in}$, it turns:

$$\frac{\dot{Q}_{in}}{\dot{m}} = \bar{T}_{in}\,(s_3 - s_2) \tag{2-5}$$

Similarly, the heat transfer from the condensing steam per unit of mass trough the condenser is given by the total area: 4-b-a-1-4. With the introduction of the temperature on the steam side of the condenser: T_{out}, we obtain the following equation:

$$\frac{\dot{Q}_{out}}{\dot{m}} = T_{out}\,(s_4 - s_1) \tag{2-6}$$

Thus, the thermal efficiency of the Rankine cycle can be expressed as a function of these heat transfer terms as:

$$\eta = 1 - \frac{\frac{\dot{Q}_{out}}{\dot{m}}}{\frac{\dot{Q}_{in}}{\dot{m}}} = 1 - \frac{T_{out}}{\bar{T}_{in}} \tag{2-7}$$

It is obvious that to improve the thermal efficiency of the cycle, the fluid must have the highest possible temperature during the heat addition process and the lowest possible temperature during the heat rejection. Therefore, there are three different ways to accomplish such condition [29].

The first option consists of having lower pressure in the condenser which imposes directly a lower fluid temperature. According to equation (2-7) the benefit of such operation are obvious. Figure 2-2 presents the *T*-*s* diagram with two different pressures of condensation.

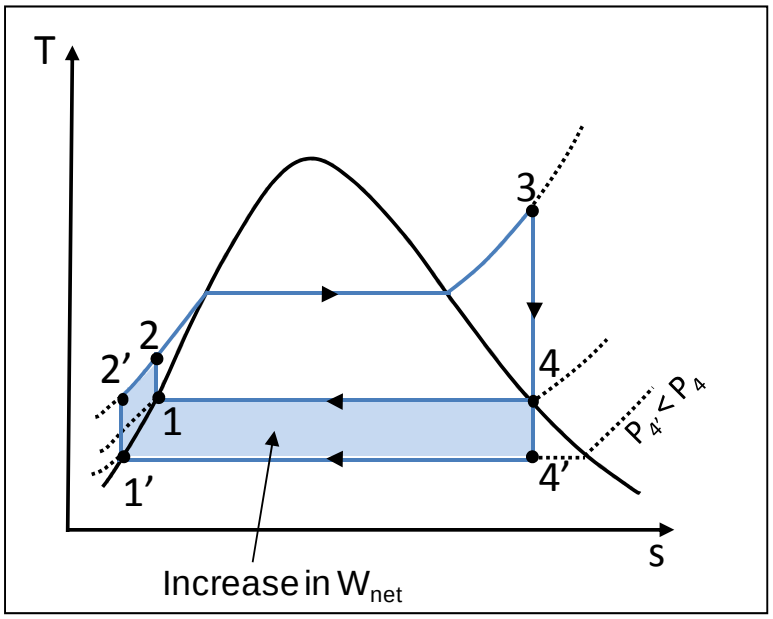

Figure 2-2: Effect of exhaust pressure on Rankine cycle efficiency.

The blue area 1'-2'-2-1-4-4' represents the increase of the available work from the cycle. Nevertheless, this solution has some physical limitations as the quantity of moisture contained in the steam at the final stage of the turbine, this can affect the efficiency of the turbine of course, but the erosion of the turbine blades may also be a very serious problem. However, the main limitation of this solution is that the condenser pressure is clearly limited by the temperature of available cooling water. It is not possible to operate at a pressure lower than the pressure of saturation given by the temperature of the cooling medium. Thus, this solution is only possible in the theory but not applicable for a real power plant.

Another way to increase the thermal efficiency of the thermodynamic cycle consists of increasing the temperature of the steam before it enters into the turbine. Figure 2-3 presents the effect of increasing the steam temperature from T3 to T3'. As illustrated by the area 3-3'-4'-4 the mechanical power is increased while the quantity of heat added and rejected are also increased but the overall effect is a net increase in the thermal efficiency. This increase in efficiency would also follow from the fact that the average temperature at which heat transferred to the steam is increased, see equation (2-7).

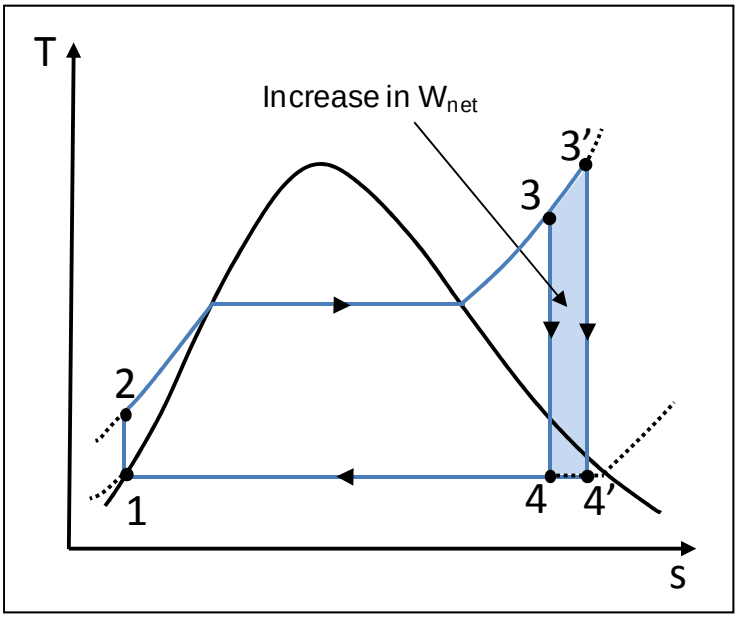

Figure 2-3: Effect of superheating the steam to higher temperatures on Rankine cycle efficiency.

Moreover, superheating the steam at higher temperature decreases its moisture content at the last stage of the turbine. From the practical point of view the limitation to this process is imposed by the characteristics of the materials (i.e., Young modulus vs. temperature).

Finally, the last method consists of increasing the boiler pressure which allows a higher average temperature during the heat-addition process. The major gain in cycle efficiency results from the reduction of the total heat rejected from the cycle while the heat input remains almost the same as illustrated in Figure 2-4. The major drawback with this method is due to the high moisture content that can occur at the last turbine stage.

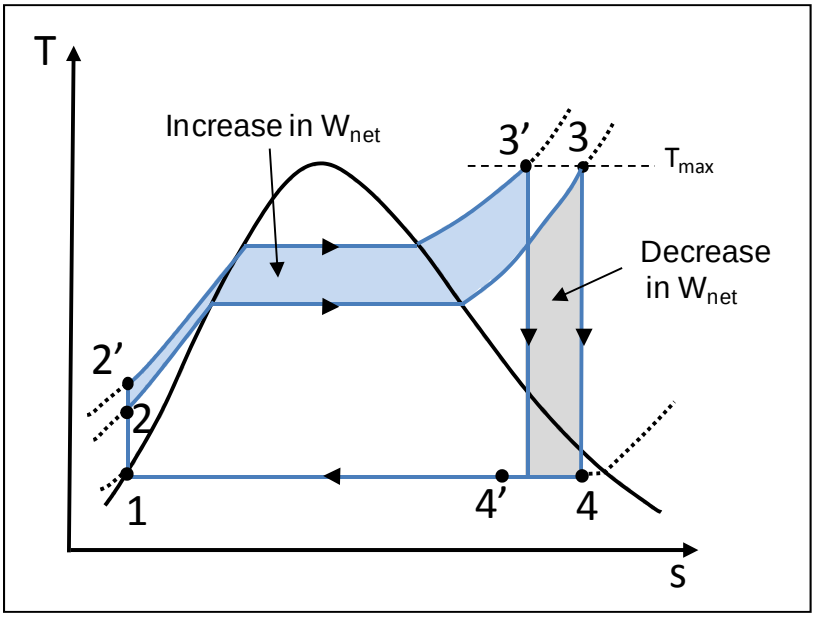

Figure 2-4: Effect if boiler pressure on Rankine cycle efficiency.

2.2 The ideal regenerative Rankine cycle

As demonstrated in the previous section increasing the average temperature during the heat addition process is a good way to increase the overall cycle efficiency. Indeed, in the Rankine cycle, as shown in Figure 2-1 heat is added to the working fluid at a lower temperature during the liquid phase and, thereby, it reduces considerably the cycle efficiency. One way to increase this temperature is to increase the temperature of the fluid before it enters into the boiler. The common process used to achieve this purpose consists of regenerating heat by extracting some fractions of steam from various turbine stages. Thus, latent heat is regenerated inside feedwater heat exchangers. Obviously, this process requires the addition of a feedwater heater (FWH) as shown in Figure 2-5. It is difficult to show the improvement of cycle efficiency graphically on T-s diagram because the mass flow rates are not the same at all stages, as shown in Figure 2-6. Nevertheless, it is obvious that the average temperature at which heat is supplied is higher; indeed, the fluid enters into the boiler at T4 instead of T2, as shown in Figure 2-5.

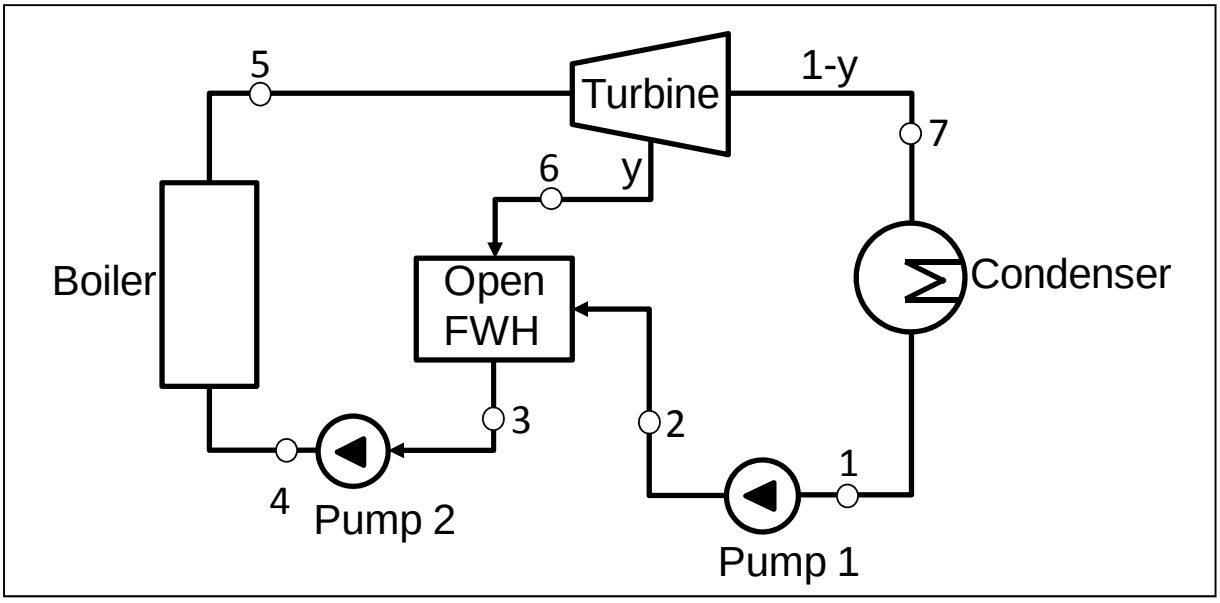

Figure 2-5: Regenerative cycle with open feedwater heater.

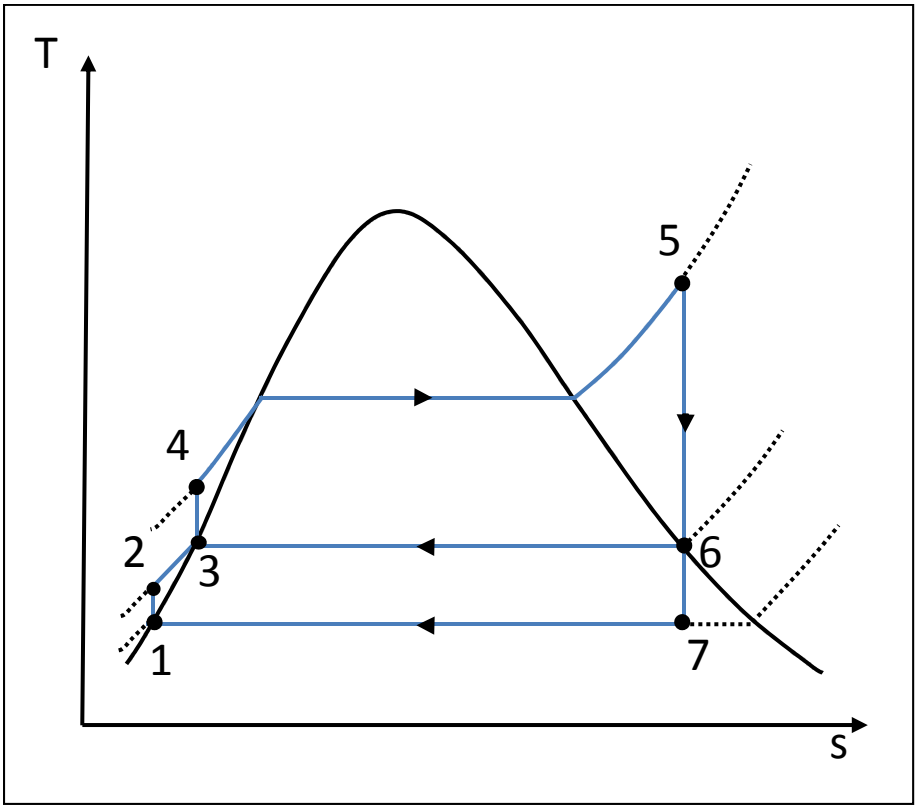

Figure 2-6: T-s diagram of the regenerative cycle.

It is obvious that the addition of other heat exchangers in the cycle enable higher temperature to be reached. Indeed, the principal idea of regeneration consists of recovering Carnot principal, where the maximum efficiency is obtained with only two thermal sources at constant temperature. Thus, this idea could be achieved by using infinity of heat exchangers to reach Carnot efficiency. Of course it is not possible in a real Rankine cycle, nevertheless the improvement in the thermal efficiency of the cycle are not negligible. In addition, Regeneration trough an open type feedwater heater (presented in detail in 2.3.3) provides a convenient mean of deaerating the feedwater and thus, removing non-condensable gases.

Therefore, regeneration has been largely used in all modern steam power plants since its introduction in the early 1920s. The power plants cycles simulated and optimized in this document are based on the process of heat regeneration. The following section presents the thermodynamic modelling to perform the simulation.

2.3 Thermodynamic modelling

All cycles presented in Chapter 1 have been simulated and optimized. The simulation module was written in Matlab (version R2009b) [30] and uses the X-Steam library [31] for thermodynamic properties of water and steam. The simulator includes specific models of different thermal equipment; the information for each one is presented in this section. The thermodynamic model requires an appropriate knowledge of working fluid properties as function of several plant operating conditions. In particular, how these properties change during the transition from subcritical to supercritical conditions. To this aim, before presenting the model, the behaviour of some key water properties as a function of both temperature and pressure are presented. Furthermore, the library used to perform the calculations is validated against thermodynamic table values.

2.3.1 Thermodynamic properties of water under critical and pseudo critical conditions.

The high-performances expected by the SCWR are mainly due to the thermodynamic properties of water under supercritical conditions. These conditions occur for pressures and temperatures higher than the critical point. The critical point is a thermodynamic condition under which the

distinction between the liquid and the gas phase disappears. Thus it is characterized by the phase state parameters: temperature, pressure and density which have unique values for each pure substance. The critical parameters of water are: pressure of 22.064 MPa, temperature of 373.95°C and density of 322.0 kg/m^3[19]. Figure 2-7 presents the variation of the specific enthalpy versus temperature for the critical pressure (22.064 MPa) and for the pressure expected to be used in the Canadian SCWR (25MPa), these properties have been determined using X-Steam library [31]. For comparison, the conditions at the outlet of the proposed CANDU –type SCWR reactor are symbolized by a square. The diamond symbol presents the conditions at the outlet of a CANDU-6 type reactor. As shown on this figure the difference between these two specific enthalpies is around 2160 kJ/kg. The thermal efficiency and the mechanical power of a thermodynamic cycle are related to these values. Thus the advantage of using water under supercritical conditions is obvious.

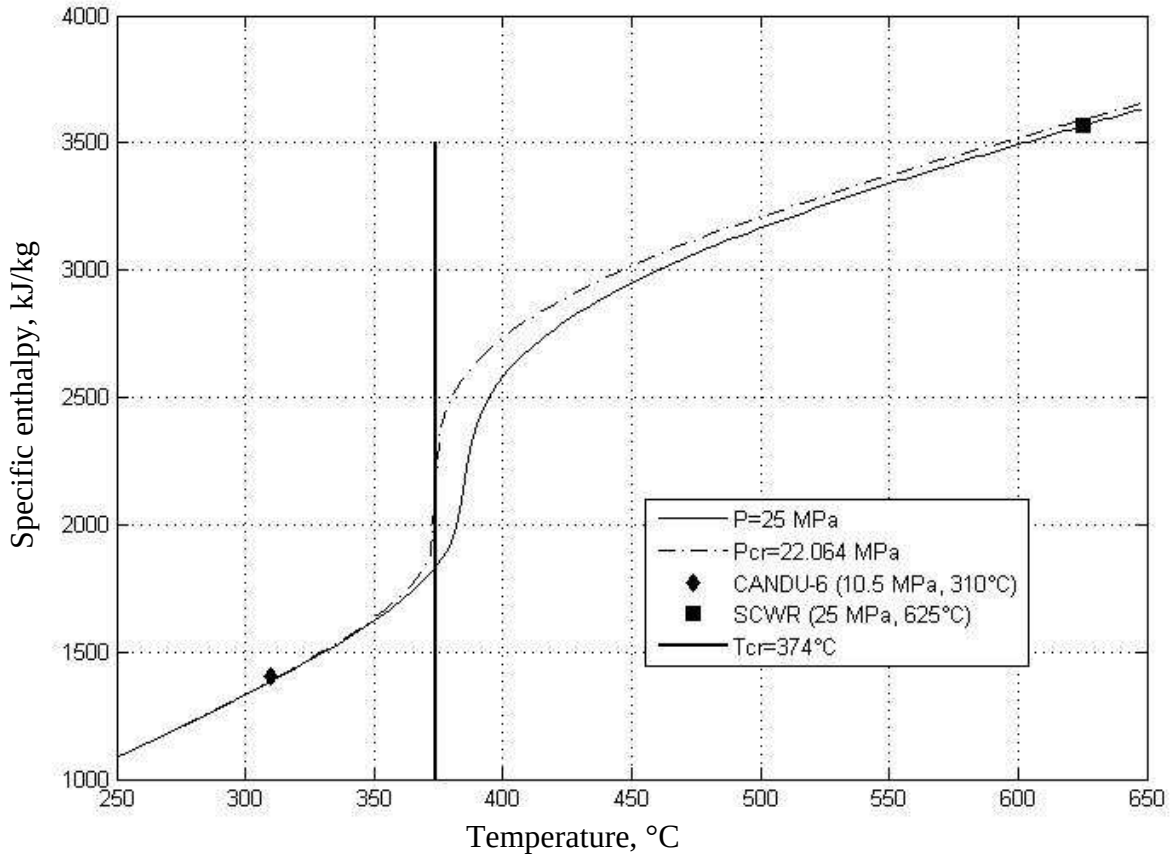

Figure 2-7: Variation of specific enthalpy versus temperature.

Also, the physical properties such as the density and the specific heat of water undergo important variations during the transition from the superheated to supercritical conditions. The variation of both density and specific heat versus temperature for the pressures of 22.064 MPa and 25 MPa are presented in the two Figures 2-8 and 2-9 respectively.

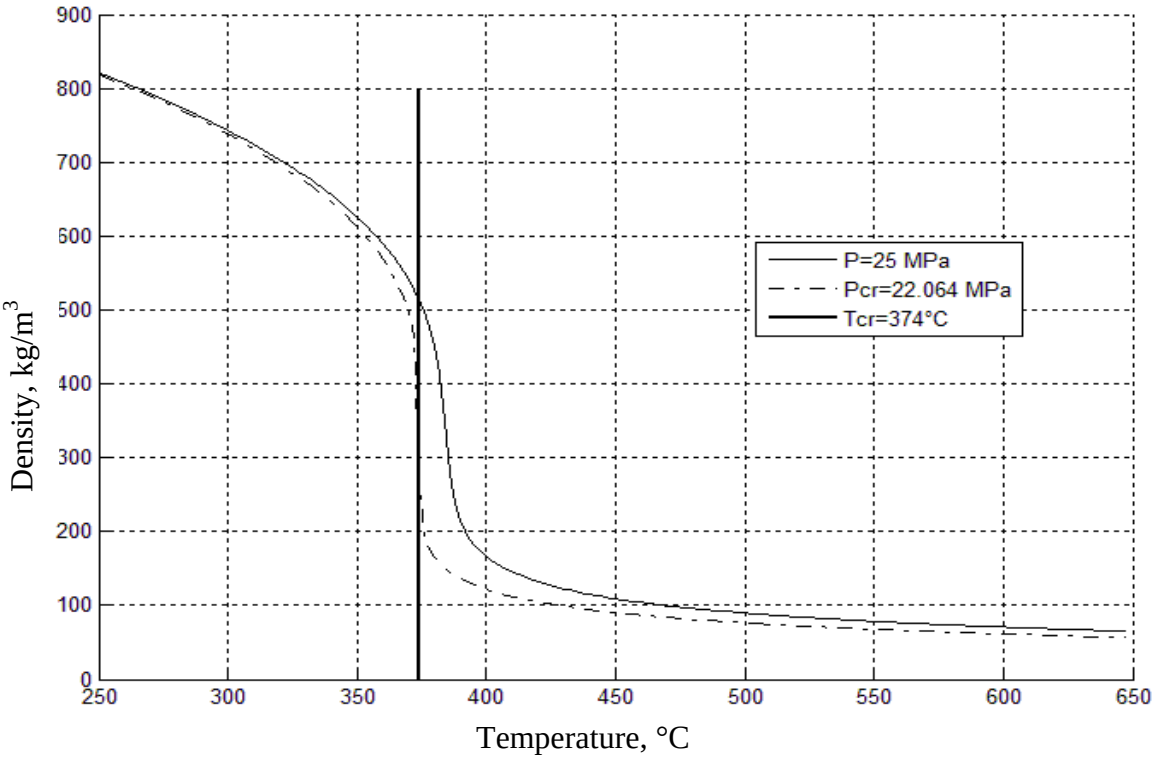

Figure 2-8: Variation of the density vs. temperature.

Both properties display rapid variations in their behaviour in vicinity of the critical and pseudo critical points. Indeed, heat transfer is strongly influenced by these thermo-physical properties variations; therefore, the heat-transfer correlations have to be adapted for supercritical water. Studies from Mokry *et al.* [32] present that there are three types of heat transfer regimes for forced convective heat transfer: normal heat transfer, deteriorated heat-transfer regime and improved heart transfer regime. The second one is characterized by a lower heat transfer coefficient than expected which means a higher wall temperatures than expected. The third regime is the contrary, a higher heat transfer coefficient characterized by a lower wall temperature. Currently, heat transfer correlation for forced convective heat transfer in the normal heat transfer regime seems to be promising. Other considerations such as neutronic field should take into account the significant change of thermo physical properties within the critical and

pseudocritical regions. In particular, the density of the coolant has a direct impact on the reactivity of the reactor. Thus, it is crucial to have a good understanding of the properties for simulating the behaviour of the fluid with sufficient accuracy to assure a safe and efficient technology. That is why; physical properties are currently being studied to gain a full understanding of the fluid under these extreme conditions [33, 34].

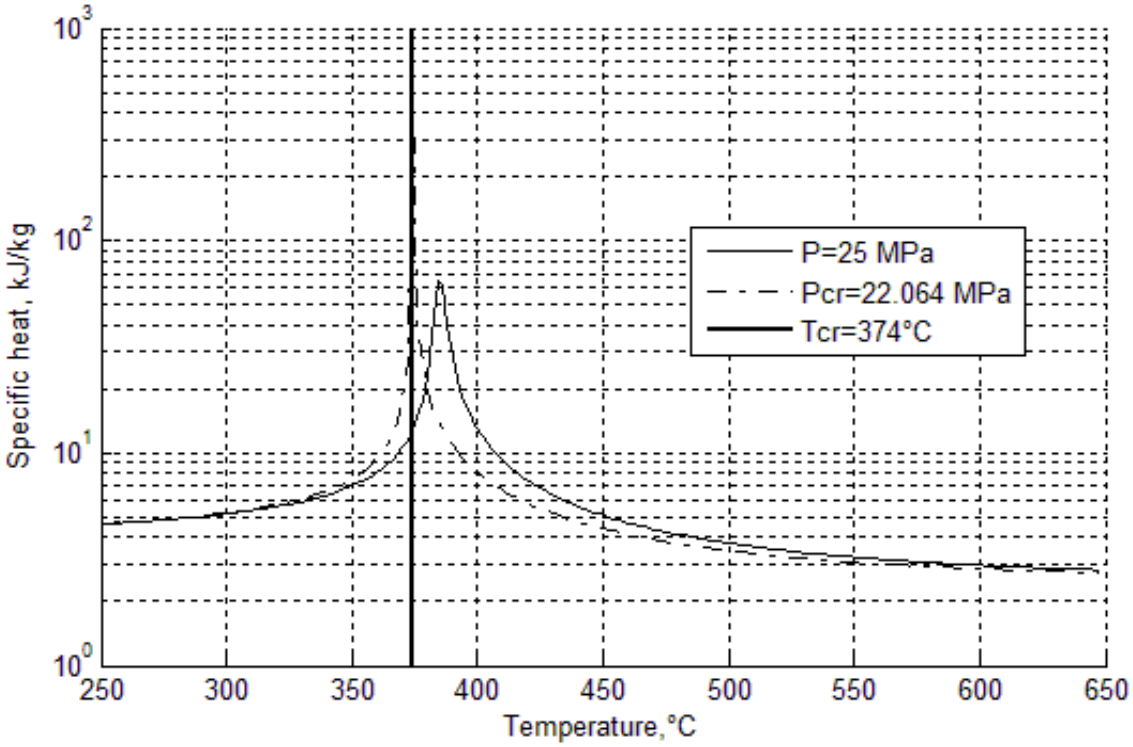

Figure 2-9: Variation of specific heat vs. temperature.

All these properties have been calculated by using X-Steam library [31], it consists of a full implementation of the formulation given in IAPWS- IF-97 [35] for industrial use including all regions and backward functions for good calculation speed. Since, the simulations require values of enthalpy and entropy, the capability of the software to calculate them has been determined.

Thus, for a wide range of temperatures and pressures covering the supercritical region, both enthalpies and entropies calculated with X-Steam are first validated against the values given in the water-steam table of Schmidt [36]. Relative differences, defined with respect to this table are partially presented in Figure 2-10 and Figure 2-11 and expressed as:

$$\text{Relative difference (\%)} = \frac{Table\ values - Calculated\ values}{Table\ values} \times 100 \qquad (2\text{-}8)$$

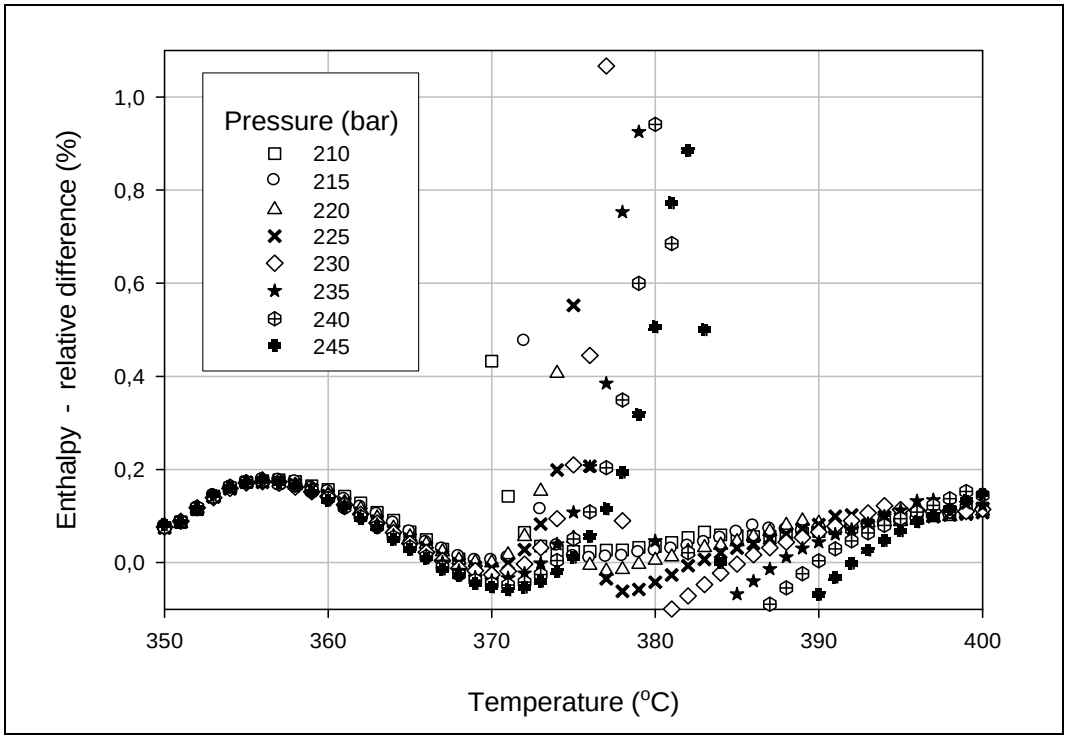

Figure 2-10: Relative enthalpy difference.

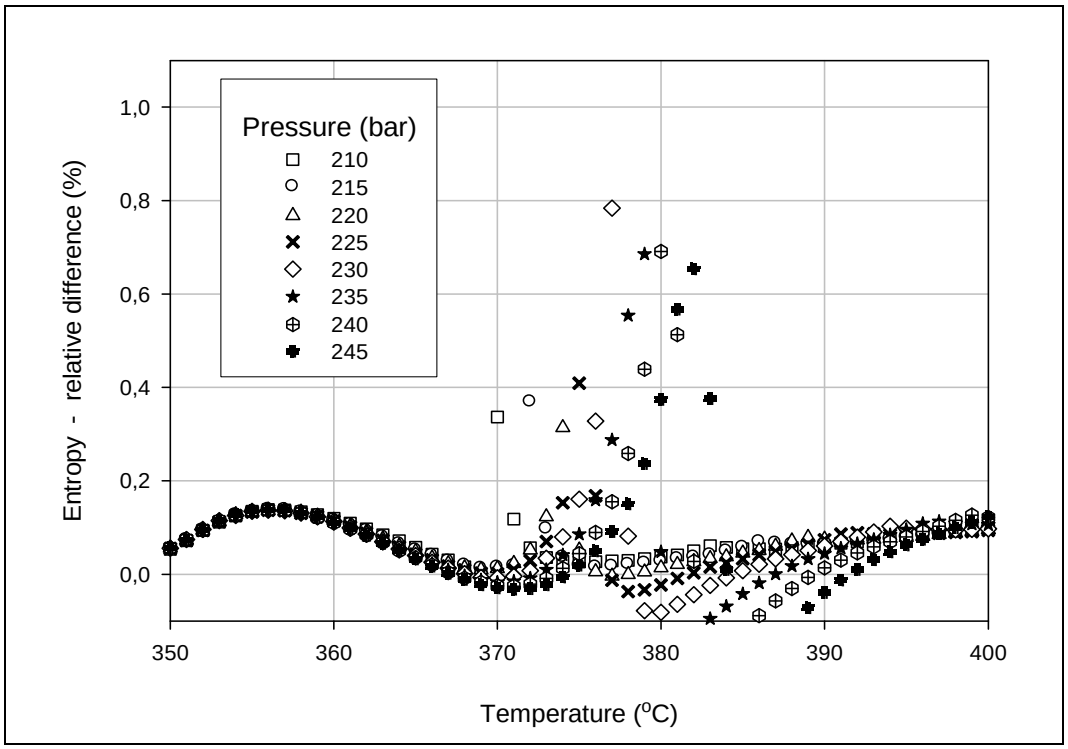

Figure 2-11: Relative entropy difference.

In general, it is observed that the X-Steam library implemented in Matlab systematically underestimates both enthalpies and entropies. However, the maximum differences of only about 1% and occurs within a limited region characterized by temperatures ranging from 375 to 385°C.

These thermodynamics properties are used by different thermal models which are implemented in the proposed plant simulation. Thus, models of different equipment and the information for each one is presented in the following sections.

2.3.2 The turbine

A turbine is a complex mechanical system formed by a series of mobile parts that permit the thermal energy of the steam to be transformed into rotational work. Most of modern systems are composed of several turbine groups that are mechanically coupled in tandem. For heat regeneration purposes, several steam extractions are usually implemented in each group [37].

Thus, a turbine can be divided into multistage groups according to steam extraction points. A simplified view of a turbine is presented in Figure 2-12. The same figure also shows the h-s diagram with the isentropic (ideal) as well as the expected real expansion of the steam along successive extraction points.

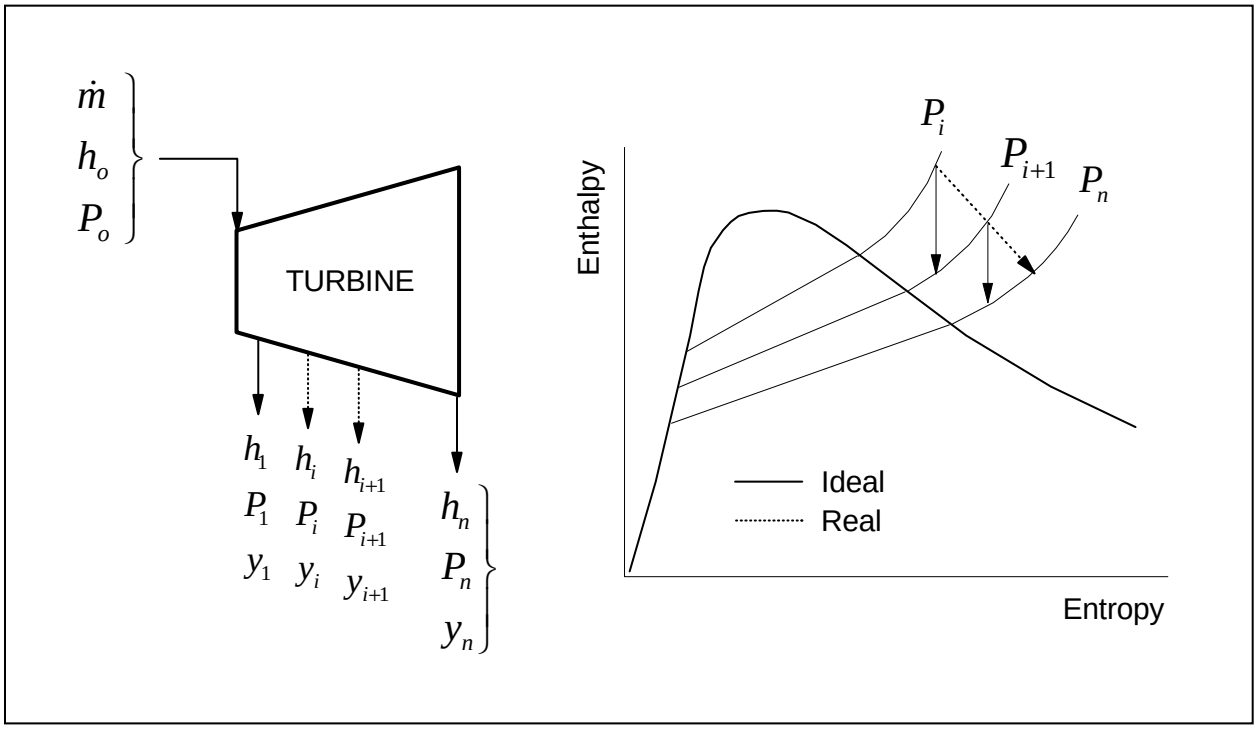

Figure 2-12: Simple modeling of multistage turbine groups.

The ideal expansion of the steam, symbolized with the solid line in the figure, is assumed as an adiabatic isentropic process. It is obvious that in real systems the entropy increases due to internal irreversibilities. The ratio of the actual work output ($h_i - h_{i+1}$) of the turbine, to the work output that would be achieved if the process was isentropic ($h_i - h_{s,i+1}$), provides the isentropic efficiency of the turbine.

$$\eta_s = \frac{h_i - h_{i+1}}{h_i - h_{s,i+1}} \tag{2-9}$$

The mechanical work produced by a turbine is expressed as a function of the enthalpies (h_i) and the fractions of steam extracted (y_i) as follows:

$$\left|\dot{W}_T\right| = \dot{m}\left[\left(h_o - h_1\right) + \sum_{i=1}^{n-1}\left(1 - \sum_{k=1}^{i} y_k\right)\left(h_i - h_{i+1}\right)\right] \tag{2-10}$$

Another important parameter to consider is the pressure drop ratio across each of turbine stages. This ratio for two successive stages should be constant for one particular turbine. This factor has not been taken into account in all simulations and thus it will be specified for each case. In the simulation tools, the pressure at the extraction is expressed by a pressure ratio (P_{ratio}) bounded between 1.3 and 2, an integer number (n_i) and the pressure at the inlet (P_0) of the turbine. Since there are more stages than extractions, so the number (n_i) allows reaching the pressure at the first, second or third stage, and so on. Therefore, the pressure at the extraction can be expressed as follows:

$$P_{ratio} \in [1.3, 2]$$

$$n_i \in \mathbb{N}$$

$$P_i = \frac{P_0}{{P_{ratio}}^{n_i}} \tag{2-11}$$

For example, if the pressure ratio of a turbine is 1.5 with the main steam pressure at the turbine inlet of 25 MPa. The extraction pressures should be taken among: 16.6 MPa, 11.11 MPa, 7.4 MPa, 4.9 MPa, 3.3 MPa, etc.

2.3.3 The condenser

The function of a condenser is to condense the steam leaving the turbine. During this process the condenser removes the latent heat of vaporization from the exhaust steam and rejects it to the environment. In general, this energy is discharged directly by using cooling water into the atmosphere [37, 38].

For all the cycles studied, it has been assumed that the condenser operates under a constant pressure which corresponds to a saturation state dictated by the temperature of the heat sink. Usually this heat reservoir can be a lake, a river or the atmosphere via the use of cooling towers. The modelling approach used for the condenser is quite simple and presented in Figure 2-13.

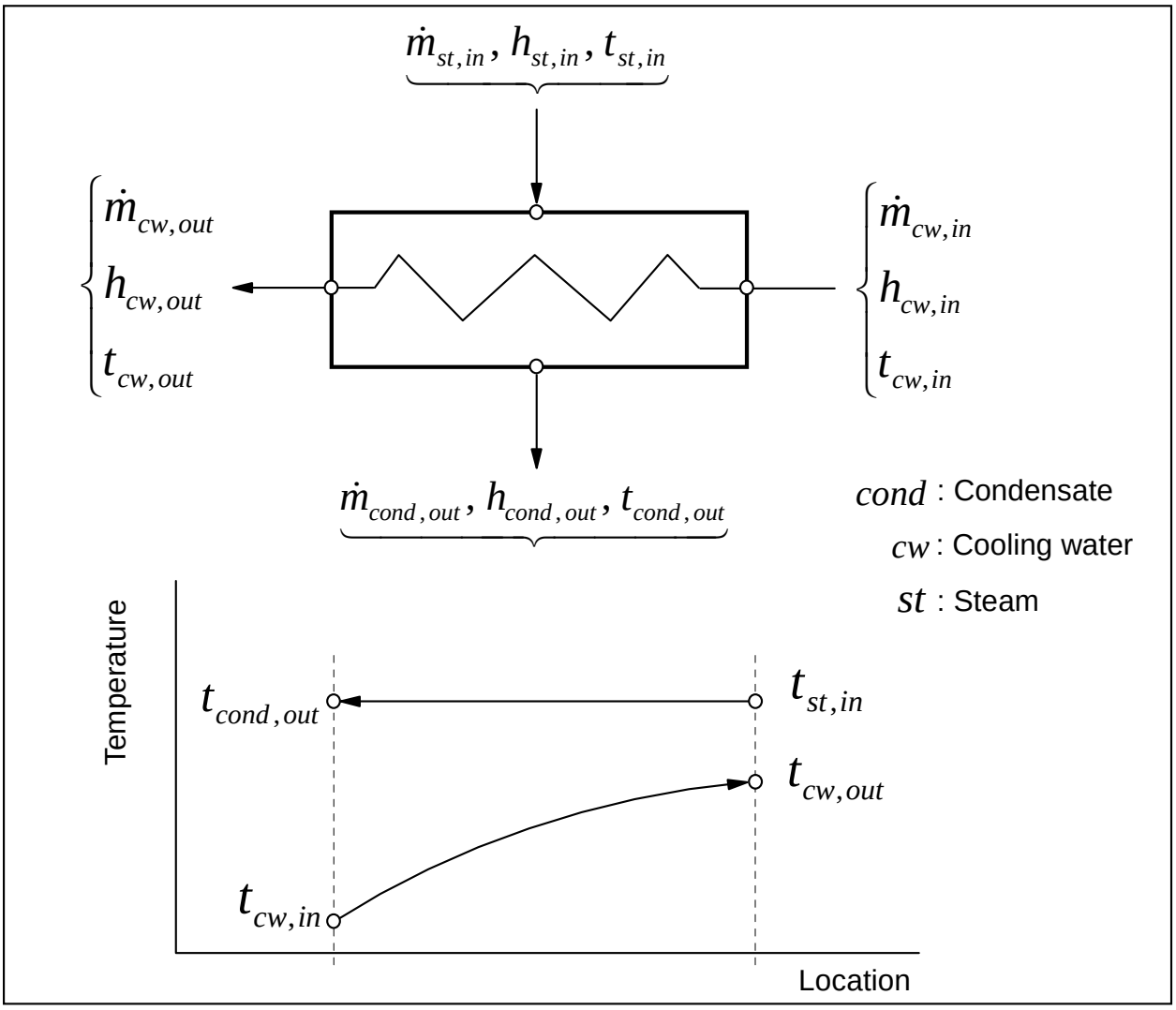

Figure 2-13: Simplified condenser model.

For each case studied, it has been assumed that the condensate leaves the condenser at a saturated liquid state. It must be pointed out that if the coolant at the outlet of the condenser is subcooled, then, overall efficiency of the plant will be reduced (Chapter 2). Following Figure 2-13, the energy balance equations are written as:

$$\dot{Q}_{cond} = \dot{m}_{st,in} h_{st,in} - \dot{m}_{cond,out}\, h_{cond,out} = \dot{m}_{cw,out}\, h_{cw,out} - \dot{m}_{cw,in}\, h_{cw,in} \quad (2\text{-}12)$$

Since $\dot{m}_{st,in} = \dot{m}_{cond,out}$ and $\dot{m}_{cw,out} = \dot{m}_{cw,in}$;

$$\dot{Q}_{cond} = \dot{m}_{st}(h_{st,in} - h_{st,out}) = \dot{m}_{cw}(h_{cw,out} - h_{cw,in}) \quad (2\text{-}13)$$

$$\dot{Q}_{cond} = \dot{m}_{cw} C_p (t_{cw,out} - t_{cw,in}) \quad (2\text{-}14)$$

where $\dot{m}_{st}$ and $\dot{m}_{cw}$ are the steam and cooling water mass flow rates respectively, and C_p is the water specific heat capacity determined at the mean cooling water temperature $= \left(\frac{t_{cw,out} + t_{cw,in}}{2} \right)$

2.3.4 Feedwater heaters

As demonstrated in Chapter 2, a considerable improvement in efficiency is obtained by reheating the feedwater before it enters into the reactor core or boiler (i.e., regeneration cycles). This process is commonly achieved by extracting a fraction of the steam from various turbine stages and by recovering the latent heat inside feedwater heat exchangers. Mainly two types of feedwater heaters are used in the power industry: direct contact (or open type) heat exchangers and tube-shell (or closed type) heat exchangers [37, 38].

In open type feedwater heaters, the extracted steam mixes with the water. They usually operate in such a way that permits both reheating the circulating fluid and extracting non-condensable gases existing in the system at the same time. This kind of process is encountered in the deaerator (see section 1.2.1). At the outlet of this kind of heaters the water is usually under the saturated liquid state. The scheme of the open feedwater heater is presented in Figure 2-14.

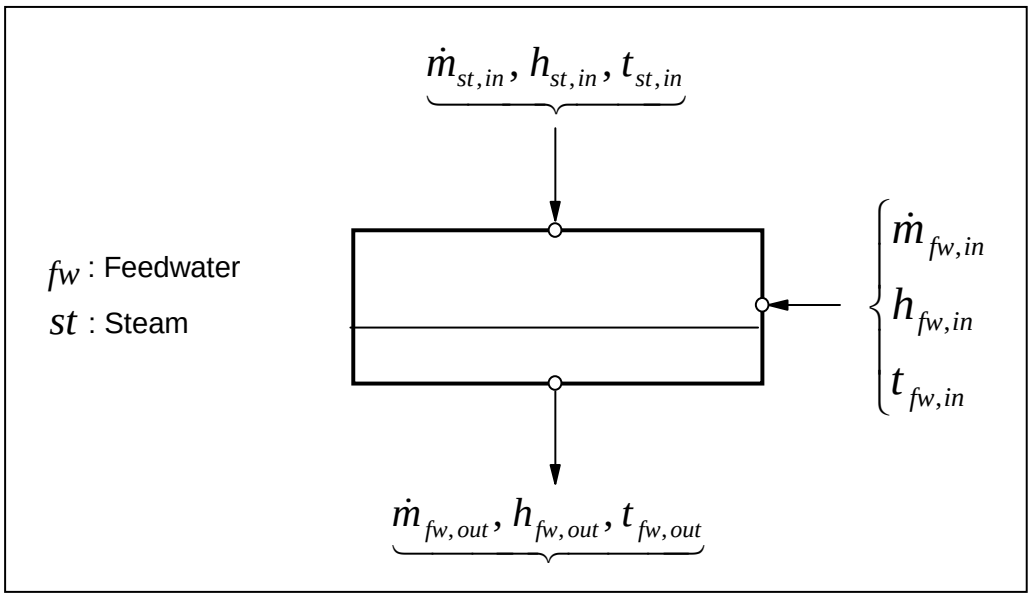

Figure 2-14: Flow diagram of an open feedwater heater.

If the partial pressure of non condensable gases is neglected, it is obvious that the simulation of this kind of heater is quite simple. It requires solving two equations (i.e., a mass balance and an energy balance) under constant pressure conditions, they are written as:

$$\dot{m}_{fw,out} = \dot{m}_{st,in} + \dot{m}_{fw,in} \tag{2-15}$$

$$\dot{m}_{fw,out}\, h_{fw,out} = \dot{m}_{st,in} h_{st,in} + \dot{m}_{fw,in} h_{fw,in} \tag{2-16}$$

As pointed out, open feedwater heaters are very useful for removing non-condensable gases. Deaeration of the condensate is based upon Dalton's and Henry's laws which express that the quantity of a gas that dissolves in a liquid decreases as the temperature of liquid rises, and if the liquid is raised to the boiling point all the dissolved gases will be liberated. Usually this process uses low pressure steam obtained from an extraction point in the steam turbine system. There are two types of deaerators: the tray-type and the spray-type as presented on Figure 2-15 and Figure 2-16, respectively. For the tray-type, a vertical domed deaeration section is mounted on top of a horizontal vessel which serves as the deaerated boiler feedwater storage tank. The spay-type consists of a horizontal cylindrical vessel for both the deaeration section and the boiler feedwater storage tank.

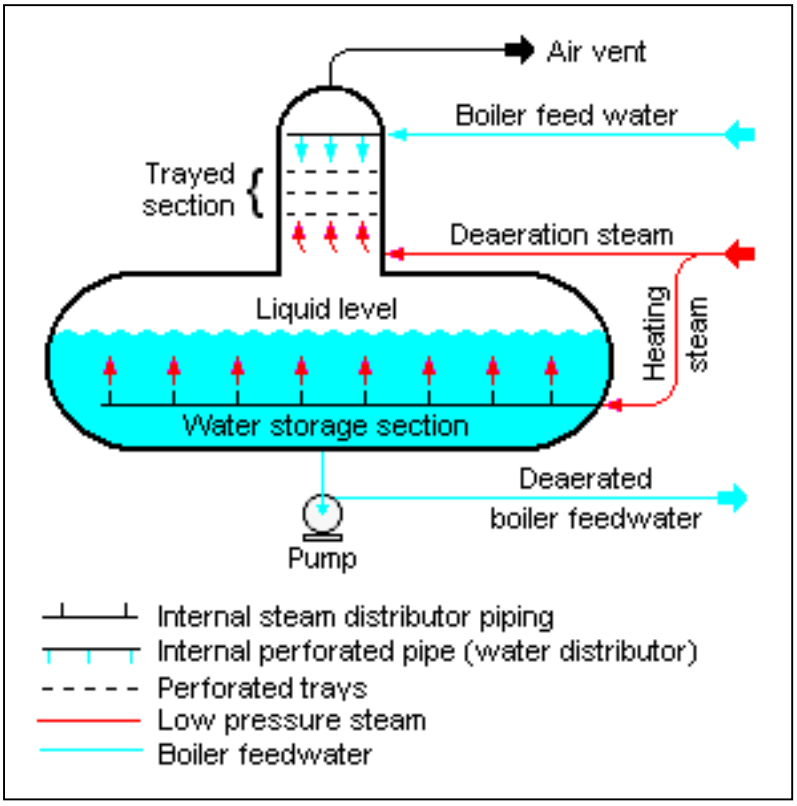

Figure 2-15: Typical tray-type deaerator [39].

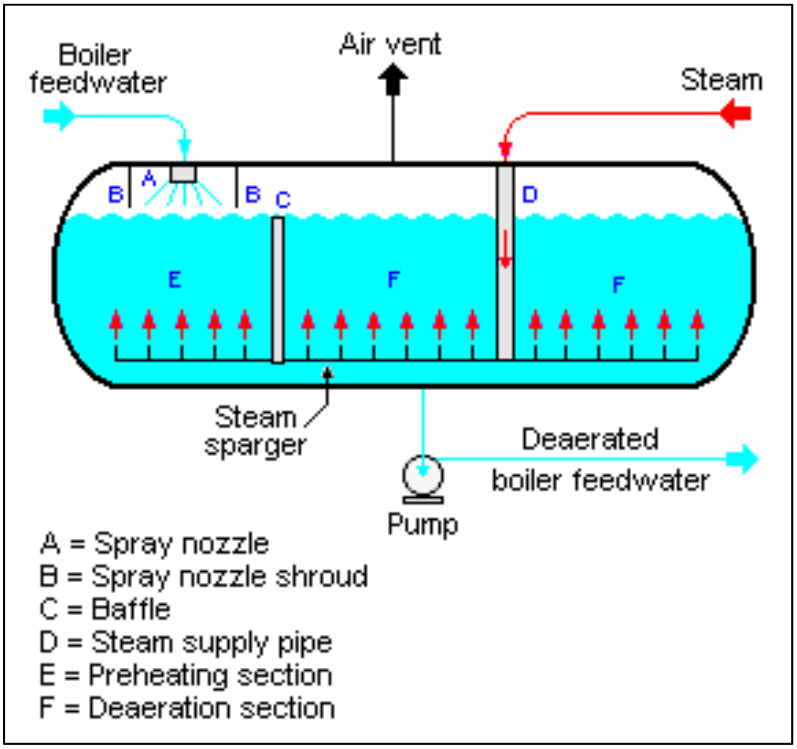

Figure 2-16: Typical spray-type deaerator [40].

In both systems an opening in the top of the heater section allows the released gasses and some steam to be vented from the heater section to the atmosphere. For this reason this unit operates under relatively low pressure conditions. To avoid pump cavitation a positive inlet pressure is achieved by placing the deaerator at the maximum height possible in the plant. The water column between this unit and the pumps assure the required NPSH (Net Positive Suction Head) for the pump.

In shell-tube type feedwater heaters, heat is transferred from the steam to the water without any direct contact between the fluids. Furthermore, since steam condenses inside the shell, the heat capacities, the temperature profiles and the heat transfer coefficients change with the process along the whole heat exchangers. To take into account different heat transfer modes encountered in these systems, they are usually arbitrary divided into different zones. Figure 2-17 shows a typical three-zone feedwater that consists of the following regions: *i*) superheating, *ii*) condensing and *iii*) drain-cooling.

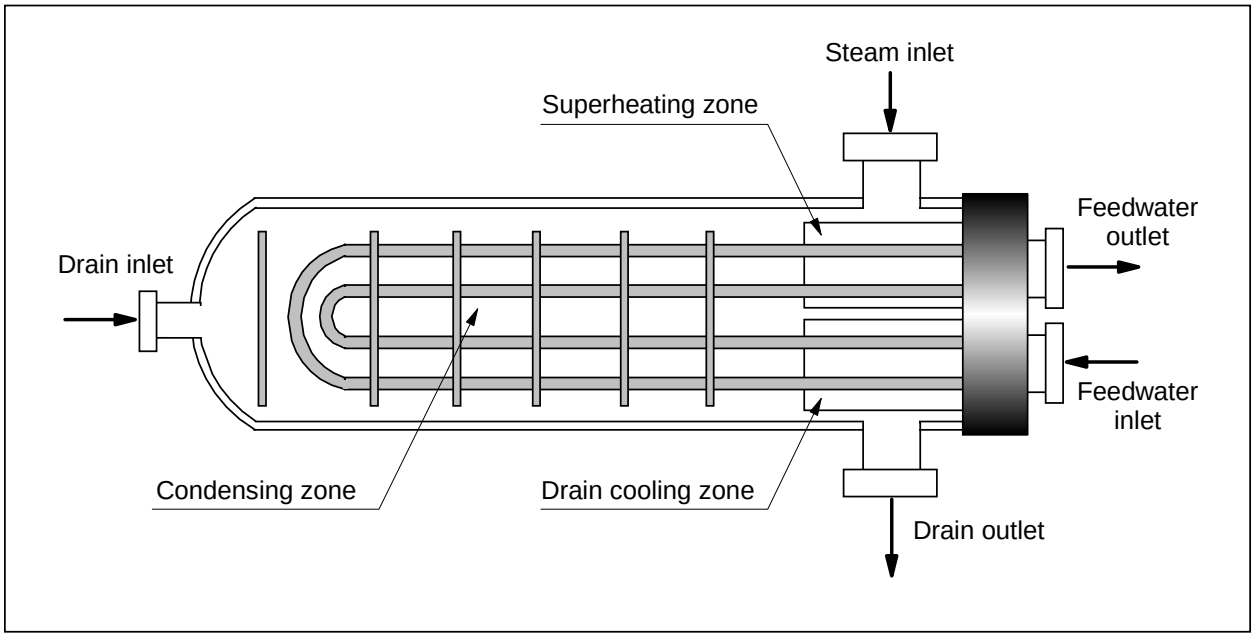

Figure 2-17: Typical three-zone feedwater heater.

In the present work neither the geometrical nor the mechanical parameters of the heat exchanger are taken into account. Therefore, the calculation scheme is relatively simple and is based on the enthalpy differences of the extracted steam and temperature differences of the feedwater. The Terminal Temperature Differences (TTD) is the difference between saturation temperature at the

operating pressure of the condensing zone and the temperature of the feedwater leaving the heater. The Drain-Cooler Approach (DCA) is the difference between the temperature of the drains leaving the heater and the temperature of the feedwater entering the heater. The TTD and DCA used in each simulation are calculated from initial plant operation conditions given in the literature [38]. Figure 2-18 shows expected temperature distributions as well as the variables used to simulate this type of feedwater heaters.

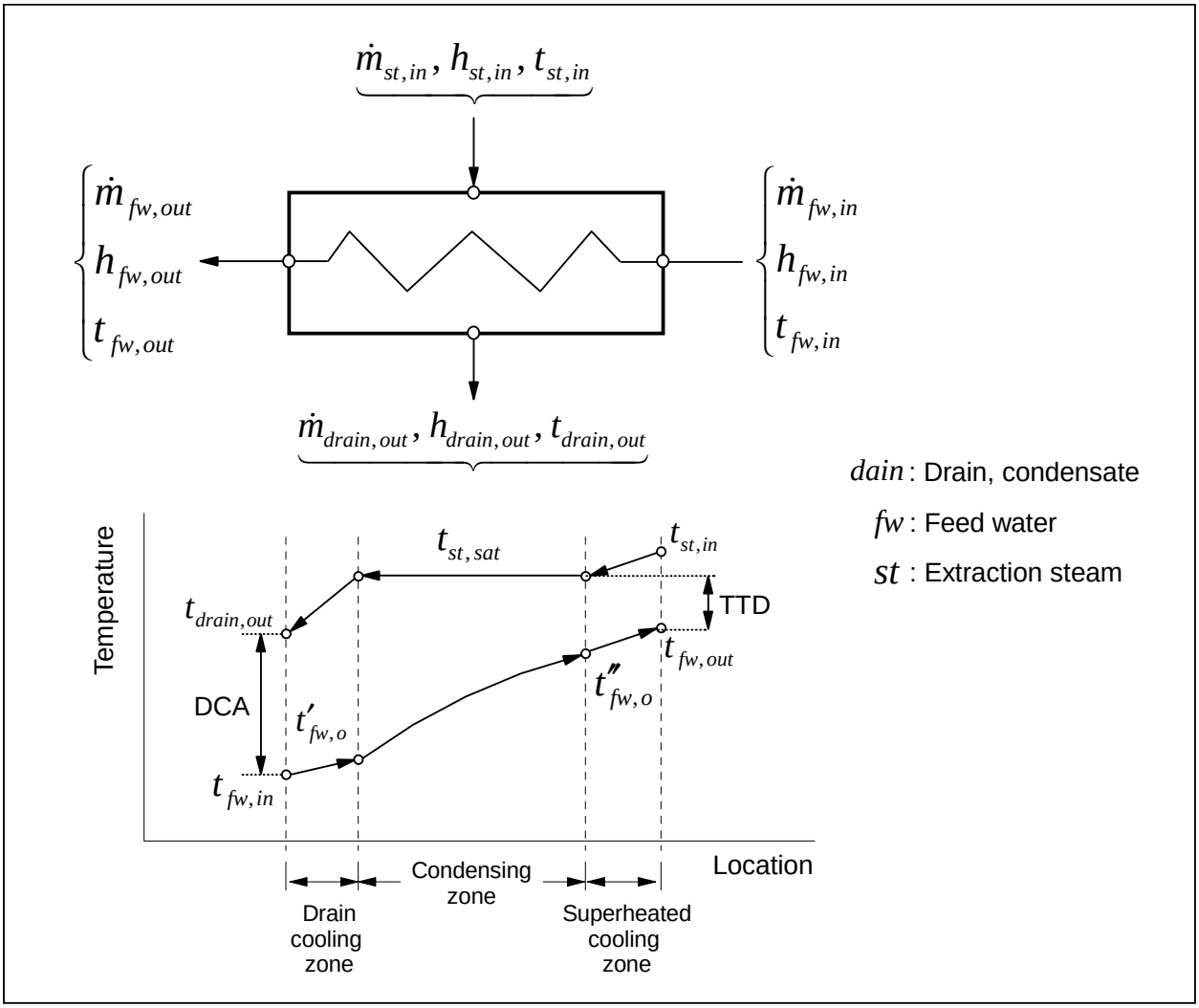

Figure 2-18: Flow diagram and temperature profiles of a three-zone feedwater heater.

Following Figure 2-18, the energy balance equations are written as:

$$\dot{m}_{fw,out}\, h_{fw,out} - \dot{m}_{fw,in} h_{fw,in} = \dot{m}_{st,in} h_{st,in} - \dot{m}_{drain,out}\, h_{drain,out} \qquad (2\text{-}17)$$

Since $\dot{m}_{st,in} = \dot{m}_{drain,out}$ and $\dot{m}_{fw,out} = \dot{m}_{fw,in}$;

$$\dot{m}_{fw,out}\,(h_{fw,out} - h_{fw,in}) = \dot{m}_{st,in}(h_{st,in} - h_{drain,out}) \quad (2\text{-}18)$$

2.3.5 Pumps

The simulation of these mechanical components is performed using the specific volume of the fluid determined at the inlet side (i.e., $\Delta h_{ideal} = v\,\Delta P$).

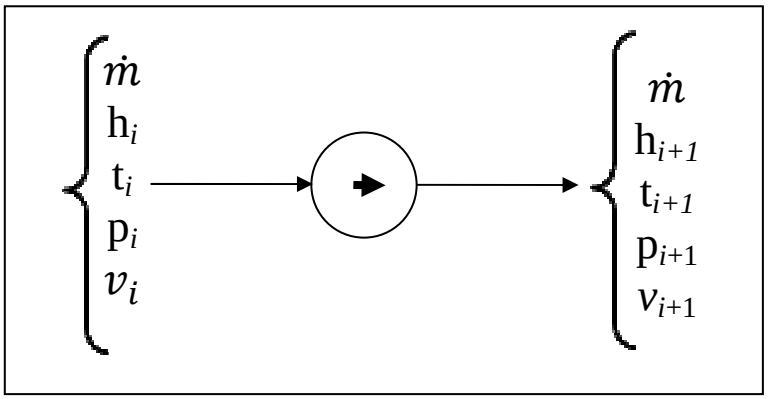

Figure 2-19: Simple modeling of pump.

In most cases of this study, the pumps are considered as isentropic components otherwise the isentropic efficiency is considered as follows:

$$\eta_s = \frac{h_i - h_{s,i+1}}{h_i - h_{i+1}} \quad (2\text{-}19)$$

Where h_s corresponds to the isentropic value of the enthalpy.

2.3.6 Pressure drops along steam extraction lines

The pressure drop along steam extraction lines are only considered in the case of Tom'Usinsk power plant presented Section 1.2.4 [17]. The reference system given in Figure 1-6, provides information about pressure losses along steam extraction lines. To take them into account, however, the simulation model may use appropriate relationships of the pressure drop as function of the mass flow rate. Thus, in this work the following proportionality is considered as suitable:

$$\Delta P = \frac{1}{2} f \frac{G^2}{\rho} \frac{L}{D} \propto \dot{m}^2 \tag{2-20}$$

The pressure loss coefficient for each line is then estimated as follows:

$$coef_{\Delta P} = \frac{\Delta P_{reference}}{\dot{m}^2_{reference}} \tag{2-21}$$

All along the plant simulation and optimization, it is assumed that this coefficient characterizes each pipe; therefore, the pressure drop caused by different flow rates than those given in the reference case [17] is calculated as:

$$\Delta P_{new} = \dot{m}^2_{new} \times coef_{\Delta P} \tag{2-22}$$

2.4 Validation of the models

For validation purposes, the original power plant of Tom'Usinsk [17] given in section 1.2.4 is simulated by including the aforementioned models. Table 2-1 presents the reference and simulated thermodynamic states at the corresponding locations shown in Figure 1-6.

It must be pointed out that the fossil-fuelled power plant has two gas cooler units (GCHP and GCLP) as well as a reheat line on the top of the heat exchanger H7. For the purpose of the present simulation, these components were represented by an external source of heat. Using the values given in the reference [17] we write:

$$\dot{Q}_{GCLP} = \dot{m}_{35}\left(h_{36} - h_{35}\right) = 9.42 \text{ MW} \tag{2-23}$$

$$\dot{Q}_{GCHP} = \dot{m}_{37}\left(h_{38} - h_{37}\right) = 17.21 \text{ MW} \tag{2-24}$$

Similar calculations performed in the reheat section shown on the top of the heat exchanger H7 resulted in an additional thermal power of 11.24 MW.

The models used for the condenser and feedwater heaters, however, require conserving simultaneously both energy and mass; therefore, an iterative calculation is implemented. Since this model also includes pressure drop along steam extractions lines which may affect local

thermodynamic states, an external iteration of the whole system of equations is also used. In all the cases a single convergence criterion of 10^{-6} is used.

In general, as shown in Table 2-1, the proposed model reproduces quite well the actual operation conditions of the power plant. The difference observed at state 16 is mainly due to the assumption that the liquid is saturated at the outlet of the heat exchanger (H1). Indeed, the enthalpy given in the reference is higher than the saturated enthalpy corresponding to the pressure at location 16. Other states shown in boldface in Table 2-1 correspond to those obtained after replacing the gas cooling units (GCHP and GCLP). Notice that these states are not included in the simulation-optimization carried out on the proposed SCWR NPPs and discussed in Chapter 4. The Table 2-1 also shows that the highest difference among calculated mass flow rates is less than 1% while for temperatures and enthalpies the highest difference is lower than 0.4%. Therefore both the thermal efficiency and the mechanical power are reproduced with acceptable accuracy. Thus, these results confirm the good performance of the plant simulator.

Table 2-1: Reference and simulated values of the fossil fuelled power plant [17].

	Reference Values					**Simulated Values**				
State #	$\dot{m}$ **(kg/s)**	T **(°C)**	P **(MPa)**	h **(kJ/kg)**	y **(%)**	$\dot{m}$ **(kg/s)**	T **(°C)**	P **(MPa)**	h **(kJ/kg)**	y **(%)**
1	475.9	600.0	30	3447.0		475.89	600.0	30	3446.9	
1'	475.9	597.0	29	3447.0		475.89	597.0	29	3446.9	
2	475.9	375.4	7.5	3079.4		475.89	375.2	7.5	3079.5	
2'	38.8	372.9	7.2	3079.4		38.70	372.8	7.2	3079.5	
3	437.1	620.0	7.3	3695.7		437.20	620.0	7.3	3695.8	
3'	437.1	619.7	7.2	3695.7		437.20	619.7	7.2	3695.8	
4	20.8	541.1	4.6	3534.5		20.80	541.3	4.6	3534.5	
4'	20.8	540.3	4.4	3534.5		20.80	540.5	4.4	3534.5	
5	29.1	457.9	2.7	3366.2		29.10	457.8	2.7	3366.2	
5'	29.1	457.2	2.6	3366.2		29.10	457.3	2.6	3366.2	
6	51.1	330.2	1.1	3113.7		51.10	330.1	1.1	3113.7	
6'	19.6	329.3	1.0	3113.7		19.60	329.1	1.0	3113.7	
6"	31.5	328.8	0.97	3113.7		31.50	328.8	0.97	3113.7	
7	9.1	235.3	0.5	2930.3		9.10	235.2	0.5	2930.3	
7'	9.1	234.7	0.471	2930.3		9.10	234.7	0.471	2930.3	
8	18.2	191.9	0.333	2847.4		18.30	191.8	0.333	2847.4	
8'	18.2	191.3	0.314	2847.4		18.30	191.4	0.314	2847.4	
9	308.8	191.6	0.32	2847.4		308.70	191.5	0.32	2847.4	
10	13.4	NA	0.104	2655.7	0.93	13.50	100.7	0.104	2655.7	0.93

Table 2-1. Continue

10'	13.4	NA	0.097	2655.7	0.79	13.50	98.7	0.097	2655.7	0.79
11	13.6	NA	0.043	2530.9	4.68	13.50	77.6	0.043	2530.9	4.67
11'	13.6	NA	0.04	2530.9	4.56	13.50	75.9	0.04	2530.9	4.54
12	17.3	NA	0.018	2422.9	7.67	17.30	57.8	0.018	2422.9	7.71
12'	17.3	NA	0.0167	2422.9	7.55	17.30	56.2	0.0167	2422.9	7.58
13	264.4	NA	0.003	2267.6	11.35	264.40	24.1	0.003	2267.6	11.35
14	313.2	24.1	0.003	100.9		313.30	24.1	0.003	101.0	
15	313.2	24.1	0.49	101.7		313.30	24.1	0.49	101.5	
16	**313.2**	**53**	**0.39**	**222.3**		**313.30**	**52.9**	**0.39**	**221.9**	
17	326.9	76.1	0.04	318.6		326.80	75.9	0.04	317.7	
18	367.6	98.8	0.097	414.1		367.80	98.7	0.097	413.8	
19	367.6	99	1.37	415.7		367.80	98.8	1.37	415.1	
20	321.8	131.9	1.27	555.2		321.90	131.9	1.27	555.0	
21	367.6	147.4	1.18	621.3		367.80	147.4	1.18	621.4	
22	475.9	180.3	1.01	764.5		475.90	180.3	1.01	764.6	
23	475.9	187.1	34.3	811.8		475.90	187.2	34.3	811.9	
24	440.8	231.6	34.0	1006.1		440.80	231.6	34.0	1006.3	
25	440.8	NA	33.7	1107.4		440.80	254.1	33.7	1107.7	
26	440.8	289.8	33.3	1277		440.80	289.8	33.3	1276.6	
27	**475.9**	**295**	**33.2**	**1302.5**		**475.90**	**294.9**	**33.2**	**1302.2**	
28	17.3	56	0.017	234.5		17.30	56.2	0.017	235.3	
29	27.4	109	0.31	457.2		27.40	108.8	0.31	456.5	
30	9.1	141.9	0.47	597.5		9.10	141.9	0.47	597.3	
31	88.7	197.1	2.6	839.9		88.60	197.2	2.6	840.3	
32	59.6	241.6	4.4	1045.4		59.50	241.6	4.4	1045.5	
33	38.8	264	7.2	1154.3		38.70	264.1	7.2	1154.6	
34	31.5	NA	0.006	2405.3		31.50	36.2	0.006	2405.3	
35	**45.8**	**99**	**1.37**	**415.7**		**45.80**	**98.8**	**1.37**	**415.1**	
36	**45.8**	**147.4**	**1.18**	**621.3**		**45.80**	**147.4**	**1.18**	**621.5**	
37	**35.1**	**187.1**	**34.3**	**811.8**		**35.10**	**187.2**	**34.3**	**811.9**	
38	**35.1**	**295**	**33.2**	**1302.5**		**35.10**	**294.9**	**33.2**	**1302.1**	

The work presented in this chapter permitted us to validate the thermodynamic modelling approach of a supercritical-boiler power plant. Thus, the same model will then be used in conjunction of an optimization technique based on the use of genetic algorithm. Before performing the optimization of the power plant, the optimization method is discussed in detail in the following chapter.

CHAPTER 3 THE OPTIMIZATION METHOD

Improving both thermal efficiency and mechanical power output constitute a multi-objective optimization problem. It is obvious that these two objectives are in competition and cannot be satisfied by a unique choice of decision variables. Thus, trade-offs between thermal efficiency and mechanical power output must be determined. To this aim, an efficient and robust evolutionary algorithm, based on genetic algorithm, is used and coupled to the power plant thermodynamic simulation model presented in the last chapter in order to determine a set of Pareto solutions.

3.1 Optimization of thermal power plants: Review

In the thermal design, the optimization of a single isolated component is not necessarily important due to its interaction with several other systems that can affect its operation conditions. In power plants, in particular, any change of a given thermodynamics states can bring about important modification of the entire cycle. Therefore, single-component optimization may be considered during the preliminary phase of optimization but has only a limited interest. For these reasons, the optimization of the overall power plant is the main goal in the thermal design [41].

A typical class of thermal system optimization is the heat exchangers network. One of the most effective and easy technique to perform the optimization of heat exchanger network is the use of the pinch analysis method. This method is largely discussed in the literature [42-44]. It uses composite curves [45, 46], which characterise the hot and cold streams of the global network. When these two curves are plotted on the temperature-enthalpy difference diagram, the pinch temperature of the whole process can be determined. Thus, the pinch method consists of determining the location of the minimum temperature difference between the two composite curves. The principal goal of this method consists of rearranging and/or modifying a topology of a system by the use of composite curves in order to improve the thermal efficiency. The pinch method for the design of heat exchanger network has, however, some limitations [41]. For instance, the effect of the pressure drop along the heat exchangers and flow lines are neglected, it also requires the previous knowledge of the mass flow rates, the average specific heats, the inlet and the outlet temperatures of each stream. They are usually decision variables and they are unknown during the design process. Furthermore, the pinch analysis might not detect some

opportunities to improve the overall design of the system. Thus, an exergy analysis should be considered as a complementary and powerful tool for the design and the optimization of thermal systems [41].

Mathematical methods have been developed for optimization to deal with different class of problems. The robustness and performance of these methods depend on the nature of the objective functions, the constraints and the number of decision variables. The case with functions of a single variable is the most elementary type. The methods used for this optimization are among other: the graphical methods, the indirect method, which includes Newton's method, the finite difference approximation of Newton's method and the secant method. Direct methods include: the two-point equal interval search, the method of bisecting, the Fibonacci method and the golden section method. Another type of optimization is the unconstrained multivariable optimization technique. Among direct methods we can cite: the random search, the grid search, the univariate search, the sequential simplex method, the hook-Jeeves pattern search method, and Powell's conjugate direction method. Indirect methods, which are more efficient and robust than direct ones, include: the steepest-descent/ascent gradient, the conjugate gradient, Marquardt's method and the Broyden-Fletcher-Gold-farb-Shanno method [41].

The optimization procedures applied to a problem in which both the objective function and constraints are linear bring about the technique known as linear programming. Some linear programming software, for problems involving more than two variables, are: linear programming simplex method, the revised simplex method and the Karmarka algorithm.

Problems with a nonlinear objective function and/or constraints are the most common type of problems encountered in thermal design optimization. The approaches for this kind of problem are: Lagrange multiplier method, iterative quadratic programming, iterative linearization, penalty function and direct-search methods.

3.2 Description of a multi-objective problem

A multi-objective optimization of power plants may contain several objective functions that must be satisfied simultaneously [47]. In this work, the objective functions are the thermal efficiency and the mechanical power of the plant which are two competitive functions. As shown in Figure 3-1, when the mass flow rate at the extraction point increases, the thermal efficiency increases at

the cost of decreasing the mechanical power. Therefore, some trade-offs between these two functions are required to achieve an optimal design of the system.

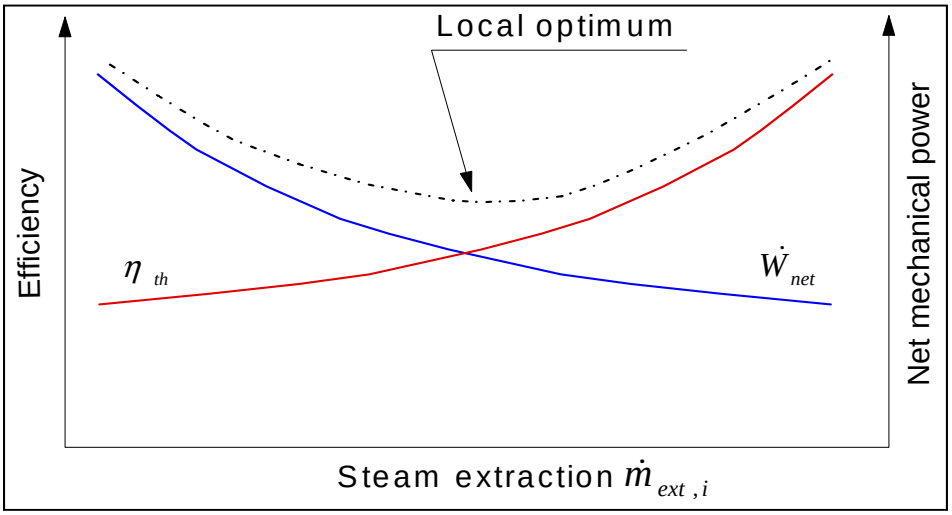

Figure 3-1: Multi-objective problem.

Thus, a general formulation of a multi-objective optimization problem having *n* objective functions and *m* decision variables can be summarized (e.g., for a minimization case) as follows:

$$\text{Minimize} \quad f_i(X) \qquad i = 1,2,...,n$$

$$\text{Subjected to the constraints: } g_j(X) \geq 0 \qquad j = 1,2,...,p$$

Where $X = (x_1, x_2, ..., x_n)$ is a vector, while $g_j(X)$ is a component of vector having p constraints. In general, there is no a single combination of decision variables x_n which is able to simultaneously minimize all components of the vector $f_i(X)$. Therefore, the optimization will be represented by a set of trade-off solutions. To determine if a solution is in fact one of the best possible trade-offs, the "Pareto optimality" concept is used [48, 49]. It permits the establishment of a hierarchy among all solutions of a multi-objective optimization problem. Thus, the best solutions of the set are called "Pareto solutions" and they can be determined using multi-objective evolutionary algorithms [50, 51]. To perform the present work, an efficient and robust evolutionary algorithm called "BEST" (Boundary Exploration Searching Technique) [52] is used and presented in the following section. The proposed algorithm allows a fast convergence and ensures a diversity of solutions. Moreover, this method overcomes difficulties associated with complex Pareto front landscapes such as: discontinuity, disjunction, etc.

3.3 Presentation of the algorithm “BEST”

This algorithm has been developed at the Institute of Nuclear Energy in collaboration with Natural Resources Canada (CANMET Energy Technology Centre-Varennes) by Jean Dipama and co-workers [52]. Unlike classical evolutionary algorithms that promote non-dominated solutions at each generation, the present approach consists of emphasizing dominated and non-dominated solutions to drive the searching process towards the boundaries of the feasible region. To fulfill this requirement, a “C*orridor Header Evolution Tracking*” strategy is successfully implemented and used to treat the power systems and any systems independently of its complexity [14, 53], see Figure 3-2. Solutions inside these corridors become parents for reproducing offspring in the next generation of a genetic algorithm [54, 55]. Thus, an evolution process is applied to captured individuals that then undergo both crossover and mutation operations. The structure of the optimization algorithm is shown in Figure 3-3. In order to increase spreading of individuals and thus to fix the boundary of the feasible region more quickly, the probability of mutations is initially quite high (70% to 80%). Moreover, there is no special mechanism for the maintenance of the diversity because the corridor strategy implicitly fulfills this task [56]. In addition, the exploration of a promising area (i.e., the contour of the feasible region) is achieved by using a crossover operator whose probability increases adaptively as mutations decrease.

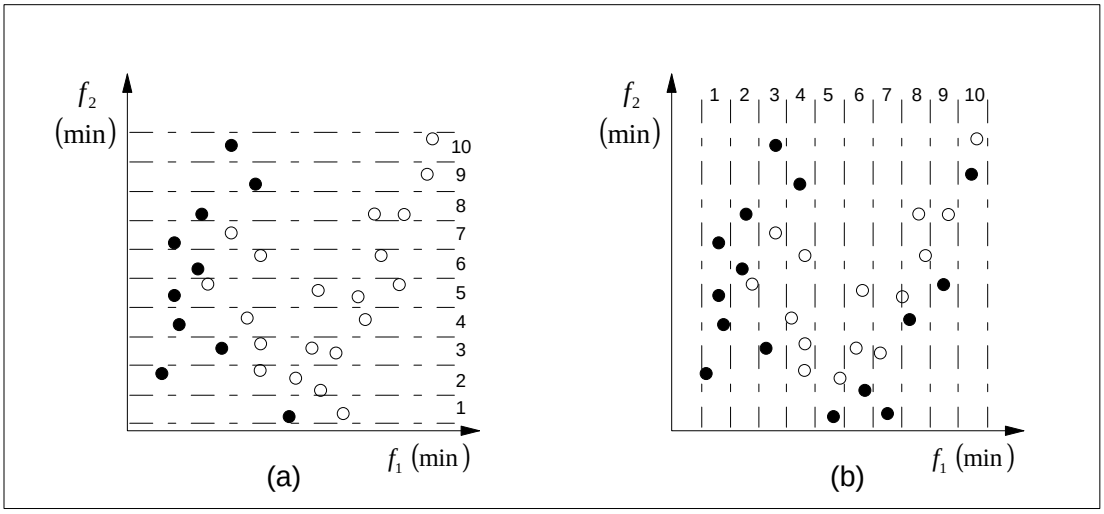

Figure 3-2: Best solutions inside corridors: (a) minimization of f1, (b) minimization of f2.

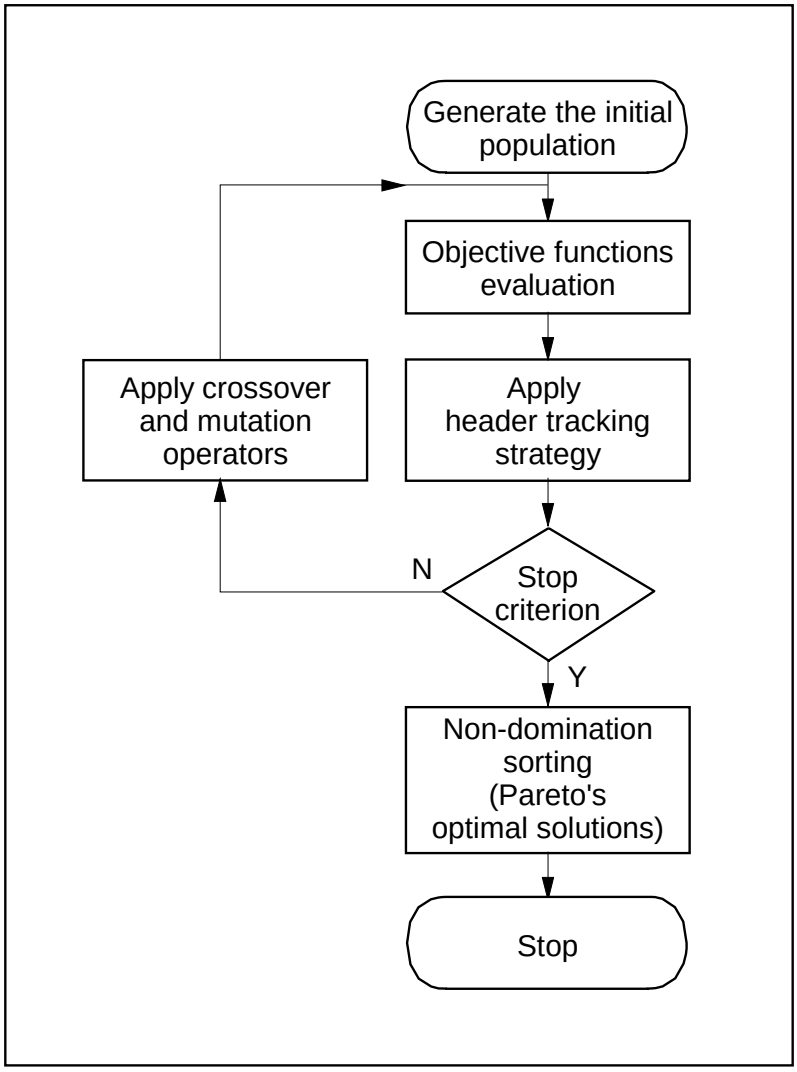

Figure 3-3: Flow sheet of the proposed algorithm.

The metric used to control mutations and crossovers is established by following the progression of the boundary formed by individuals in the corridors; this metric is calculated with the following equation:

$$d = \sum_{j=1}^{N} \left[\frac{1}{C} \sqrt{\sum_{i=1}^{C} \left(\frac{f_{j,i}^{t} - f_{j,i}^{t-1}}{f_{\max} - f_{\min}} \right)^2} \right] \tag{3-1}$$

In this equation, $f_{j,i}^{t}$ represents the evaluation of objective j of an individual inside the corridor i at generation t; $f_{\min}$ and $f_{\max}$ are the lower and upper bounds of the objective j; N is the number of objectives and C is the number of corridors.

The value obtained from Equation (3-1) is then used to determine a "*control*" parameter calculated as: $control = \ln(d)$. After multiple trials, a triggering between operations was established based on this parameter and the best values are suggested in Table 3-1. The solution searching process is based on the strategy given in Herrera *et al.* [57]. The probabilities used for each operator during the present work are summarized in Table 3-2. As the population converges towards the contour of the feasible region, it is apparent that parameter d decreases, which allows a convenient limit at which the algorithm stops the searching process, to be introduced. Finally, a non-domination sorting procedure is executed to determine Pareto's optimal solutions.

Table 3-1: Suggested values for the *control* parameter.

Trigger or action	***control* parameter**
Exploration triggering	$control \geq -8$
Hybrid triggering	$-12 \leq control \leq -8$
Exploitation triggering	$-18 \leq control \leq -12$
Stop process	$control \leq -18$

Table 3-2: Summary of searching process operators.

Searching phase	**Operator**	**Probability (%)**	**Type**
Exploration	Mutation	90	Random
	Crossover	10	Uniform
Hybrid	Mutation	10	Probabilistic
	Crossover	90	Simulated binary
Exploitation	Mutation	10	Probabilistic
	Crossover	90	Arithmetic

To handle thermodynamic power-cycles, the optimization technique should be coupled with an appropriate power plant thermodynamic model discussed earlier. Figure 3-4 represents the framework implemented to perform both plant simulations and optimization.

The strategy is composed of the optimizer and the power plant simulator based on a specific plant thermodynamic model. The two modules communicate to each other by exchanging data from two blocks. To this aim, a “Dynamic Data Exchange” (DDE*) protocol running under the Windows XP environment is implemented. The first block converts the data into physical variables that are sent to the simulator, while the second one evaluates objectives and constraints imposed to the problem by using the results from the simulations. The optimizer generates an initial random population of solutions or individuals. They are then used by the plant simulation module to evaluate thermodynamic states that are invoked to calculate objectives and constraints required to run the optimizer. Based on the fitness of the individuals, the best ones are selected to pass crossover and mutation operators and thus, to reproduce a new population that should be more efficient than the initial one. This new population seeds the simulator and the process continues until a convenient stop criterion is reached.

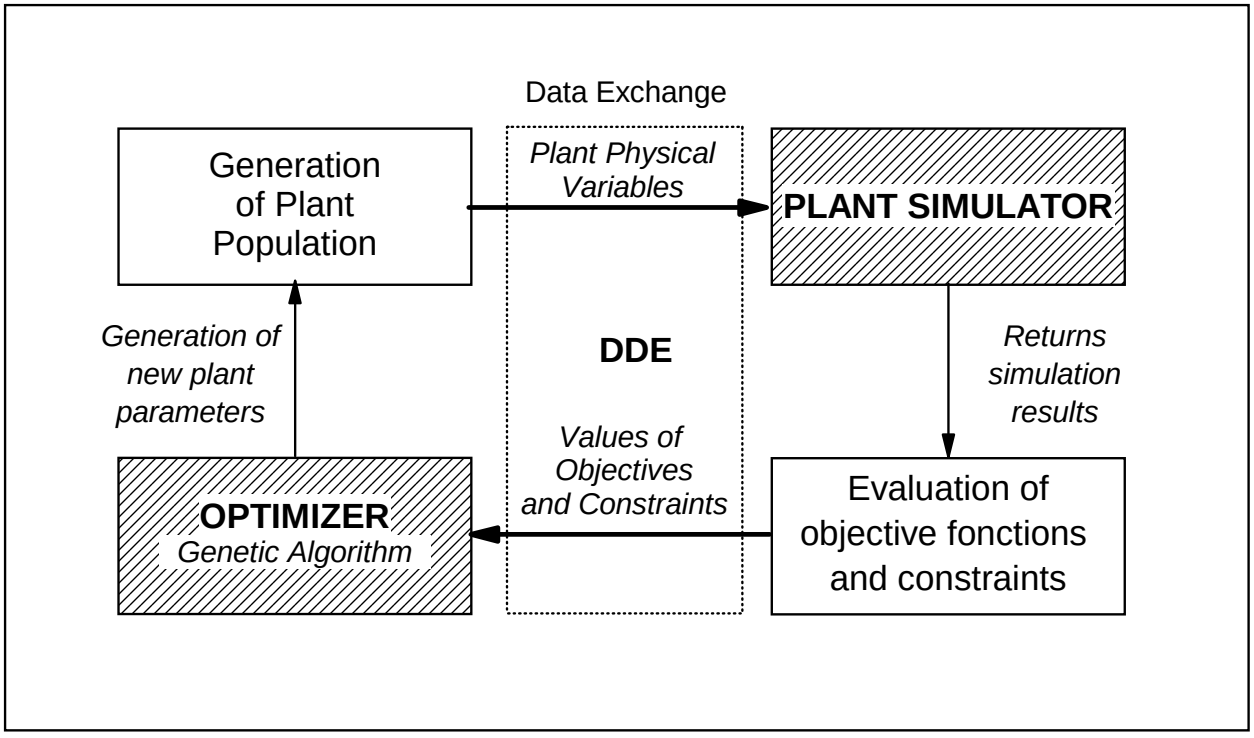

Figure 3-4: Optimization procedure framework.

* Trademark of Microsoft

The proposed methodology has been largely validated. In fact, the same optimization scheme has been used in conjunction with appropriate models to optimize cogeneration and advanced steam power plants [14, 52, 56]. In addition, a thermodynamic model quite similar to that used in this work was also applied to simulate the Gentilly-2 nuclear power plant [15]. These calculations, which include models for major thermal equipment, were able to reproduce very closely actual operation conditions of the nuclear power station.

3.4 Validation of the optimizer against a pinch and exergy analysis method

The optimization procedure has been applied on a real steam power plant given in Sefei *et al.*[58] and schematically shown in Figure 3-5. The system is mainly composed of a boiler, a reheater, high-, intermediate- and low-pressure turbine groups, the condenser, feedwater pumps, eight water pre-heaters and a deaerator unit. This power plant has an output of 368 MW with a thermal efficiency of 46.29%. These authors applied the method of pinch and exergy analysis to optimize this thermodynamic cycle and they obtained a thermal efficiency of 46.7%.

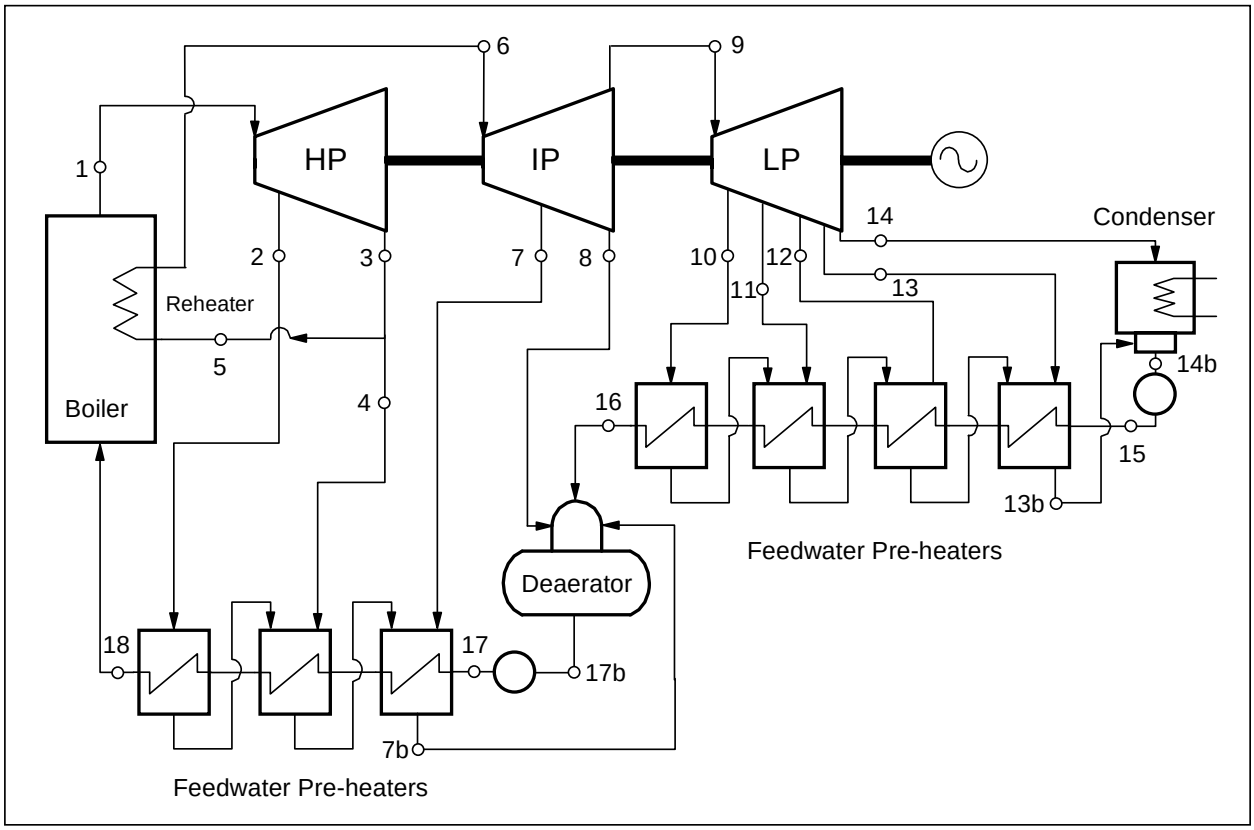

Figure 3-5: Advanced steam power plant [58].

This power plant is optimized using the optimization-simulation methodology described in this chapter. The first step consists of validating the proposed model by comparing its results with those given in reference [58]. The proposed model reproduces quite satisfactorily the actual state of the power plant as shown in Table 3-3 (errors equal to zero in the table means that they are lower than 10E-12).

Table 3-3: Comparison of present simulation with actual power plant conditions.

State #	**Actual power plant state**			**Present Matlab model**	
	$\dot{m}$ **(kg/s)**	**P(MPa)**	**T(°C)**	**T(°C)**	**Relative error (%)**
1	315.1	17.8	538	538	0
2	25.1	6.9	397.7	397.7	0
3	290	3.94	323.2	323.2	0
4	30.3	3.94	323.2	323.2	0
5	259.7	3.94	323.2	323.3	0
6	259.7	3.55	538	538	0
7	12.66	1.51	415.9	415.9	0
8	11.53	0.733	324.3	324.3	0
9	235.51	0.733	324.3	324.3	0
10	10.33	0.363	244.7	244.7	0
11	10.1	0.164	165.2	165.2	5.45E-05
12	9.2	0.064	87.62	87.63	1.28E-04
13	8.65	0.022	62.17	62.13	5.10E-04
14	197.23	0.0051	33.1	33.07	9.00E-02
15	235.51	1.031	33.15	32.27	2.66E-02
16	235.51	0.671	132.96	132.6	2.72E-03
17	315.1	20	166.94	166.99	3.23E-04
18	315.1	19.67	280.47	280.22	9.02E-04
$\dot{Q}_{in}$ (MW)		809.37		811.03	2.06 E-03
$\dot{Q}_{out}$ (MW)		434.65		436.12	3.38 E-03
η_{th} (%)		46.29		46.23	1.30 E-03

To perform the optimization, the algorithm is initiated with 60 corridors along each objective functions and the size of the initial population was 250. In all simulations, the program stops after reaching 200 iterations. Information about optimization process such as: decision variables, their

upper and lower bounds as well as the constraints imposed during the optimization of the power plant are summarized in Table 3-4. The objective functions of this problem are the maximization of both the efficiency and the net work output of the plant, given by:

$$\eta_{th} = 1 - \frac{\dot{Q}_{out}}{\dot{Q}_{in}} \text{ and } \dot{W} = \dot{W}_{turbine} - \dot{W}_{pumps} \quad (3\text{-}2)$$

Where $\dot{Q}_{out}$ and $\dot{Q}_{in}$ are the thermal power rejected at the condenser and the total thermal power consumed by the plant, respectively. Further, the mechanical power $\dot{W}_{turbine}$ takes into account high pressure (HP), intermediate pressure (IP) and low pressure (LP) turbine groups running in tandem.

Table 3-4: Advanced power plant decision variables and constraints.

Decision variables	**Lower bound**	**Upper bound**
Steam extractions (kg/s)		
$\dot{m}_2$	19.14	31.90
$\dot{m}_4$	23.11	38.51
$\dot{m}_7$	9.65	16.10
$\dot{m}_8$	8.79	14.65
$\dot{m}_{10}$	7.88	13.13
$\dot{m}_{11}$	7.70	12.84
$\dot{m}_{12}$	7.016	11.69
$\dot{m}_{13}$	6.60	10.99
Constraints		
$\frac{\sum_i \dot{m}_i}{\dot{m}}$	≤ 0.6	
Steam quality		
x_{14b}	0	
x_{17b}	0	
Coolant temperature ($°C$)		
t_{13b}	$t_{13b} = t_{15} + 5$	
$t_{7b} - t_{17}$	$3.5 \leq t_{7b} - t_{17} \leq 6.5$	
$t_{sat\ 10} - t_{16}$	$t_{sat\ 10} - t_{16} \geq 0$	

The Pareto's front obtained during the optimization process is presented in Figure 3-6. The values shown in this figure correspond to the overall thermodynamic cycle efficiency versus the net output mechanical power. The optimized plant conditions given in the reference [58] are also shown in Figure 3-6.

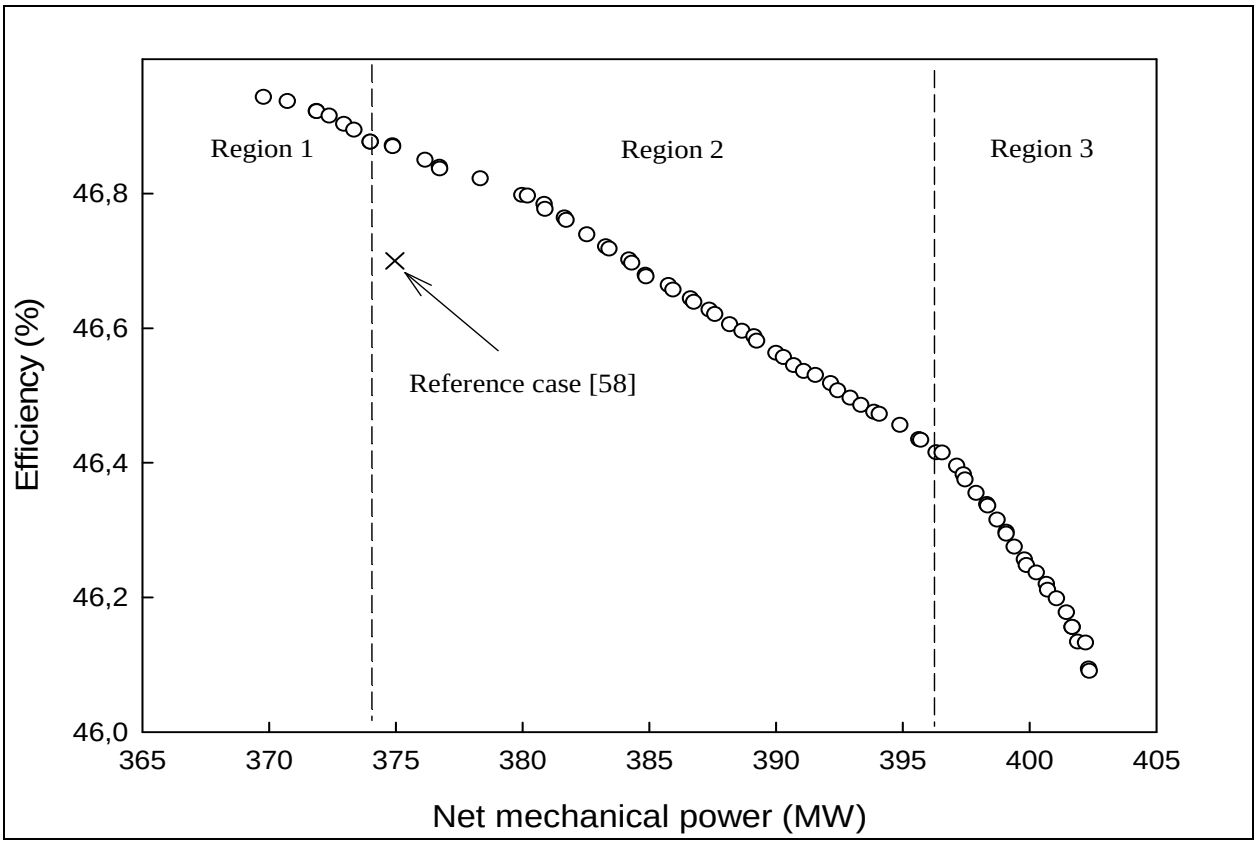

Figure 3-6: Best trade-off power plant solutions – Pareto's front.

This figure clearly shows that it is still possible to increase the thermal efficiency by about 0.2 point of percentage by selecting the best combination of steam extraction values. A comparison between the optimized values of steam extractions given in reference [58] with those obtained by the present method, for a Pareto's point close enough to the reference case, is shown in Table 3-5. Furthermore, Pareto's front shown in Figure 3-6 can be subdivided into almost three distinct regions. From detailed analyses of the data, we have observed that for efficiencies higher than 46.9 %, the front is almost controlled by extraction 2 (see Figure 3-5), where the efficiency decreases and mechanical power increases with decreasing mass flow rate. The region 2, which corresponds to power plant efficiencies lower than 46.8 % and higher than 46.4 %, the

optimization seems to be controlled by extraction 12 where the plant efficiency decreases and the net work increases with increasing extraction mass flow rate. In addition, Pareto's front shows a sharp knee change at about 46.4 % of plant efficiency where it appears to be controlled by extraction 7. In this region, the efficiency decreases and the work increases with decreasing extraction mass flow rate.

Table 3-5: Comparison of closer Pareto point with optimal reference case.

Steam extractions (kg/s)	**Reference case**	**Present work (closer Pareto's point)**
$\dot{m}_2$	25.884	23.448
$\dot{m}_4$	32.881	38.498
$\dot{m}_7$	15.852	16.090
$\dot{m}_8$	11.366	9.311
$\dot{m}_{10}$	11.156	7.886
$\dot{m}_{11}$	10.202	8.205
$\dot{m}_{12}$	9.882	8.204
$\dot{m}_{13}$	9.771	7.590
Thermal power (MW)	$\dot{Q}_{in}$ 802.7 $\dot{Q}_{out}$ 427.7	$\dot{Q}_{in}$ 799.9 $\dot{Q}_{out}$ 425.0
Efficiency (%)	46.7	46.9

It is important to note that while performing these analyses, even though the rest of the extractions randomly change during the optimization procedure, they do not show any correlation with a particular landscape of Pareto's front.

In general the steam extractions predicted with the present method are quite similar to those given in the reference and the efficiencies are also quite close. However, applying the present methodology allows the determination of a much larger range of optimum operation conditions of the power plant. Thus, the Pareto's Landscape can permit decision makers to modify the actual operation conditions of the plant accordingly to other external constraints, i.e., fuel costs vs. energy demand, etc.

In fact, for a substantial reduction in thecost, it would be more convenient to operate the plant under conditions that permit a higher efficiency even if the total generated power is significantly reduced. The fact that each region of Pareto's front seems to be controlled by only few decision variables makes it easier to better operate the power plant.

In this chapter we have validated the optimization-simulation methodology by comparing our results with those obtained by using other techniques. Thus, we have demonstrated the robustness of the proposed algorithm, its stability and capacity of handling quite complex conventional power plants. In the following chapter, the same methodology is used to simulate and optimize supercritical water-cooled nuclear power plants.

CHAPTER 4 OPTIMIZATION OF SCW NUCLEAR POWER PLANTS

Once the plant modelling and the optimization strategy are validated against available power plant data, they are applied to perform the optimization of the thermodynamic cycles presented in Chapter 1. Thus, this chapter presents, in detail, each case with the decision variables and constraints used to run the algorithm as well as the interpretation of the Pareto's front.

4.1 Optimization of the SCW NPP simplified thermodynamic cycles

All optimizations are carried out by running the algorithm under the conditions given in the previous sections and schematized in Figure 3-3 and Figure 3-4. Thus, a constant population of individuals (=200), with the same number of generation (=100) and corridors (=60) are used. Previous trials have shown that these values are not very critical, thus they are arbitrarily selected. It is obvious, however, that the computation time increases by increasing any of these quantities. Furthermore, the initial population of 200 solutions (i.e. number of individuals) required to run the genetic algorithm is generated by the thermodynamic model, where key thermodynamic variables (control parameters) are randomly changed. Depending on the type of cycle, these variables can be different. For instance for the simplest case shown in Figure 1-2 (a), only the pressures at states 5 and 6 are considered. Instead, for the complex case of Figure 1-3 (b) both pressures and extractions constitute the control variables of the problem.

In addition, the optimization must simultaneously satisfy the objectives, which are again the thermal efficiency and the mechanical power, as well as several constraints that are specific to each case. In order to correctly compare the thermal efficiency and the mechanical power obtained from the present optimization with those given in reference [10], the same assumptions and definitions are used. Therefore, major equipments are considered adiabatic and the pressure losses in the heat exchangers and in steam extraction lines are neglected. Furthermore, turbines and pumps are assumed to operate under ideal isentropic conditions. It must be pointed out that the definition of efficiency used in the reference [10] differs from the most common form, i.e., it does not include the mechanical power of the pumps. On the other hand, the amount of the power consumed by the pumps is usually very low compared to the output power of the turbines; therefore, this effect is generally insignificant.

The Pareto's front obtained for the simplest cycle given in Figure 1-2(a) is shown in Figure 4-1 and key values used for the optimization are summarized in Table 4-1.

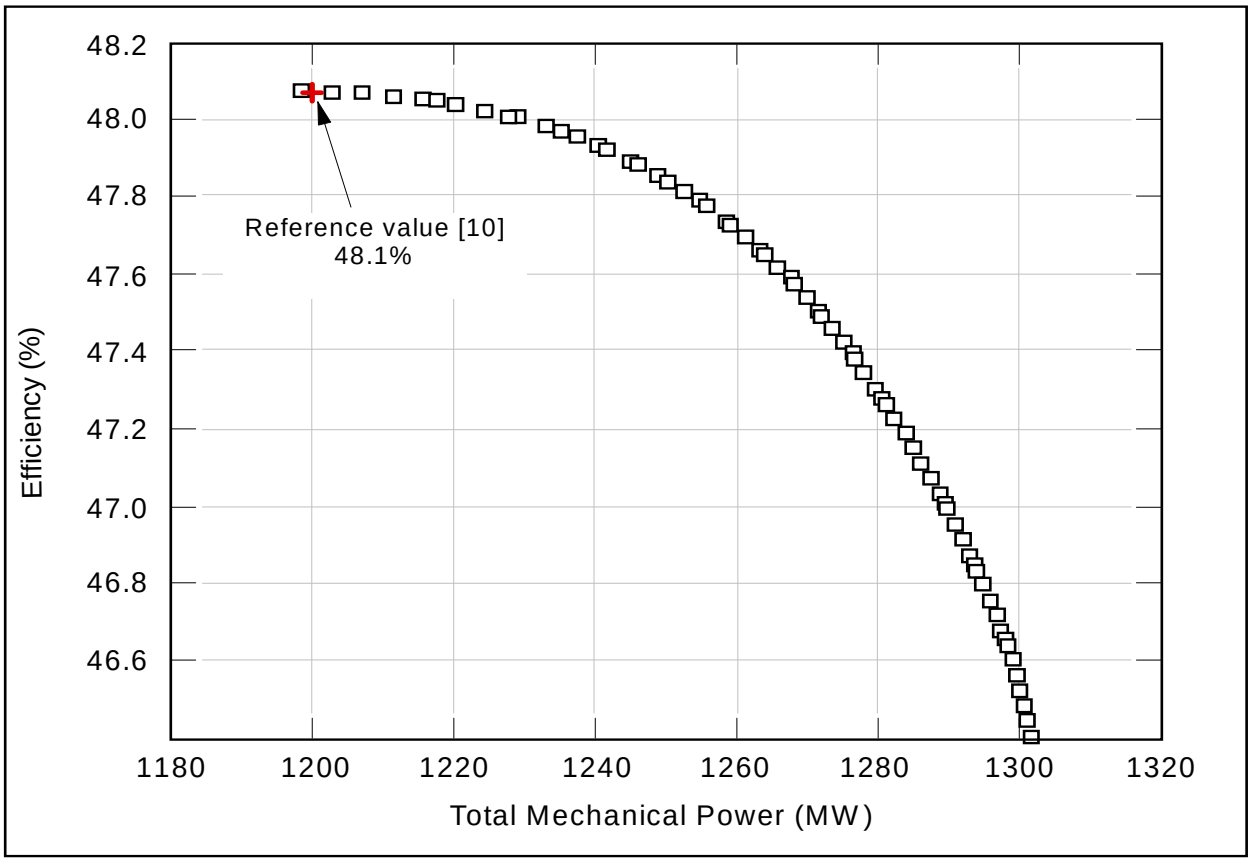

Figure 4-1: Pareto's front obtained for the single-reheat cycle shown in Figure 1-2(a).

Table 4-1: Optimization values for single-reheat cycle.

Variables	Min.	Max.
Pressures at 5 and 6 (MPa)	0.5	10
Constraints		
Steam quality	x_1=0	
Optimization Results		
Pressures at 5 and 6 (MPa)	0.5	4.98
Efficiency (%)	46.4	48.1
Mechanical power (MW)	1198	1301

As it can be observed, the efficiency and the mechanical power given in Naidin *et al.* [10] are within the predicted Pareto's landscape. However, the present optimization results indicate that there exist other operation conditions that produce higher mechanical power at the cost of decreasing the overall efficiency. It is interesting to note that the efficiency given in the reference corresponds to almost the maximum output power that this plant can produce.

For the double-reheat cycle shown in Figure 1-2(b), the optimization variables are the pressures at the exit of the HP and IP turbines respectively with a single constraint imposed to the quality at the inlet of the circulation pump. Other key values of optimization are presented in Table 4-2.

Table 4-2: Optimization values for double-reheat cycle.

Variables	Min.	Max.
Pressures at 5 and 6 (MPa)	4	10
Pressures at 7 and 8 (MPa)	0.4	4
Constraints		
Steam quality	$x_1=0$	
Optimization Results		
Pressures at 5 and 6 (MPa)	4	5.6
Pressures at 7 and 8 (MPa)	0.4	1.05
Efficiency (%)	49.2	49.4
Mechanical power (MW)	1269	1333

Similarly to the former case, the objective functions are the thermal efficiency and the mechanical power. Pareto's front obtained in this case is compared with reference values in Figure 4-2. It is interesting to observe that in this case both efficiency and mechanical power given in reference [10] are much lower than the optimal conditions predicted by using the present methodology.

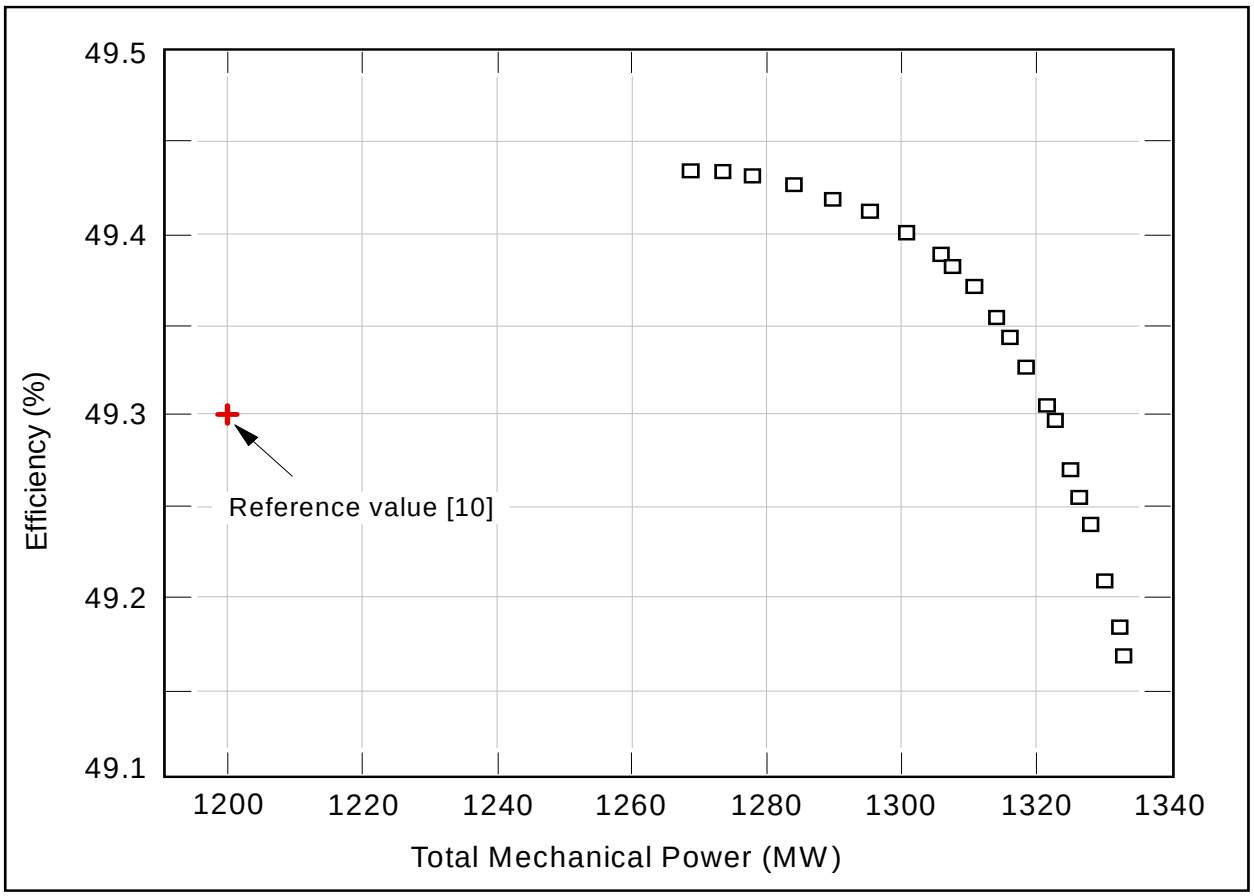

Figure 4-2: Pareto's front obtained for the double-reheat cycle shown in Figure 1-2b.

Nevertheless, Pareto's front clearly shows the competition between the two objective functions, that is: the efficiency decreases with increasing the mechanical power and vice-versa. Note that, in general, the variations in discharge pressures permit better trade-offs to be achieved. It must be pointed out, however, that these changes must be validated against real operation conditions of the turbines. Therefore, the final optimization is not necessarily useful without introducing a tight interaction with plant design engineers.

The single-reheat cycle with heat regeneration through an open type feedwater heater shown in Figure 1-3(a), is optimized by changing the pressures at the extraction and at the exit of the HP turbine, as well as the fraction of the extracted steam. At least three constraints must be satisfied during the process, beside the restrictions imposed to some steam qualities. To avoid cavitation, the liquid entering into the pumps is forced to be slightly sub-cooled. Table 4-3 summarizes decision variables and constraints used for the optimization, as well as the optimization results.

Table 4-3: Optimization values for the single-reheat cycle with heat regeneration through single deaerator.

Variables	Min.	Max.
Pressures at 3,2 and 9 (MPa)	6	20
Pressures at 6 and 7 (MPa)	2	6
Steam extraction y (%)	0.05	6
Constraints		
Steam quality	$x_1=0$ $x_3=0$	
Enthalpy difference	$h_{f3} - h_3 \geq 0$	
Optimization Results		
Pressures at 3,2 and 9 (MPa)	8	9.6
Pressures at 6 and 7 (MPa)	2	3.6
Steam extraction y (%)	0.05	4
Efficiency (%)	47.9	50.5
Mechanical power (MW)	1374	2028

The results of the optimization are presented in Figure 4-3; they show some particular features. In fact, Pareto's front is characterised by three distinct zones. The analysis of this behaviour is quite complex. As a matter of fact, the representation given in Figure 4-3 corresponds to a simple projection of a multi-dimensional space into two dimensions (i.e., in this case this space has at least five dimensions). Therefore, only a careful representation of all variables that control the solution space can help us to understand the particular behaviour of Pareto's front. In some cases there are preponderant variables that seem to determine the dynamics of the system.

In this particular case we have observed that the first zone (Figure 4-3) seems to be controlled by the pressure in such a way that the efficiency decreases and the mechanical power increases by decreasing the pressure at the extraction and at the exit of the HP turbine.

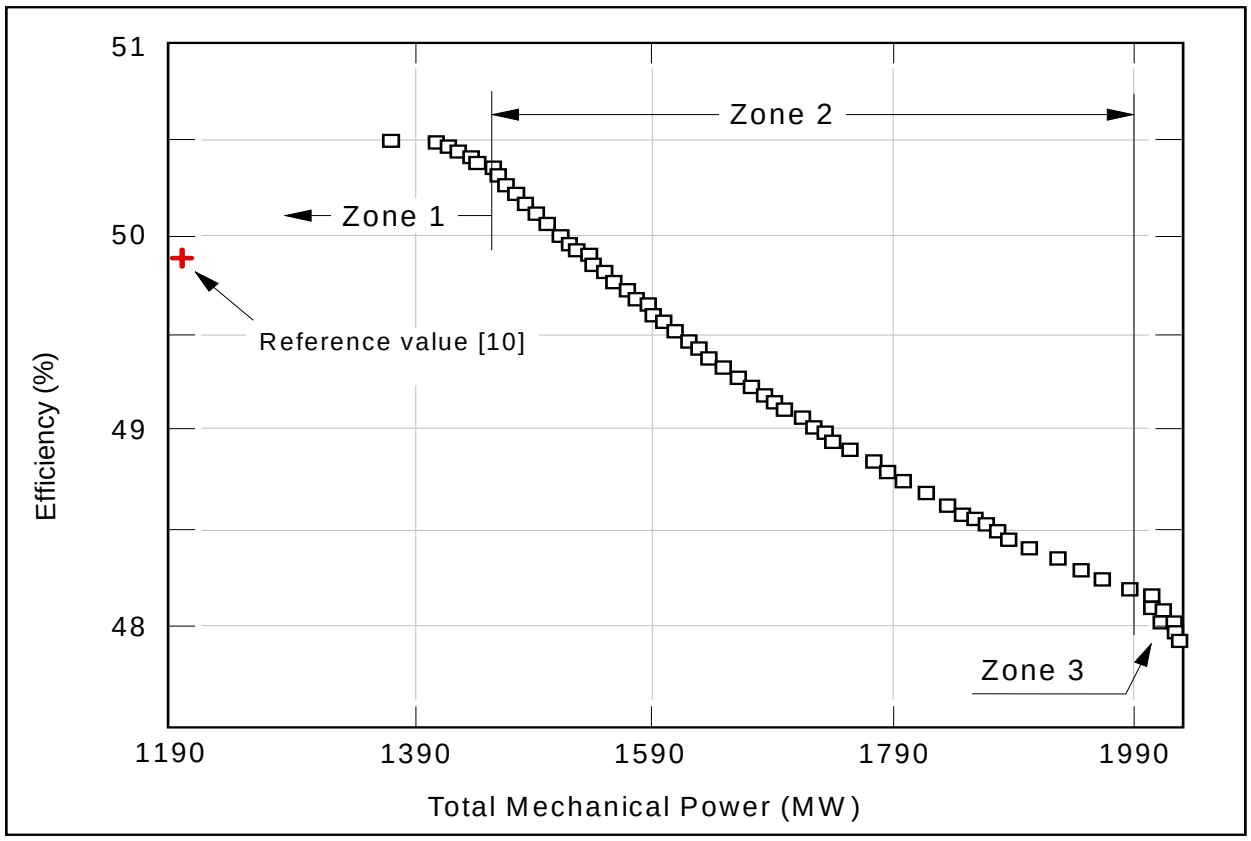

Figure 4-3: Pareto's front obtained for the single-reheat cycle with heat regeneration through single deaerator shown in Figure 1-3a.

The second zone seems to be controlled by the fraction of extracted steam; thus, the efficiency decreases and the mechanical power increases by decreasing the extraction mass flow rate. Finally, zone 3 appears to be mainly controlled by the pressures (at 9 and 6) in a similar way as zone 1. Furthermore, it is interesting to note that Pareto's front provides a large number of possible solutions which permit higher efficiencies and mechanical work than that given reference [10, 28].

The regeneration cycle shown in Figure 1-3 (b) is optimized by considering a larger number of degrees of freedom. Its optimization is based on pressures at the extractions and at the exit of the HP-turbine as well as steam fractions at points 11 and 12. Note that the fraction of steam extracted from point 8 is imposed by the balance of mass and energy applied to the open reheater that works as the deaerator unit of the power plant. Therefore, the flow at the exit of this reheater is considered to be under saturated liquid condition, which is considered as an additional constraint of the problem. To avoid cavitation, subcooled conditions are also imposed to the

liquid at the inlet of both circulation pumps. The control variables and constraints are summarized in Table 4-4.

Table 4-4: Optimization values for the single-reheat cycle with heat regeneration through single deaerator and two feedwater heaters.

Variables	Min.	Max.
Pressures at 11 (MPa)	12.15	20.25
Pressures at 8 (MPa)	3.75	6.25
Pressures at 12 (MPa)	1.2	2
Temperature 6 (°C)	270	370
Steam extraction 11, y_{11} (%)	15	25
Steam extraction 12, y_{12} (%)	10	20
Constraints		
Temperature		
$\lvert t_6 - t_8 \rvert \leq 30°C$	$t_{11} - t_6 \geq 0$	
$t_{12} - t_3 \geq 0$	$t_{13} = t_5 + 6°C$	
$t_{14} = t_2 + 6°C$	$t_{sat14} - t_{14} \geq 0$	
$t_{sat13} - t_{13} \geq 0$		
Steam quality		
$x_1 = 0$	$x_4 = 0$	
$x_{10} \geq 0.85$	$x_{12} = 1$	
Extraction	$y_{11} + y_8 + y_{12} \leq 60\%$	
Optimization Results		
Efficiency (%)	52.78	56.9
Mechanical power (MW)	1109	1361

Figure 4-4 presents the Pareto's front obtained for this system as well as the reference plant state [10]. The front is characterized by four distinct zones. Even though all control parameters vary randomly along the front, each zone seems to be essentially conditioned by one preponderant variable. Hence, careful analyses of the predicted data (i.e., eight dimensional space) show that the first zone is mostly conditioned by the pressure at the exit of the HP-turbine i.e., point 8 in Figure 1-3(b). In this zone, the efficiency decreases and the mechanical power increases by decreasing the pressure.

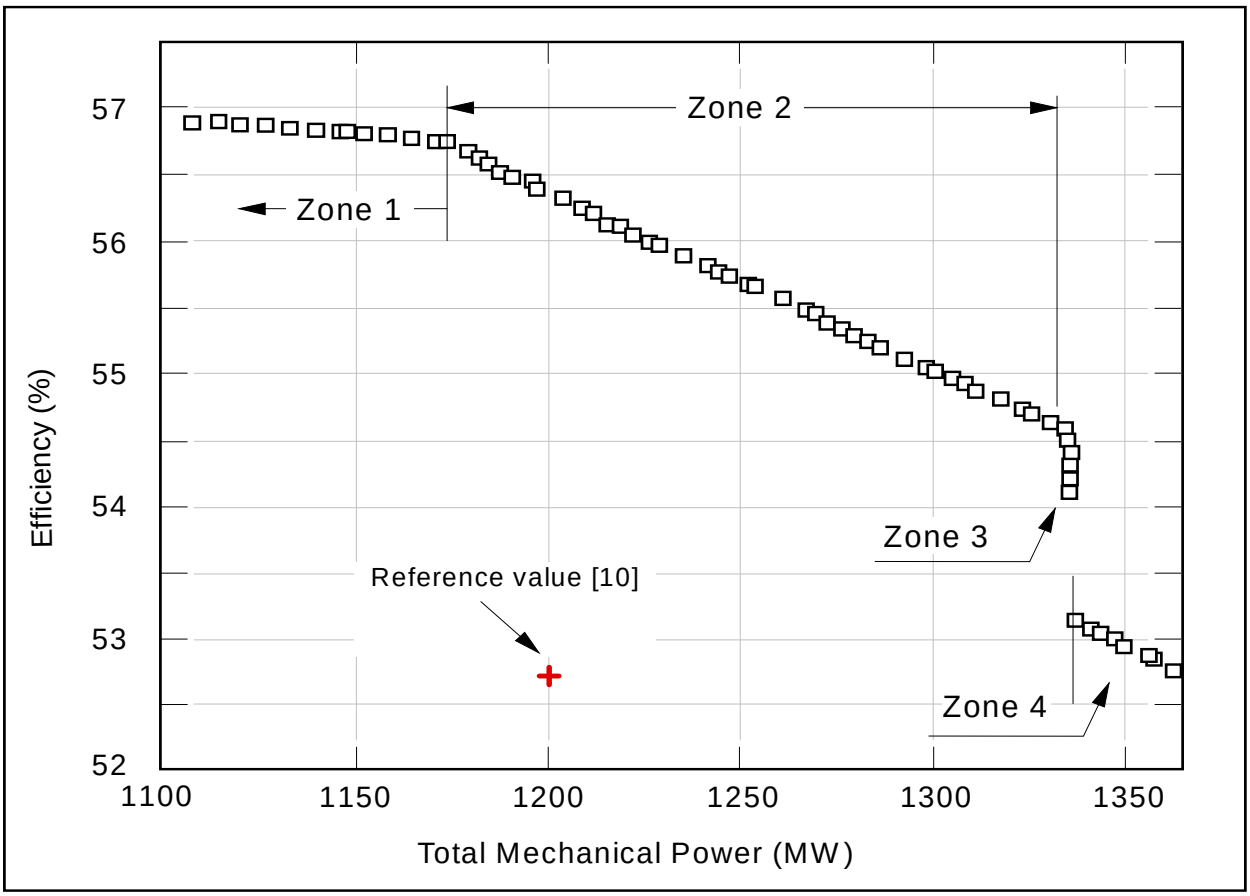

Figure 4-4: Pareto's front obtained for the Single-reheat cycle with heat regeneration through single deaerator and two feedwater heaters shown in Figure 1-3b.

The second zone is mainly controlled by the fraction of steam extracted at point 11. It is observed that the efficiency increases and the mechanical power decreases by increasing the extraction mass flow rate. This result corroborates basic thermodynamic principles, i.e., the extraction of a fraction of steam allows a gain in efficiency at the expense of losing some turbines' work.

The abrupt knee change observed in zone 3 of Figure 4-4, seems to be mostly controlled by the steam extracted at point 12; thus, the thermal efficiency increases and the mechanical power decreases by increasing the extraction mass flow rate.

Finally the last region is conditioned by the pressure at point 8 following similar trend to zone 1. It must be pointed out that the pressures at point 11 and 12 do not considerably change; they remain almost constant to their lowest limit imposed by the optimizer and therefore they do not have a significant effect on Pareto's front.

Similarly to other cases studied, the present optimization method provides a wide range of thermodynamic conditions under which both the thermal efficiency and the mechanical power are much higher than the values suggested in Naidin *et al*. [10].

Due to the relative complexity of this cycle, however, a comparison between the optimum conditions, near 1200 MW, selected from the Pareto's front and the reference case is also presented in Table 4-5.

Table 4-5: Comparison between the reference case [10] and optimized system of Figure 1-3b.

	Reference case			**Present optimization**		
State #	**T (°C)**	**P (MPa)**	**h (kJ/kg)**	**T (°C)**	**P (MPa)**	**h (kJ/kg)**
1	38.3	0.00677	160.8	38.4	0.00677	160.8
2	38.5	5.0	166.0	38.51	4.15	164.9
3	200.0	5.0	850.0	210.3	4.15	899.9
4	265.0	5.0	1155.0	252.53	4.15	1098.1
5	270.0	25.0	1180.0	257.93	25.0	1124.1
6	350.0	25.0	1624.0	351.99	25.0	1637.9
7	625.0	25.0	3567.0	625.0	25.0	3566.8
8	350.0	5.0	3065.0	322.57	4.15	3018.8
9	625.0	5.0	3725.0	625.0	4.15	3731.3
10	38.3	0.00677	2270.0	38.38	0.00677	2300.0
11	540.0	16.2	3415.0	489.81	12.15	3320.3
12	450.0	1.6	3314.0	412.18	1.20	3287.3
13	275.0	16.2	1210.0	263.93	12.15	1153.2
14	45.0	1.6	185.0	44.51	1.20	187.4
Extractions (%)						
y_{11}	20.0			23.7		
y_8	10.0			6.5		
y_{12}	15.0			20.0		
Efficiency (%)	52.7			56.4		
Mass flow rate (kg/s)	1030.0			1030.0		
Mechanical power (MW)	1200.0			1197.3		

In general, although the values of most thermodynamic variables are quite similar, major differences are observed around steam extractions. Thus, the total mass flow rate of steam extractions for the optimized system is about 11 % higher than the reference case. However, it is interesting to note that a higher total value of the extractions permits both the thermal efficiency and the mechanical power to be considerable higher than the reference case. This constitutes an interesting result that could not be obtained without using an optimization linked to a plant simulation model. In fact, this strategy permit a large range of possible plant operation conditions to be taken into account. In turn, the optimizer determines whether or not the outcomes from the simulations are feasible-solutions.

Once again, these results show plenty of possibilities for increasing both the efficiency and the mechanical output of the plant. In some cases, we were able to determine that the landscape of Pareto's front was mostly controlled only by few numbers of key parameters. Even though, the cycles presented in this section are quite simple, their optimization shows the powerful tool that represents the Pareto's front. The simulations and optimizations of thermodynamic cycles more closely related to modern power plants are presented in following sections.

4.2 Optimization of the no-reheat and single reheat power cycles.

In this section, both thermodynamic cycles presented in section 1.2.2 (Figures 1-4 and 1-5) are optimized in two different ways according to the definition of decision variables. As pointed out in section 2.3.2, the pressure of the steam at the extraction point for reheating the feedwater should respect a pressure ratio across the turbine stage. According to Hitachi, this pressure ratio must be bounded between 1.3 and 2 (equation 2-6). Therefore, this part presents two different optimizations strategies; the first one (Case 1) consists of selecting pressures as decision variables in a given range of values, similar to the previous cases studied. For the second one (Case 2) a given pressure ratio for each turbine group (i.e., high-, intermediate-, low- pressure sections) is considered.

The optimization-simulation procedure is performed according to the models given in previous sections. Turbines and pumps are characterized by isentropic efficiencies given in the references [8, 9]. These values are considered constant for each group of turbines; the isentropic efficiency is around 0.89 for high pressure turbine and 0.92 for intermediate and low pressure turbines.

Pumps are simulated with an isentropic efficiency of 0.84 and the condenser is assumed to operate under a constant pressure of 6.77 kPa in both cases. The condition at the outlet of the reactor core is 625°C and 25 MPa. The same exit temperature is also valid for the reheat process. Heat exchangers are simulated according to the values of Terminal Temperature Differences (TTD) and Drain Cooling Approach (DCA) given in references [8, 9] and summarized in Table 4-6. In addition, the outlets of the condenser and the deaerator are assumed to be under saturated liquid conditions.

Table 4-6: Feedwater heaters parameters.

Heater identifier	**DCA (°C)**	**TTD (°C)**
H1	5.6	2.8
H2	5.6	2.8
H3	5.6	2.8
H4	5.6	2.8
H5	5.6	2.8
H6	5.6	1.5
H7	5.6	0
H8	5.6	-1.6
H9	-	-

In this study, the pressures at the steam extraction points are considered as decision variables. For the Case 1, these pressures are taken randomly inside the boundaries given by the operator. Instead the case 2 must respect the pressure ratio across turbine stages as explained in section 2.3.1. Constraints consist of temperature differences as well as the second law of thermodynamics. The most important values of decision variables and constraints are summarized in Table 4-7. All the optimizations have been carried out by running the algorithm under the same conditions as discussed before. Thus, a constant population of 200 individuals with the same number generations and 100 corridors are used.

The Pareto's fronts obtained for the no-reheat cycle using the two ways of optimization are presented in Figure 4-5 and Figure 4-6 . It is obvious that the solutions given by the Pareto's front for Case 2 are fewer in number than for Case 1. The use of a given pressure ratio for the definition of the decision variables, significantly limits the extent of the space of potential

solutions as compared to Case 1. On the other hand, the second case is closer to a real turbine design and also offers more than a single solution for such a multi-objective problem.

Table 4-7: Optimization decision variables and constraints.

Decision variables		
No-reheat and single-reheat cycles Case 1 (Figure 1-4)	**No-reheat and single-reheat cycles Case 2 (Figure 1-4)**	**Constraints**
$7.5 \leq P_2 \leq 18$ $6 \leq P_3 \leq 7.5$ $4 \leq P_4 \leq 6$ $2.5 \leq P_5 \leq 4$ $1.5 \leq P_6 \leq 2.5$ $0.8 \leq P_7 \leq 1.5$ $0.3 \leq P_8 \leq 0.7$ $0.01 \leq P_9 \leq 0.3$ $0.01 \leq P_{10} \leq 0.3$	$1.3 \leq P_{ratio} \leq 2$ $1 \leq n \leq 3$	$270°C \leq t_{13} \leq 370°C$ $\eta_{th} \leq 0.65$ $t_{13} < t_4$ $0.75 < x_{11}$ Single reheat: $270°C \leq t_{14} \leq 370°C$ $\lvert t_{14} - t_3 \rvert \leq 100°C$

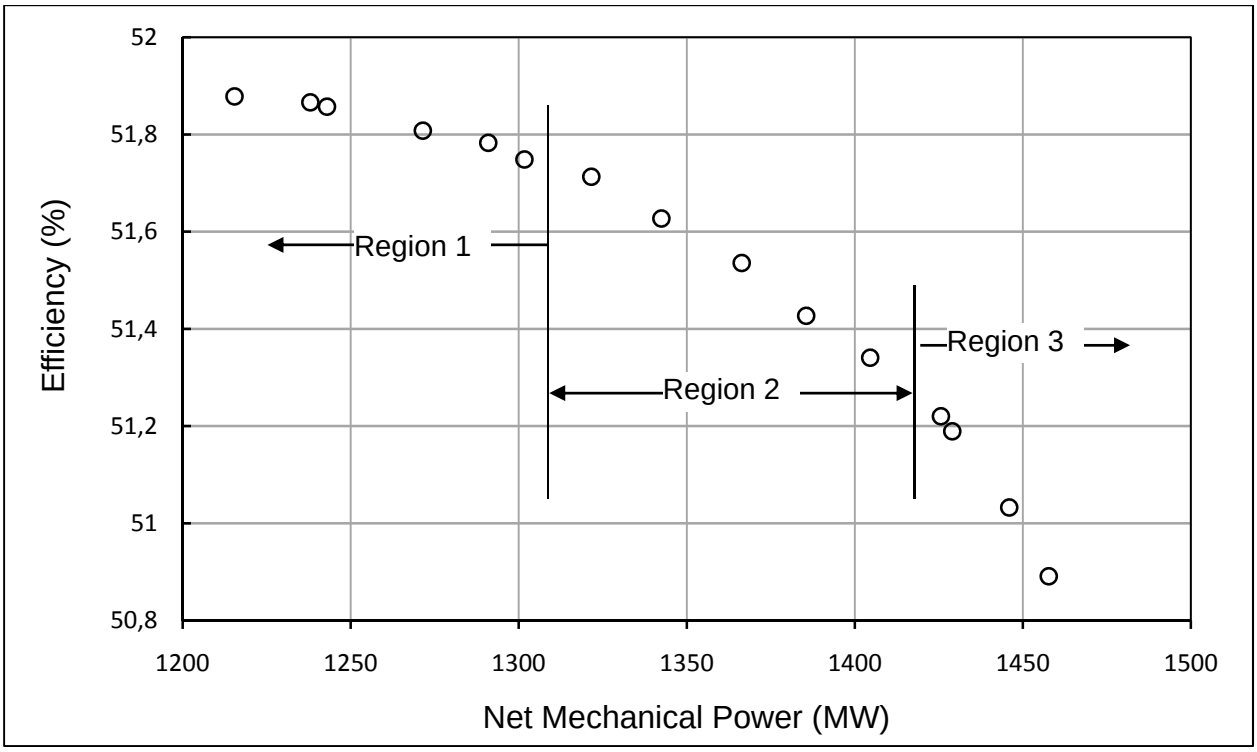

Figure 4-5: Pareto's front obtained for the no-reheat cycle for Case 1.

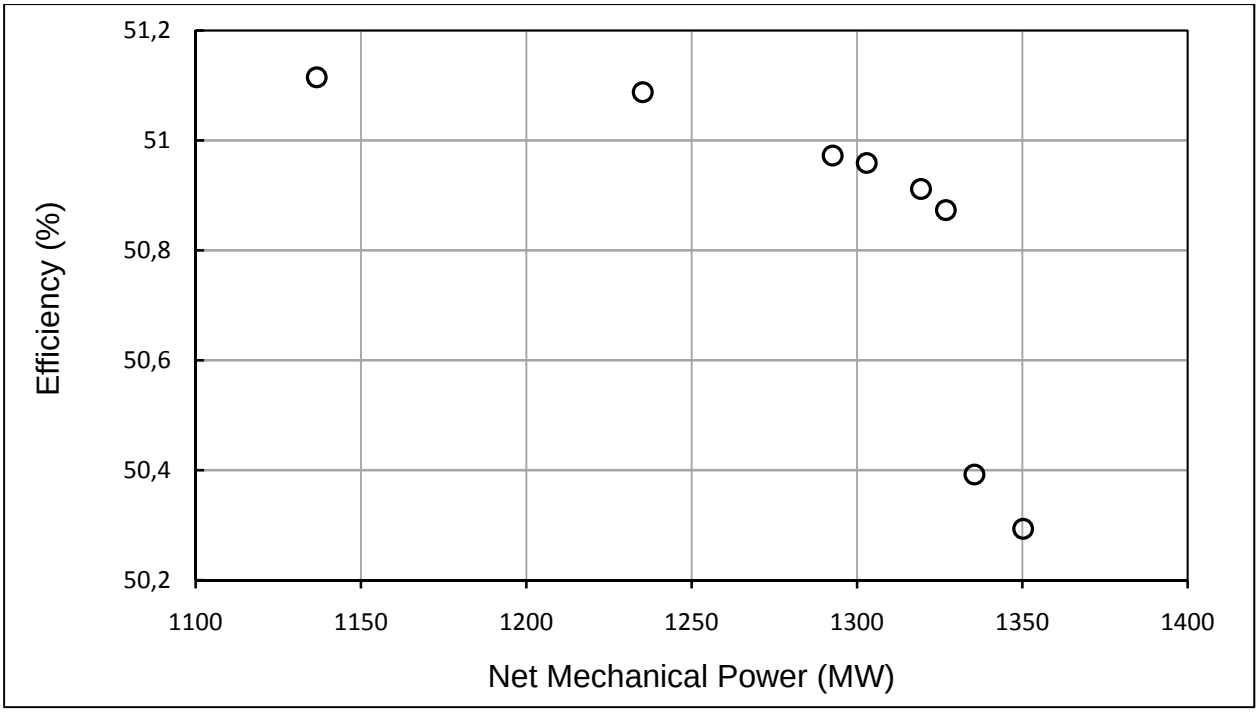

Figure 4-6: Pareto's front obtained for the no-reheat cycle for Case 2.

A brief analysis of the optimization results obtained for Case 1, shows that the Pareto's front is characterized by three distinct regions. The first one, which goes up to a thermal efficiency of 51.75 %, is mainly controlled by the pressures at states 2 and 4 and in a less significant manner by the pressures at states 5 and 6. When these pressures increase, the thermal efficiency increases and the mechanical power decreases. The conservations of energy and mass impose the modification of mass flow rates at the extractions. Thus, the efficiency increases with mass flow rates at states 2 and 4. This behavior is due to the fact that the last two heat exchangers are fed by these two extractions. The mass flow rates decrease at states 5, 8 and 10 along with the thermal efficiency. This phenomenon may be linked to the quantity of heat rejected through the condenser, which increases with increasing these mass flow rates.

The second region shown in the Figure 4-5 is once again controlled by the pressure at state 2 and corresponds to the increase of mass flow rates at states 4 and 2. The mass flow rates which feed H1, H2 and H3 also have a negative impact on the thermal efficiency. Similar to the previous case heat rejected to the condenser increases with increasing these mass flow rates.

The last region has no significant behavior, neither for decision variables nor for mass flow rates.

The second cycle with the addition of one steam-reheat (Figures 4-7 and 4-8), allows an increase of the thermal efficiency of about 10 point of percentage. Again, for Case 2, the number of solutions is limited compared to the optimization for Case 1. Furthermore, for the first case the front of Pareto can be divided into four regions as shown in Figure 4-7. The first one consists of only two points and thus, cannot be rigorously analyzed. Nevertheless, it is interesting to note that these solutions are obtained for the highest values of the pressure at the extraction of the high pressure turbine.

The second region seems to be mainly controlled by the pressures at states 2 and 7 where the thermal efficiency increases with increasing these pressures. At the same time, it can be observed that the mass flow rates at states 2 and 5 increase, whereas at points 3, 6, 7, 8 and 11 they decrease.

The third zone is again mainly controlled by the pressure at the first extraction (state 2) and the mass flow rates at extractions 2 and 5. Here, it is observed that the thermal efficiency increases with the pressures. The main decision variable for the last region is the pressure at state 5, where the efficiency increases with decreasing this pressure. At the same time, the mass flow rate at state 3 increases while the one at state 6 decreases.

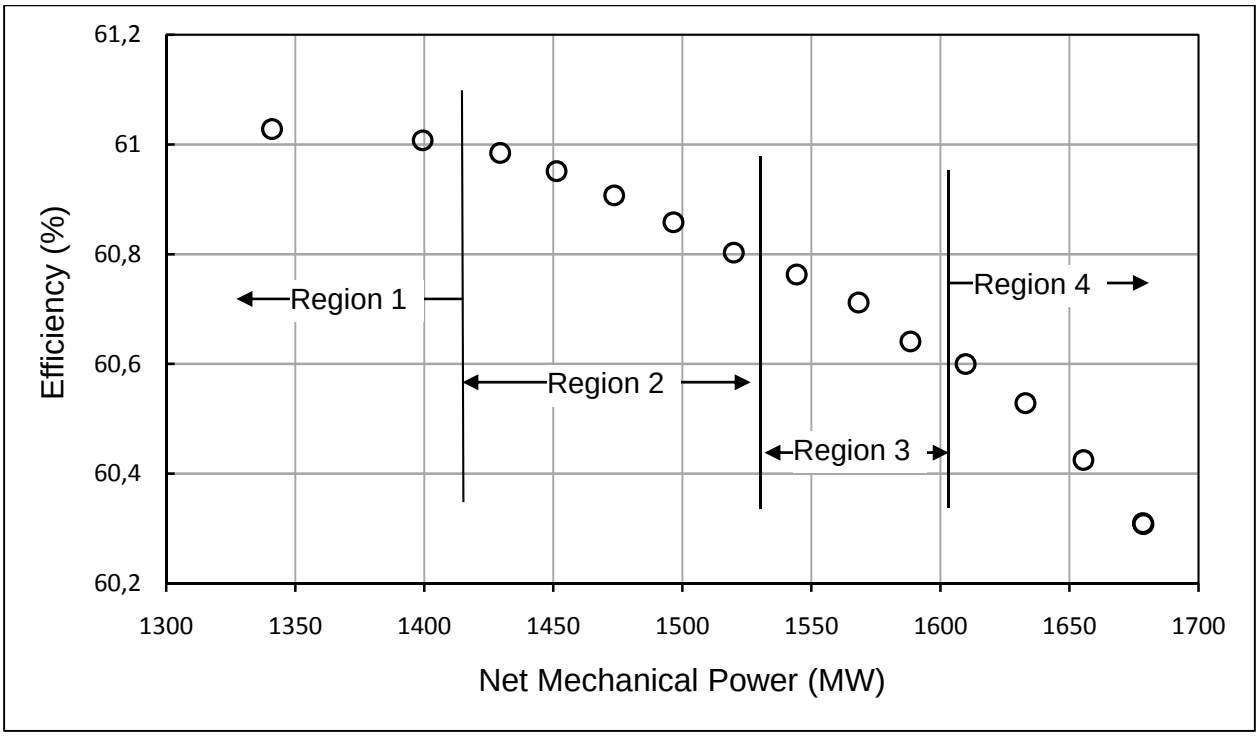

Figure 4-7: Pareto's front obtained for the single-reheat cycle for Case1.

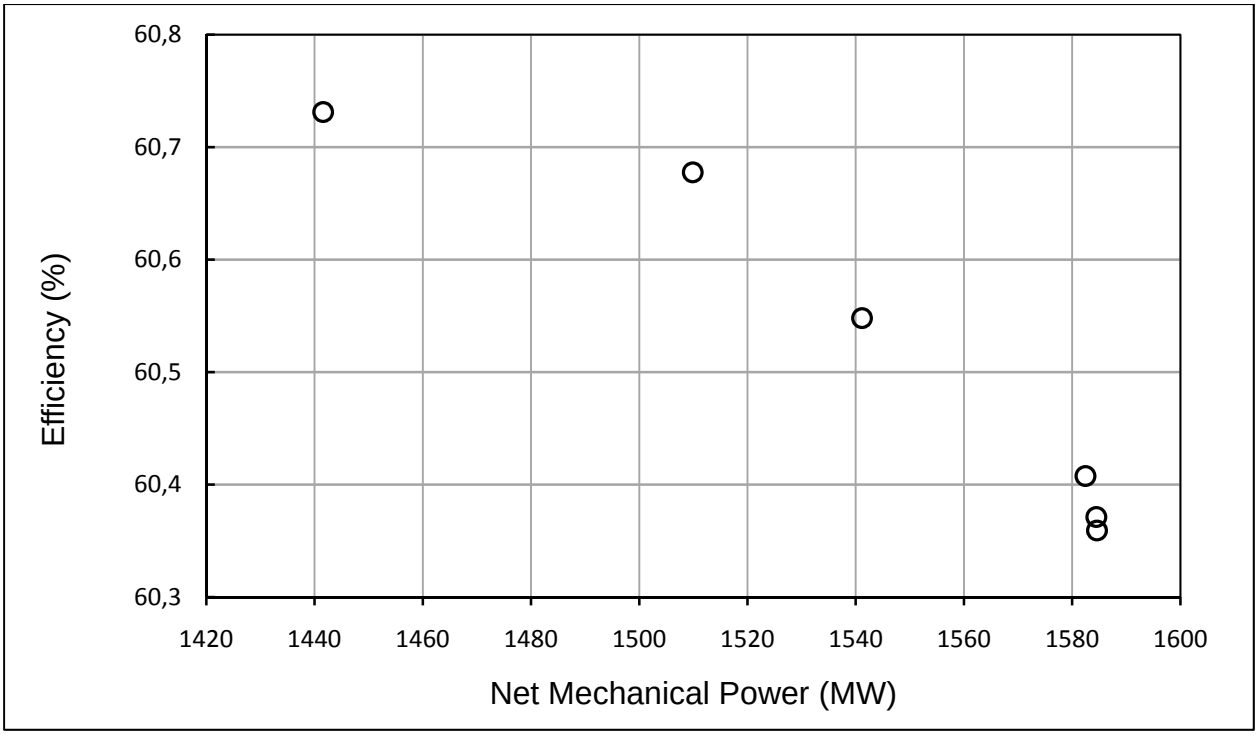

Figure 4-8: Pareto's front obtained for the single-reheat cycle for Case2.

The comparison between the Pareto's fronts obtained for these two cycles clearly shows the benefit achieved by a single-reheat cycle. The major advantage is the high thermal efficiency. It is also interesting to note that the mass flow rate required to obtain the desirable mechanical power of 1200 MW with reheat is lower than that without reheat. However, this option increases substantially the design complexity of the machine by the introduction of steam-reheat fuel channels into the reactor core.

The concept of pressure ratio across the turbine stage has been considered for both cycles. The higher efficiency obtained for the Case 1 cannot be achieved for Case 2, which is characterized by low number of solutions. Nevertheless, the optimizer gets at least 6 solutions for both cycles and thus, offer the possibility to the operator or designer to choose the most suitable compromise between thermal efficiency and mechanical output of the plant. It is obvious that the use of fixed pressure ratios should be developed in more detail, in particular to satisfy turbine design criteria. However, the lack of information on supercritical turbine design is the major barrier encountered during the development of this work.

4.3 Optimization of two cycles adapted from a supercritical fossil-fuelled power plant

Once the plant modelling method is validated against power plant data (see Section 2.4) it is used to perform the optimization of a supercritical boiler power plant given in [17]. The flow diagram of this system is shown in Figure 1-6 (Section 1.2.3). This plant is used as a blue print to develop two different SCWR NPP configurations. It is apparent that a multi-objective optimization procedure may handle a large number of decision variables and constraints. In this investigation, pressures at different locations along the cycle are considered as decision variables. Similarly to other cases already presented, the constraints are imposed based on temperature differences as well as on the second law of thermodynamics. For all the cases studied, the most important values of decision variables and constraints are summarized in Table 4-8. The same temperature constraints used for running the reference case are also used to treat the other ones, while the qualities x_{14}, x_{17}, x_{18} and x_{22} are forced to zero. Furthermore, for all cases treated, the mass flow rate at state 12 in Figure 1-6 is used as an additional decision variable. It is obvious that to satisfy the optimum values of the pressures, the optimizer forces the associated mass flow rates to change. This is an important point that should be considered in future engineering work.

Table 4-8: Optimization decision variables and constraints.

Decision variables: Pressure (MPa)		**Temperature Constraints (°C) All systems (Figure 1-6)**
Reference Case 668-MW Fossil Fuelled Supercritical Power Plant (Figure 1-6)	**Proposed SCWR NPPs 600-MW and 1200-MW (Figure 1-6)**	
$6.6 \leq P_2 \leq 9.0$	$5.0 \leq P_2 \leq 6.5$	$t_{sat\,H8} - t_{33} > 0$ $t_{sat\,H7} - t_{32} > 0$ $t_{sat\,H6} - t_{31} > 0$ $t_{sat\,H5} - t_{30} > 0$ $t_{sat\,H4} - t_{29} > 0$
$3.6 \leq P_4 \leq 6.5$	$3.5 \leq P_4 \leq 4.8$	
$1.5 \leq P_5 \leq 3.5$	$1.2 \leq P_5 \leq 3.4$	
$0.4 \leq P_6 \leq 0.8$	$0.4 \leq P_6 \leq 0.8$	
$0.2 \leq P_8 \leq 0.4$	$0.2 \leq P_8 \leq 0.4$	
$0.07 \leq P_{10} \leq 0.20$	$0.07 \leq P_{10} \leq 0.20$	
$0.03 \leq P_{11} \leq 0.06$	$0.03 \leq P_{11} \leq 0.06$	
$0.015 \leq P_{12} \leq 0.02$	$0.015 \leq P_{12} \leq 0.020$	

The Pareto's front obtained for the reference case given in [17] is shown in Figure 4-9.

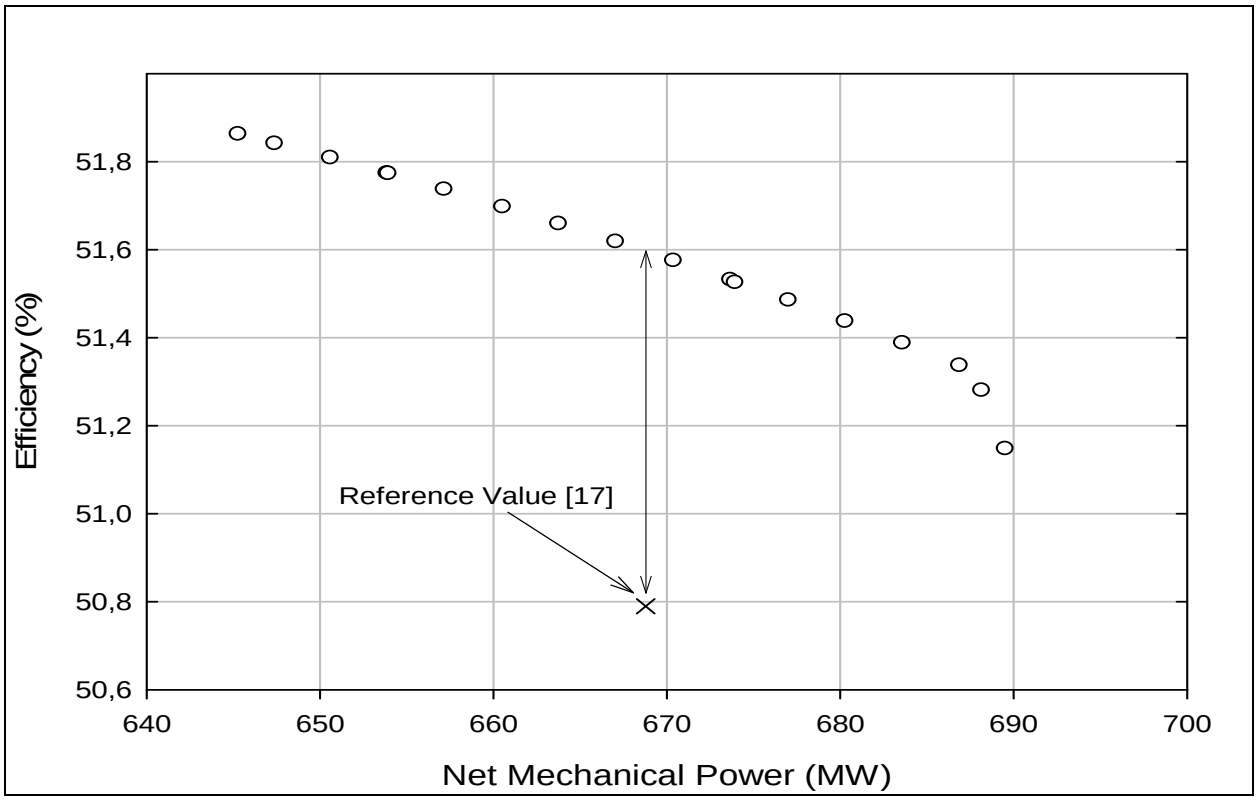

Figure 4-9: Pareto's front obtained for a fossil fuelled supercritical power plant [17].

It is interesting to observe that the actual operation conditions of this fossil fuelled power plant are quite close to Pareto's boundary (i.e., $\dot{W} = 668.7\,\mathrm{MW}$ and $\eta = 50.8\%$); thus, the difference with respect to the front is less than 1 point of percentage. The project described by Kruglikov *et al.*[17] seems to have been already optimized and well designed to obtain an almost optimal value of thermal efficiency. From Figure 4-9, it is obvious that the present optimization method provides a wider range of conditions under which the plant could perform better by decreasing the net mechanical power or vice-versa (i.e., two competing objectives). The final selection of best trade-offs must consider not only economical criteria (reduce fuel expenditures by decreasing the net available power) but also technical criteria in the design of the plant, (i.e., turbines, heat exchangers, condenser, etc.).

It is obvious that for the SCWR NPP cases, temperatures, pressures and mass flow rates are different from those of the reference case. In particular, pressures and temperatures have been modified to satisfy the anticipated operation conditions of future SCWR's [19]. Thus, the pressure in the reactor core is fixed to 25 MPa and the outlet fluid temperature to 625°*C*. However, the pressure during the second passage of the fluid in the reactor core is less than 6.5 MPa.

The Pareto's front obtained for the proposed SCWR NPP configurations as well as the values obtained from the simulations before the optimization is performed, are shown in Figure 4-10 and Figure 4-11. For two 600-*MW* SCWR units running in parallel a steam mass flow rate of 412 kg/s for each loop is used whereas for the 1200-MW system this value is obviously doubled.

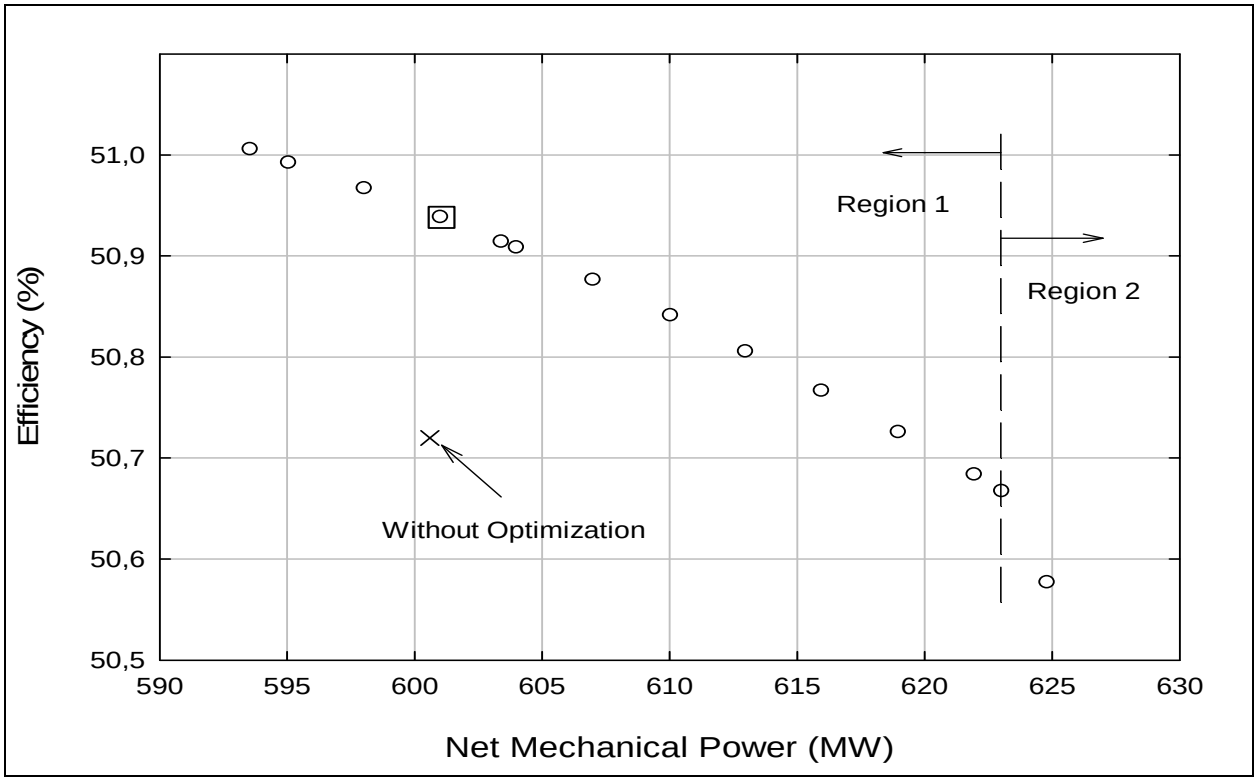

Figure 4-10: Pareto's front for SCWRNPP's: 600-MW units.

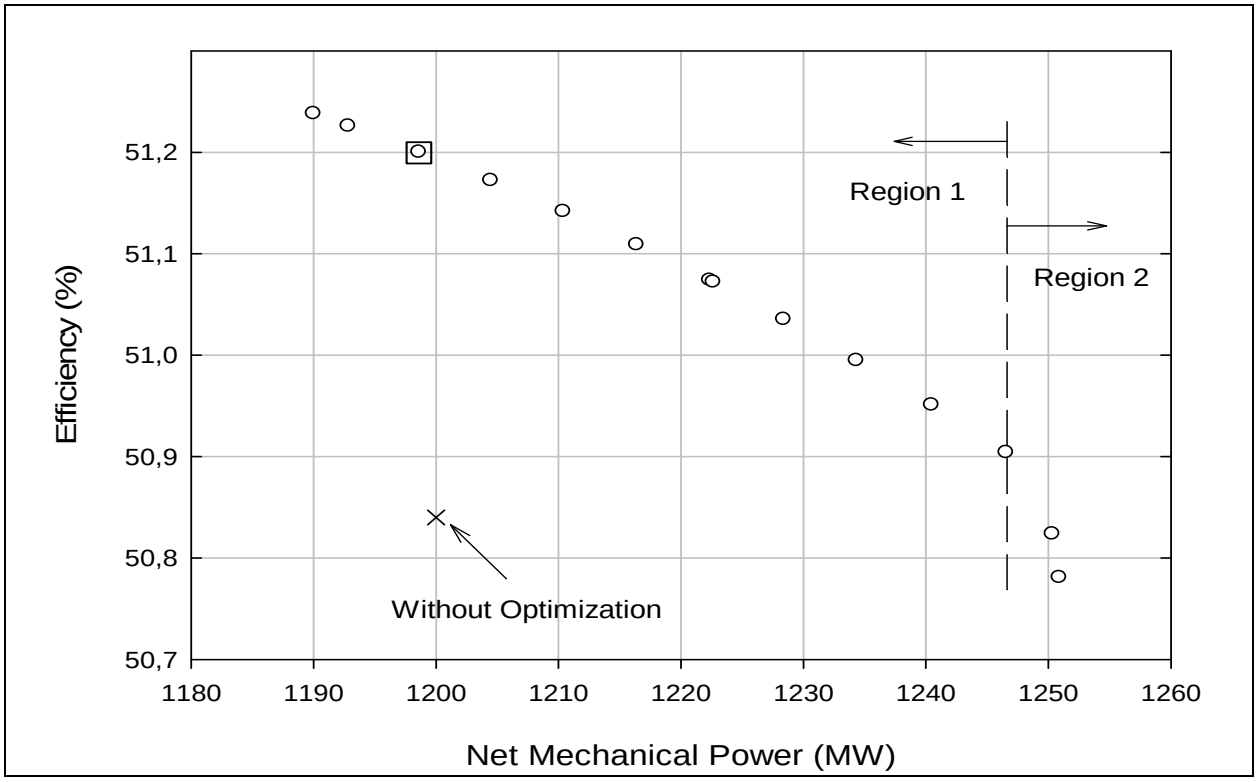

Figure 4-11: Pareto's front for SCWRNPP's: single 1200-MW unit.

It is apparent that for a net mechanical power equal to the non-optimized value, the optimization increases the efficiency between 0.2 and 0.35 point of percentage. Once again, it is observed that both the optimum values of efficiency and the net power vary in opposite directions. The results of these cycle simulations for a net power close to the stipulated values (points signposted) on the Pareto's front in Figure 4-10 and Figure 4-11 are given in Table 4-9. The results of both optimizations are very close: the thermal efficiency for the single 1200-MW unit is only 0.2 point of percentage higher than that of the 2 X 600-MW units. This may be explained by the higher temperature at the inlet of the reheat process at state 2 (see Figure 1-6). On the other hand, the net mechanical power produced by the 2 X 600-MW units is about 4 MW higher. Thus, the optimization reaches almost the same global behaviour for both cycles. Broadly, values of pressure at the extractions, which are the decision variables in the optimization process, are quite similar. Whereas, the mass flow rate at the extraction at state 12 (see Figure 1-6) which is a decision variable, is 2.6 times higher than the value for the 2 X 600-MW units. This fact has an impact on the value of the temperature for states 16 to 21, and can probably affect the overall thermal efficiency of the thermodynamic cycle.

Table 4-9: Simulation-optimization results for reference case and proposed SCWRNPP's.

	Initial values for fossil-fuelled power plant			**Optimized values for 2x 600 *MW* SCWRNPP**			**Optimized values for 1200 *MW* SCWRNPP**		
# State	**T (°C)**	**P (MPa)**	**$\dot{m}$ (kg/s)**	**T (°C)**	**P (MPa)**	**$\dot{m}$ (kg/s)**	**T (°C)**	**P (MPa)**	**$\dot{m}$ (kg/s)**
1	600	30.0	475.9	625	25.0	412.0	625.0	25.0	821.3
2	375.4	7.5	475.9	394.9	6.11	34.0	399.6	6.3	69.2
3	620.0	7.3	437.1	625	5.96	378.0	625	6.05	752.1
4	541.1	4.6	20.8	534.4	3.50	11.1	532.7	3.50	21.8
5	457.9	2.7	29.1	466.8	2.27	23.2	466.3	2.29	45.7
6	330.2	1.1	51.1	361.3	1.10	51.1	359.8	1.10	51.1
7	235.3	0.5	9.1	236.9	0.40	10.1	235.7	0.40	15.4
8	191.9	0.333	18.2	182.6	0.24	17.5	195.6	0.28	28.0
9	191.6	0.32	308.8	182.2	0.23	264.9	195.3	0.23	590.1
10	100.7	0.104	13.4	89.9	0.07	11.7	110.4	0.10	14.8
11	77.6	0.043	13.6	65.8	0.026	10.0	85.8	0.0597	10.0
12	57.8	0.018	17.9	54.0	0.015	10.6	54.0	0.015	55.5
13	24.1	0.003	264.4	24.1	0.003	232.6	24.1	0.003	509.7
14	24.1	0.003	313.2	24.1	0.003	272.0	24.1	0.003	572.6
16	53.0	0.39	313.2	44.7	0.39	272.0	76.1	0.39	572.6
17	76.1	0.04	326.9	64.4	0.02	282.0	85.6	0.06	582.6
18	98.8	0.097	367.6	87.8	0.06	321.3	100.1	0.10	640.8
19	99.0	1.37	475.9	87.9	1.37	321.3	100.2	1.37	640.8
23	187.1	34.3	475.9	186.0	28.22	412	186.2	29.30	821.3
24	231.6	34	440.8	223.0	28.00	412	223.0	29.00	821.3
25	254.0	33.7	440.8	239.6	27.77	412	239.3	28.70	821.3
26	289.8	33.3	440.8	276.2	27.47	412	277.0	28.30	821.3
27	295	33.2	475.9	276.2	27.47	412	277.0	28.30	821.3
η (%)		50.79			50.94			51.20	
$\dot{W}$ (MWe)		668.78			601.06			1198.66	

Even though, Figure 4-10 and Figure 4-11 correspond to plane projections of a multidimensional space, the Pareto's fronts, according to their slopes, can be divided into two distinct regions. A close analysis of changes observed in the decision variables (Table 4-8) during the optimization

given in Figure 4-10 shows that the first region is mainly controlled by the pressure at state 2 (Figure 1 - 6) and efficiencies increase with increasing the pressure. However, in the same region the net mechanical power decreases with increasing pressures. It is also observed that the corresponding mass flow rate of extracted steam tends to increase. This change increases feedwater reheating which in turn increases the water enthalpy at the entrance of the reactor core. This behaviour is directly related to the thermal efficiency of the cycle. Instead, the second region follows a more complex behaviour and seems to be controlled by pressures at state 4 and 5 and by the mass flow rate at extraction 12 (Figure1-6). Even though other variables also varied during the process, no apparent correlation between them and the Pareto's landscape could be established.

For the second SCWR NPP configuration, the change in mass flow rate affects the overall mass balances along the cycle. Figure 4-11 shows that the Pareto's front can also be divided into two regions. The behaviour of the several decision variables is quite similar to those of the previous case (Figure 4-10), i.e.; region 1 is mainly controlled by the value of pressure at state 2 as shown in Figure 4-12.

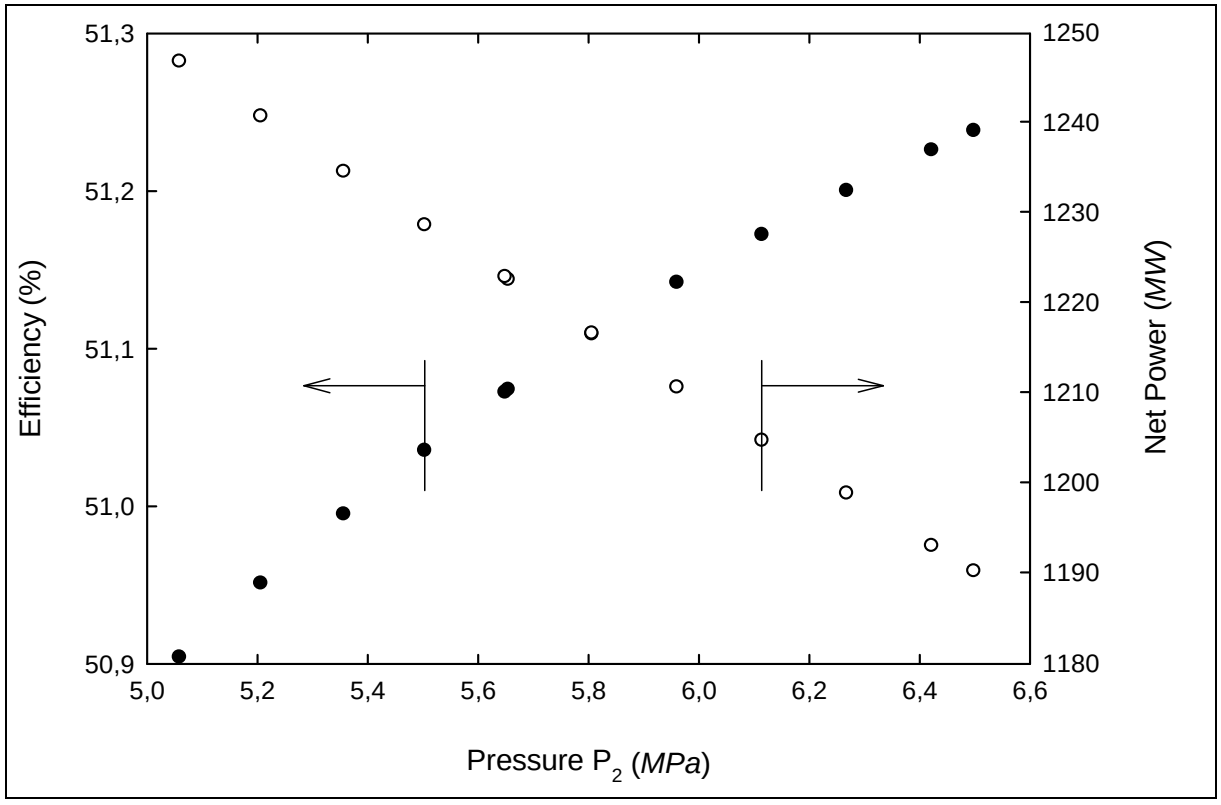

Figure 4-12: Variations of efficiency and net power as a function of pressure P_2.

Thus, efficiency increases and net mechanical power decreases with increasing pressure P_2. Increasing the reheat pressure allows a higher temperature average during heat-addition process which is a common way for increasing the thermal efficiency in a Rankine cycle. For this case, it is also observed that within a very limited range, the efficiency is essentially affected by the extractions 2 and 12 (Figure1-6) while the effects of variations on other mass flow rates are negligible.

Figure 4-13 shows the effect of the mass flow rate at state 2. In the same way as increasing the pressure, increasing extracted mass flow rates allows the average temperature to increase during the heat-addition process, and thus increases the thermal efficiency of the cycle. The second region (Figure 4-11) seems to be controlled by the pressure at the first steam extraction (#4) from the IP turbine while all other decision variables remain almost constant in this region.

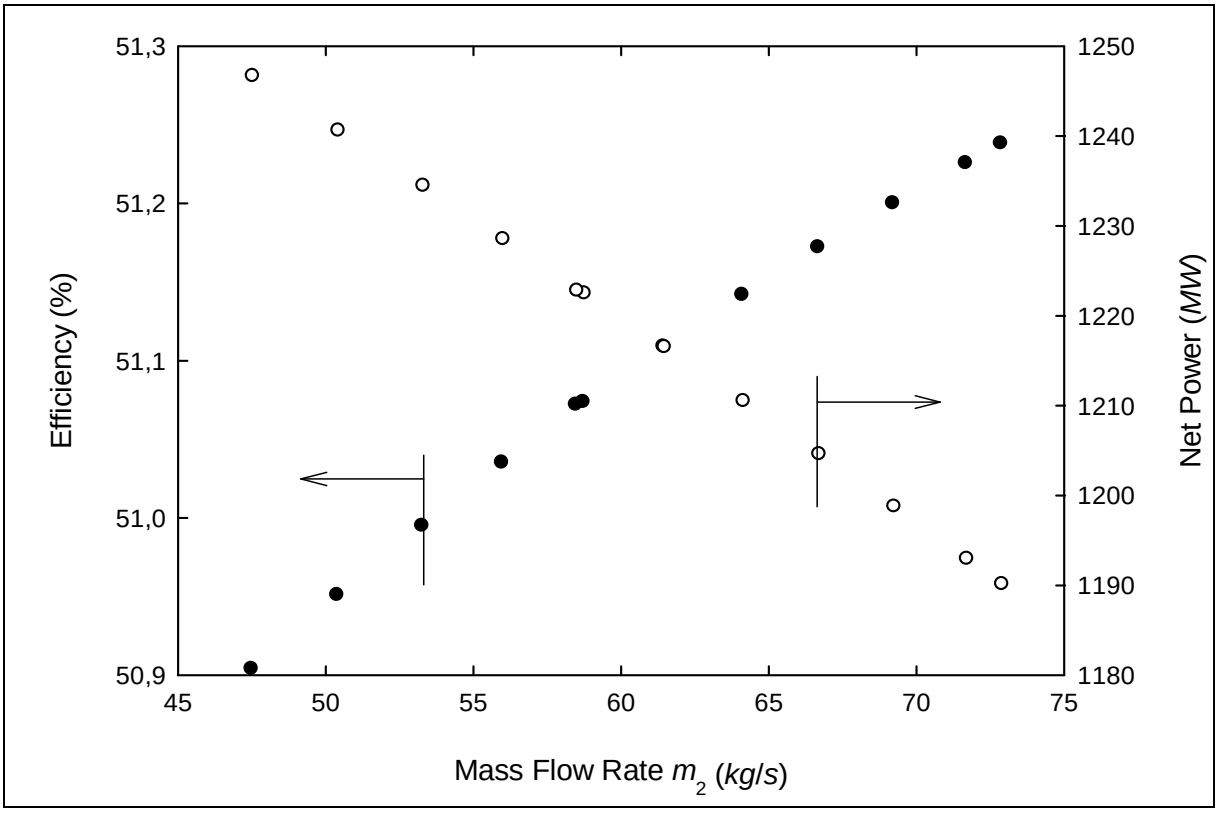

Figure 4-13: Variations of efficiency and net power as a function of mass flow rate $\dot{m}_2$.

In general, it is observed that the improvement in the mechanical power can be substantial, while conditions imposed by the deaerator considerably limit the possibility to enhance the plant's

efficiency. These conditions, however, are necessary to guarantee acceptable removal of non-condensable gases. From an engineering view point, the first SCWR NPP configuration will necessitate the doubling of the mechanical and nuclear components which will increase both investment and operational cost. In turn, the fact that the second configuration requires much higher mass flow rates, will involve different dimensioning of major thermal components, i.e., turbines, heat exchangers, condenser, etc. A trade-off between these two possibilities will still necessitate a multi-objective optimization that should include appropriate economic models.

CHAPTER 5 PROPOSITION OF CANDU TYPE SCWR'S

In this chapter after at first a brief description of current CANDU systems a proposition for the thermal hydraulic circuit associated to a CANDU SCWR is presented. Some basic mechanical dimensioning and temperature profiles are also discussed in order to gain an appreciation on their order of magnitudes and thus, determining the feasibility of such type of nuclear reactor.

5.1 Principal characteristics of CANDU reactors

The CANDU (CANada Deuterium Uranium) reactors were initially developed by Atomic Energy of Canada Limited (AECL) in the 1950s and 1960s. The CANDU reactor is one of the three major commercial power reactors in operation worldwide. Currently, 48 heavy water moderator reactors, based on the CANDU design, are in operation, under construction, or under refurbishment.

A simplified view of a CANDU reactor is presented in Figure 5-1. Pressurized heavy water is heated in the primary cooling loop by fission reactions in the reactor core. The heated water is transported to the steam generator for heating the light water of the secondary cooling loop. The vapour created under 4.5 MPa goes to the turbines and produces electricity via the generator [59].

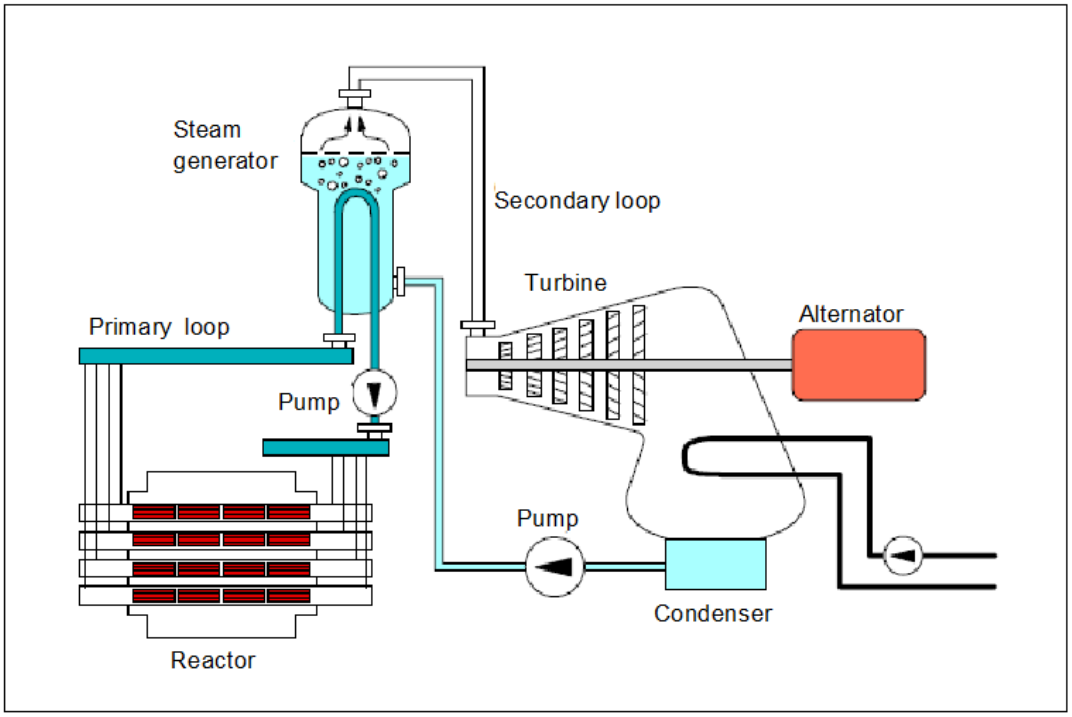

Figure 5-1: Simplified view of a CANDU reactor.

This Canadian-designed power reactor is conceptually similar to light water reactors, although it presents specific features and advantages that are not common in other reactors types.

- Instead of a pressure vessel , the reactor core is composed of 380 of pressure tubes with much smaller diameter;
- In traditional light water reactors, the pressure vessel contains the light water which acts as moderator and coolant. In CANDU reactors, the moderator and the coolant are separated from each other forming two completely independent circuits;
- The use of heavy water (D_2O) as a moderator and coolant permits natural uranium to be used as the fuel;
- The pressure tubes containing the fuel bundles are horizontal, that permits under operation refuelling.

The internal structure of a CANDU reactor is presented in Figure 5-2. Each pressure tube contains 12 fuel bundles lining end to end. Each bundle measures 0.495 m in length and has a diameter of 0.102 m, the cladding material is zircaloy. The number of fuel rods per bundle is 37, with an outside diameter of 13.1 mm[59]. The main operating conditions of a CANDU type reactor are given in Table 5-1.

Table 5-1: Typical operating condition for a CANDU type reactor[59].

Power thermal	2064 MW
Net electrical power	600 MW
Coolant pressure inlet / outlet	11.3 MPa / 10.0 MPa
Temperature inlet / outlet	266°C / 310°C
Moderator outlet temperature	71°C
Average linear heat rate	30.5 kW/m

The critical components for thermo hydraulic dimensioning of an SCWR are among others: the calandria vessel, the pressure tubes, the outlet and inlet flow collectors and the feeder pipes (Figure 5-2, Figure 5-3). In the following sections, some calculations are made to estimate the

order of magnitude of the wall thickness of these pipes if the coolant is replaced by supercritical waeter.

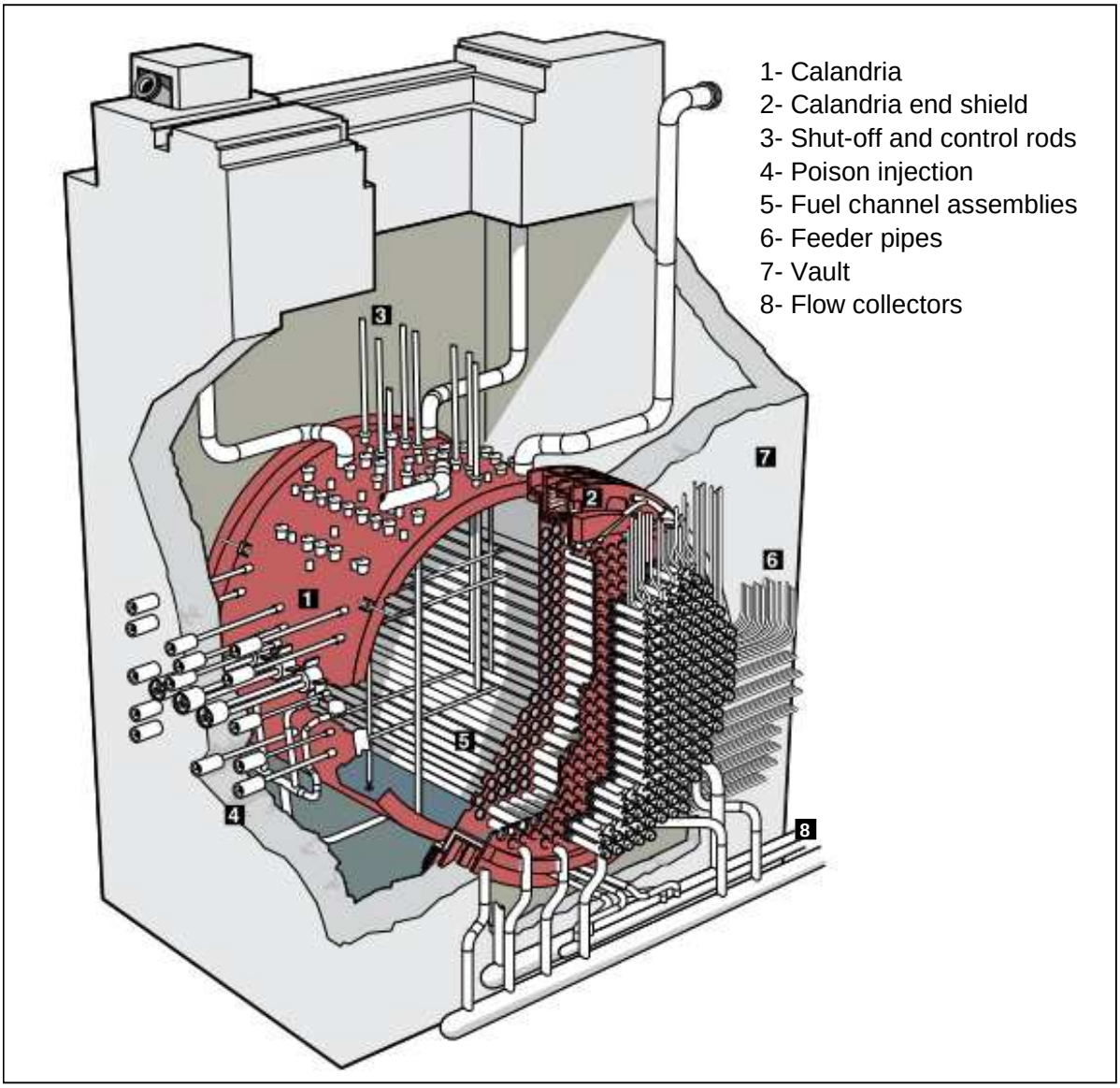

Figure 5-2: Internal structure of a CANDU reactor (taken from [60]).

CANDU units are operating worldwide: North America, South America, Europe and Asia. These nuclear power stations have consistently proven to be competitive with other types of nuclear reactors. CANDU reactors are potential candidates to be adapted to the new SCWR technology which will operate at or above supercritical conditions. The pressure tube can easily be designed and manufactured to support the high pressure of 25 MPa. However, the design and manufacturing will be more challenging for reactors with pressure vessel. Further CANDU

reactors seem to be particularly suitable for using supercritical water, especially with regard to variation of coolant density [61]. This variation may complicate the neutron flux gradient and consequently flux shaping requirements. However, the main advantage of CANDU reactors is due to the fact that the moderator and the coolant are separated and that the coolant may have less effect on the neutronics. Secondly, the density gradients can be balanced by the bi-directional flow in the neighbouring channels as shown in Figure 5-3.

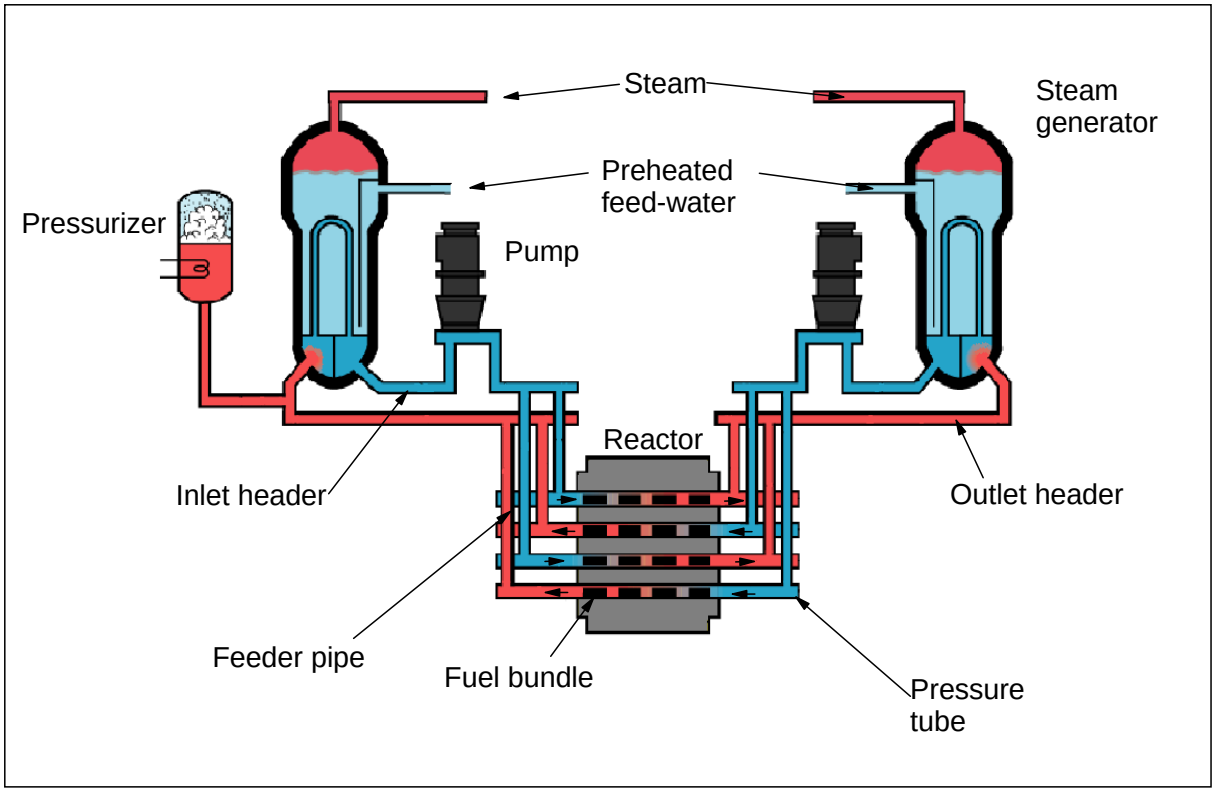

Figure 5-3: Simplified thermal hydraulic circuit of current CANDU.

5.2 Simplified thermal hydraulic circuit of CANDU type SCWR's

In this document, thermodynamic cycles with steam-reheat options have been proposed and optimized: this, however, implies technological challenges in the design of the reactor core. Nevertheless, nuclear reactors with steam-reheat have been developed in Russia since 1954. According to Saltanov *et al.* [62], the challenge is to develop a reactor which will produce a steam between 500–540°C and 8.8–12.7 MPa under a heat flux of up to 1.2 MW/m^2 with acceptable reactor-physics parameters and an economically achievable depletion of the uranium.

In 1964, the first reactor with a nuclear steam reheat was put into operation. This unit, of 100 MWe, was followed by another one of 200 MWe in 1967, and thermal efficiency for both reactors was about 37-38 %. These units consist of a uranium-graphite channel-type reactor with high pressure steam-reheat. Main thermal parameters of these systems are summarized in Table 5-2 and their thermal cycles are shown in Figure 5-4 and Figure 5-5.

Table 5-2: Main thermal parameters [63].

Parameters	**1st Unit**	**2nd Unit**
Electrical power (MW)	100–105	180–190
Thermal power (MW)	285–290	490–515
Outlet steam temperature (°C)	505–510	515–518
Outlet steam pressure (MPa)	8.6–8.8	6.9–7.4
Pressure in steam separators (MPa)	11.8–12.3	11.3–11.6
Uranium enrichment (%)	3.3	3.4

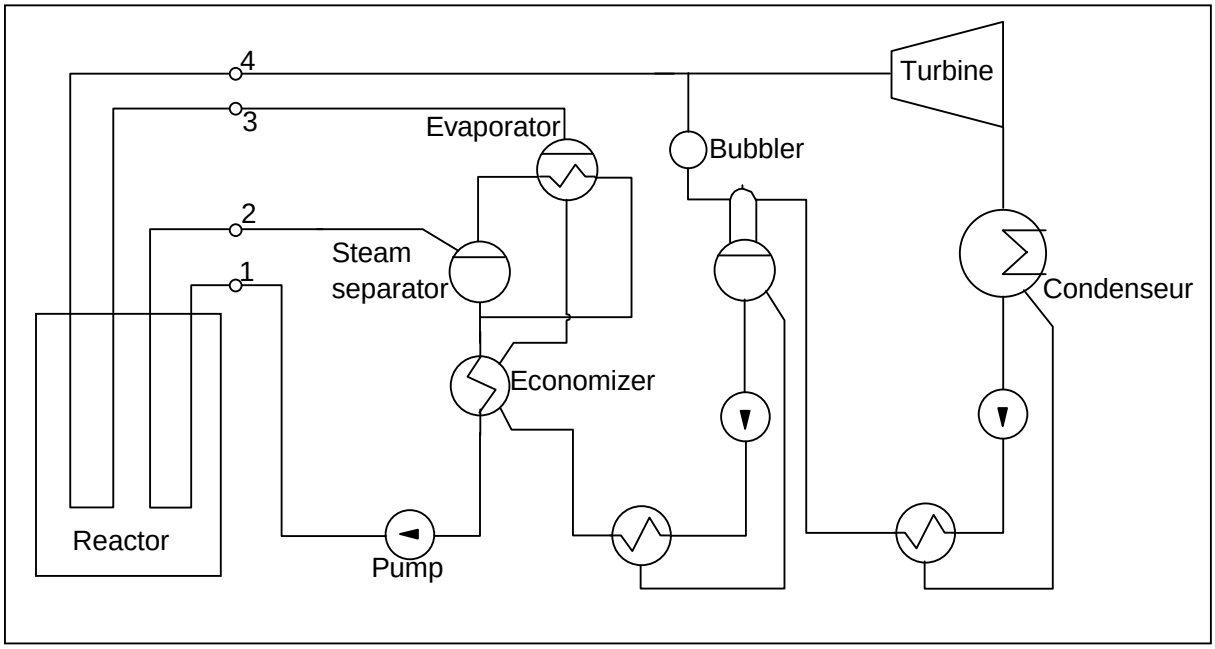

Figure 5-4: Schematic of BNPP unit 1 [64].

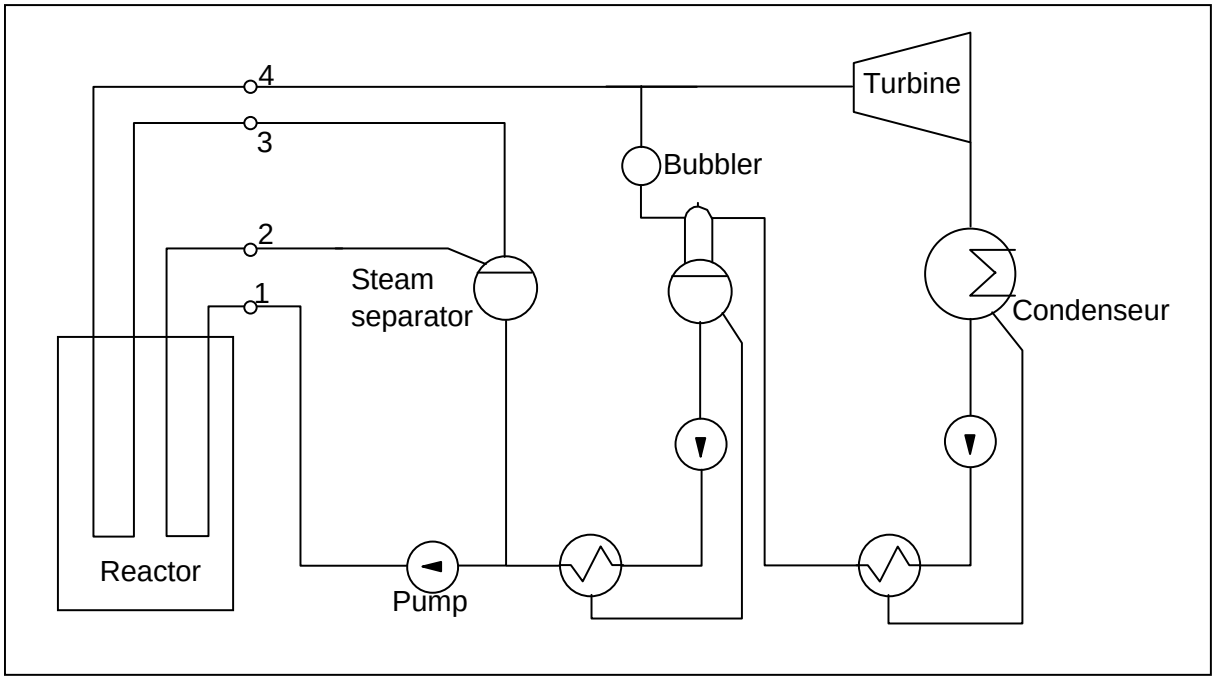

Figure 5-5: Schematic of BNPP unit 2 [63].

Both cycles are very similar; nevertheless the second unit is simplified and uses a direct cycle. The fluid enters into the reactor at state 1, under 15.5 MPa and 300°C, after being heated the steam content at the exit of the reactor (state 2) is around 33.6 % for the first unit, and 31 % for the second unit [65]. At state 3, the steam passes once again through the reactor core for the first unit, under 11 MPa and 316°C, to leaves at state 4 under a pressure of 10 MPa and a temperature of 510°C. For the second unit, it enters at state 3 with a pressure of 13.2 MPa and temperature of 328°C and leaves at state 4 at 508°C and 11 MPa. In the later unit, the steam is superheated in a U-shaped channel (Figure5-6), the fluid goes through three fuel element downwards and then through the next three fuel element upwards [65]. This design enable a reduction of the graphite temperature by 100°C in comparison with the design used in the first unit, in which steam enters by the central channel (replaced by a control rod in the new design) and goes through the 6 channels upwards.

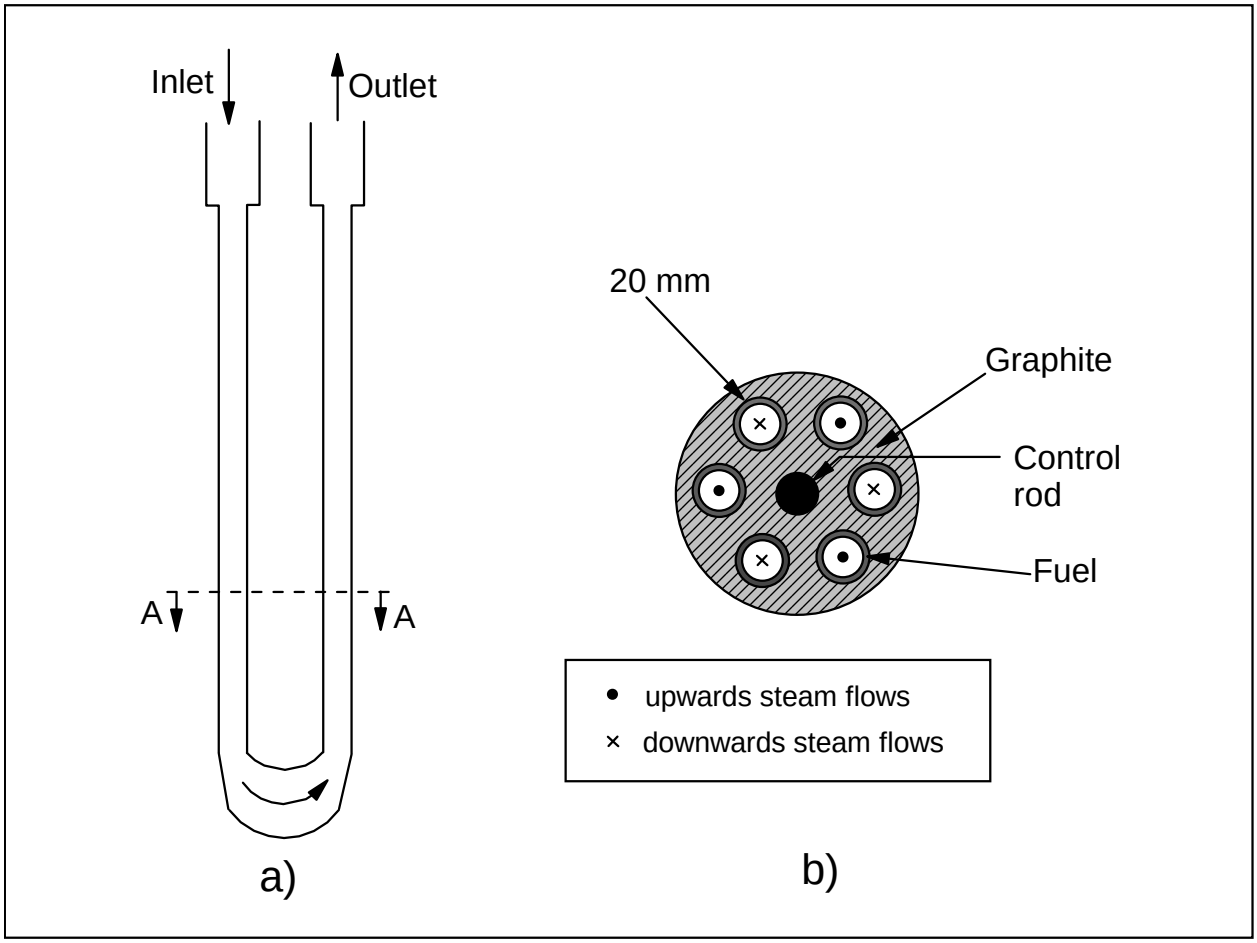

Figure 5-6: a) U-shaped steam superheating channels. b) Cross-section of steam-reheat channel [65, 66].

Another improvement between these two units is the arrangement of the steam superheating channels in the reactor core. In the first unit, the steam reheat channels were located in a ring alternating with the evaporating channels as shown in Figure 5-7 [64]. Whereas in the second unit reheat channels are in the central part in alternate location with respect to the evaporating channels as seen in Figure 5-8 [65]. The thermal neutrons density distributions in the radial direction for both reactors (Figure 5-7 and Figure 5-8) show that the second configuration enables a more uniform distribution to be achieved [65]. This is a very interesting aspect for the design of the distribution of the superheating channels and the supercritical channels of future CANDU type SCWR core. In fact, it is easier to work with a thermal neutron distribution which is almost uniform. Thus, an appropriate distribution of both kinds of channels should be accomplished.

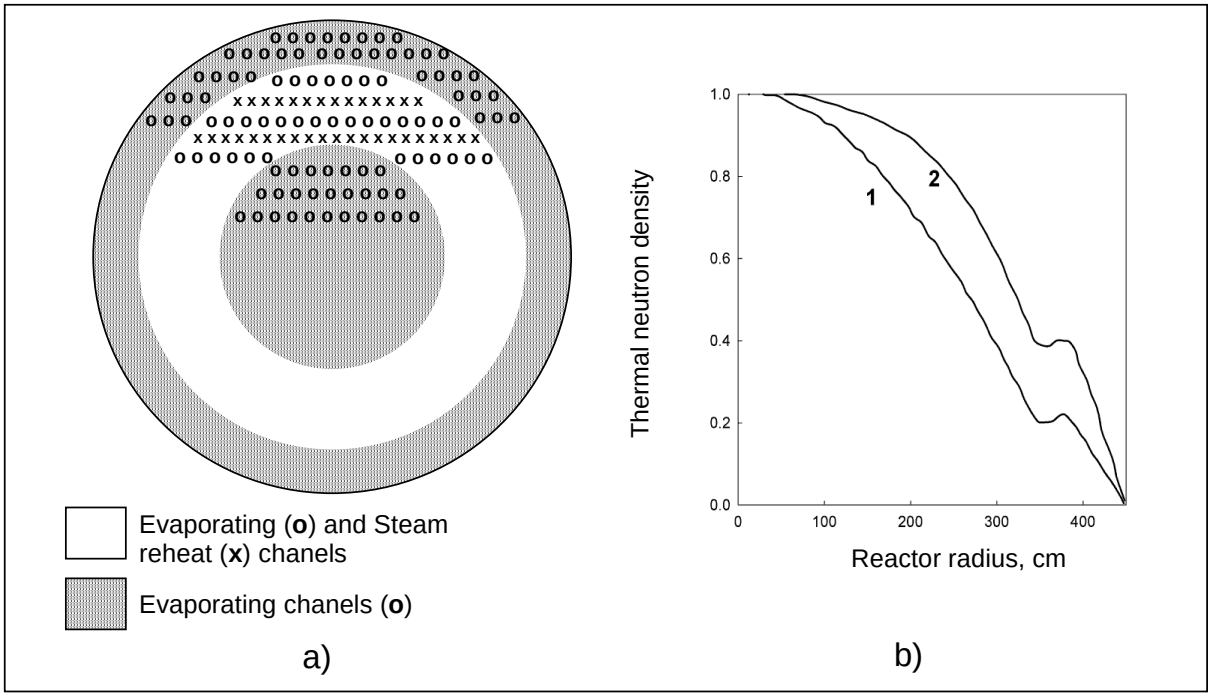

Figure 5-7: a) Unit 1 channels layout. b) Radial thermal neutron distribution (1-begginning of operating period, 2- end of the operating period) [64].

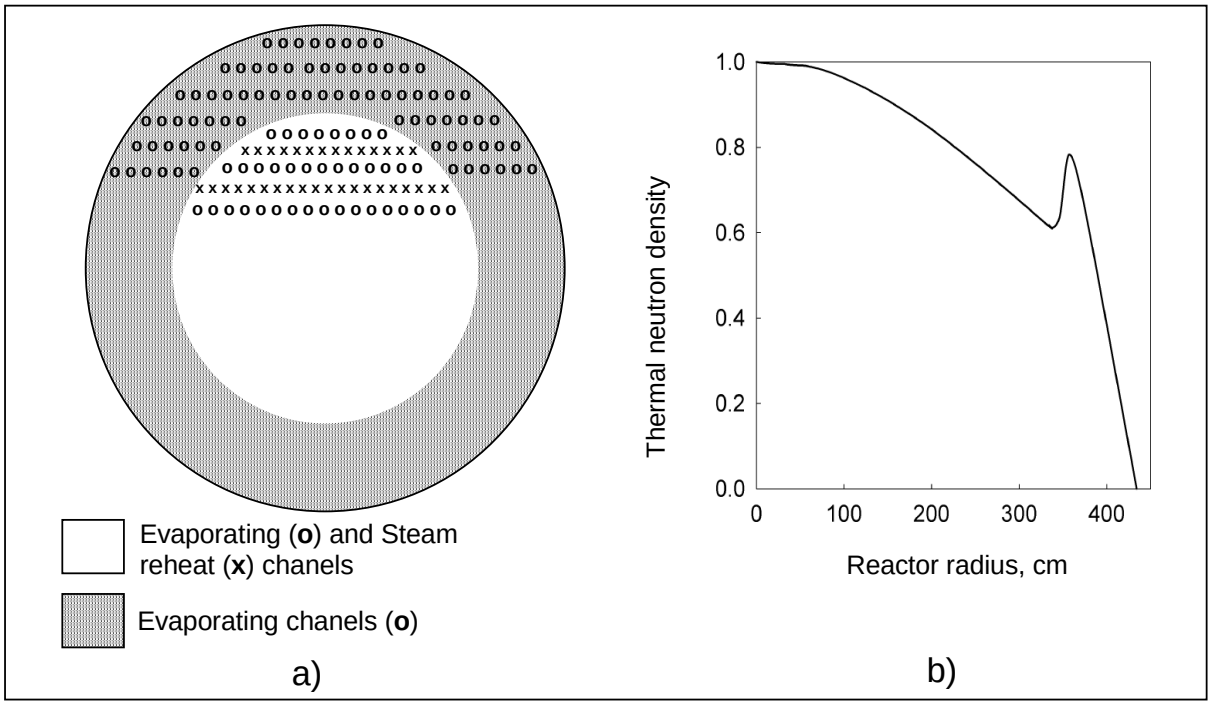

Figure 5-8: a) Unit 2 channels layout. b) Radial thermal neutron distribution [65].

The United States Atomic Energy Commission (USAEC) was in charge of an active program for the development and demonstration of Boiling Water Reactors (BWRs) with nuclear steam reheat. This program ensured the construction of three reactors: Boiling Reactor Experiment V (Borax-V) entered into operation in 1962 followed by the Boiling Nuclear Superheater (BONUS) in 1964 and Pathfinder in 1966 [67]. The feasibility of two types of reactors was demonstrated, one in which steam was generated and reheated in the same core and the other one used an external reheating with another source. Some problems of corrosions, erosion and deposits on the surface of fuel elements have been encountered during this program. Furthermore, fission product carry-out in direct-cycle system and inadvertent flooding of the reheating zone lead to reactivity changes. The principal parameters of these reactors are summarized in Table 5-3.

Table 5-3: Main thermal parameters of BWR NPPs [67].

Parameters	**BORAX-V**	**BONUS**	**Pathfinder**
Net electric Power (MW)	3.5	16.5	62.5
Thermal power (MW)	20	50	200
Net cycle thermal efficiency (%)	-	33	31
NPP steam cycle	Direct	Direct	Direct
Reheating-zone location	Central or peripheral	Peripheral	Central
Nominal operating pressure (MPa)	4.1	6.7	4.1
Turbine inlet-steam pressure (MPa)	2.4	5.9	3.7
Saturated steam temperature (°C)	254	284	254
Reheated steam temperature (°C)	454	482	441
Maximum fuel-sheath temperature (°C)	590	635	677

This worldwide experience of reactors with steam-reheat provides, however, important information on physical and engineering challenges for future SCWR designs. It is obvious that a

lot of work should be carried out to improve steam-reheat channels design and reactor design. The above experiments constitute a good starting point.

To this aim, a simplified thermo hydraulic circuit appropriate to the SCWR is presented in Figure 5-9; this figure also illustrates the concept of steam-reheat inside the SCWR core.

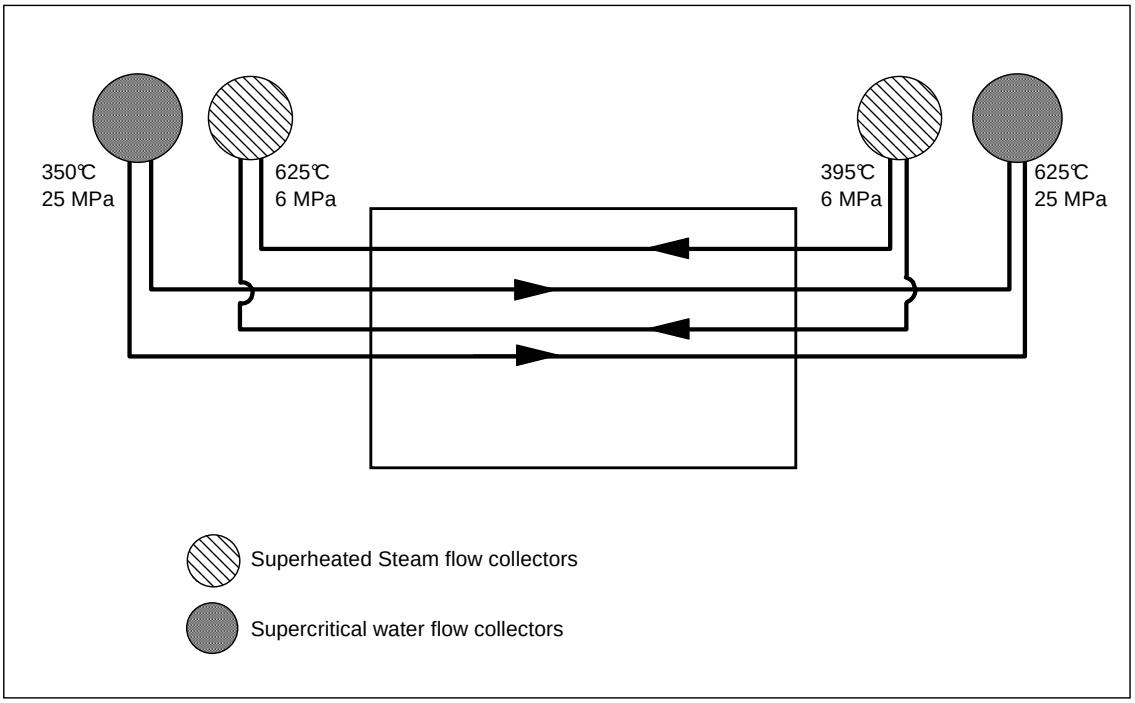

Figure 5-9: Proposition of a thermo hydraulic circuit for the SCWR.

The bidirectional flow configuration and alternating supercritical and the steam reheat channels should enable a reduction of axial temperature gradients and almost the same average temperature on both sides. Moreover, with the conditions of pressure and temperature given on the Figure 5-9, the supercritical channels require 1870 MW whereas the steam-reheat channels require only 430 MW of thermal power. In a CANDU type reactors the radial thermal neutron distribution is quite uniform, thus the power of the supercritical channels (SC) and the reheating channels (RC) should be almost the same (i.e., both channels are subjected to the same neutron flux distribution). The energy balance between these two channels can be expressed as follows:

$$\dot{Q}_{SC} = \dot{Q}_{RC} \tag{5-1}$$

$$\dot{m}_{SC}\Delta h_{SC} = \dot{m}_{RC}\Delta h_{RC} \tag{5-2}$$

$$\rho_{SC} V_{SC} A_{SC} \Delta h_{SC} = \rho_{RC} V_{RC} A_{RC} \Delta h_{RC} \quad (5\text{-}3)$$

The values of density as well as the values of the variation in enthalpies are fixed by the system, thus the only way to satisfy equation (5-3) is to balance the product between the flow cross-section of the channels and the velocity.

As shown in Chapter 2, the density changes sharply near the critical point, thus an arithmetic mean is used to express ρ_{SC}. After replacing by the appropriate values in the equation (5-3), the product of velocity and section for the reheat channel is about 37.5 times higher than that for the supercritical ones. This ratio is very high and it should be considered in detail in the design of the channels.

The Russian experience has shown that central reheating with alternating steam-reheat channels and supercritical channels provides better neutron flux distributions. However, a lot of work is still necessary to determine the best arrangement by performing thermal-hydraulic calculations linked to neutronic considerations. In particular, to better understand how density changes, which varies from 625 kg/m^3 at the inlet of the reactor to 67 kg/m^3 at the outlet, may affect the reactivity of the system. It must be pointed out that, the question of handling the high power difference between the supercritical water channels and the steam-reheat channels is still open to a more rigorous study.

5.3 Mechanical dimensioning of critical core components

This section presents some calculations carried out to determine pipe wall thickness for different pipe diameters and materials. The equations used herewith are taken from AMSE code Section 304.1.2 “straight pipe under internal pressure” [68]. Two expressions of thickness are used depending on the ratio of the thickness calculated and the outside diameter of the pipes. Indeed, if this ratio is higher than 1/6 the theory of thin shell is not applied anymore. Both expressions are expressed as follow:

$$t_w = \frac{P(d + 2c)}{2[SE - P(1 - Y)]}; \qquad \text{available for } t_w < \frac{D}{6} \quad (5\text{-}4)$$

$$t_w = \frac{d + 2c_I}{2}\left[\exp\left(\frac{1.155P}{S}\right) - 1\right]; \qquad \text{available for } t_w > \frac{D}{6} \tag{5-5}$$

The following nomenclature is used in these equations:

t_w: pressure design thickness

P: internal design gage pressure

D: external diameter

d: inside diameter of pipe

S: stress value for material from Table A-1 in ASME code

Y: coefficient from Table 304.1.1 in ASME reference

c: the sum of the mechanical allowances (thread or groove depth) plus corrosion and erosion allowances

According to ASME code, the minimum thickness should not be less than:

$$t_m = t_w + c \tag{5-6}$$

The high pressures and temperatures conditions are critical constraints for materials selection. Indeed, the allowable stress of materials decreases with temperature. Two materials have been selected for their best allowable stress for the temperature that concerns SCWR's (about 625°C) among the tables given by ASME code [68]. These materials are classified as nickel alloy. The first one is called Hastelloy and it is composed of nickel, chromium, molybdenum and iron. This material is well known for the high-performance under high-temperature and high-stress service, and it is a highly corrosion-resistant metal alloy. The second one is Inconel-625, the composition of which is predominantly nickel, with chromium and molybdenum. This alloy is mostly used in an environment that requires resistance to heat and corrosion and also retains strong mechanical properties.

To illustrate the allowable stress of these two materials which are classified as nickel alloy, Figure 5-10 shows the variation of allowable stress (MPa) given by ASME [68] versus the temperature (°C). The values for the common stainless steel 316L have also been added as a reference case.

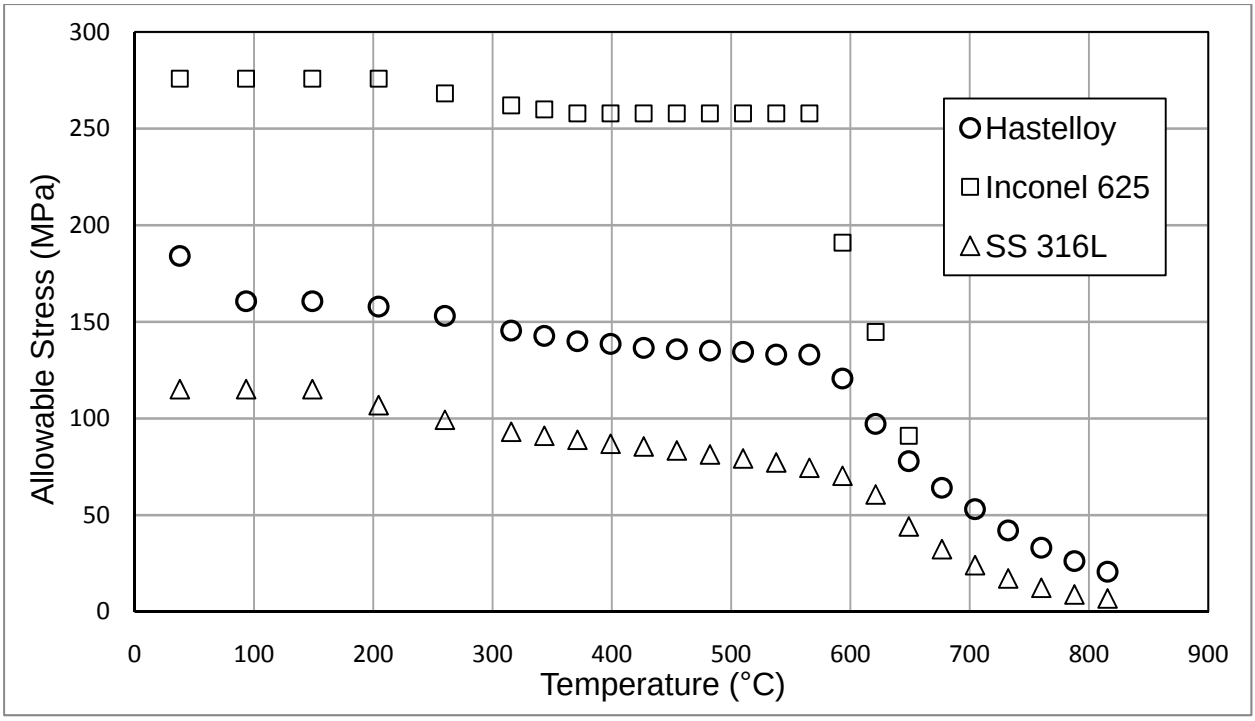

Figure 5-10: Variation of the allowable stress versus temperature for three different materials.

As shown in Figure 5-10, Inconel-625 has a high allowable stress for temperatures under 600°C after which it starts to decrease quickly as compared to the other materials. The range of temperature for the SCWR is around 620-650°C, which corresponds to the last two points on the graphic for Inconel-625.

A lot of work is currently carried out to find new materials performing better at high temperatures and pressures. Overcoming the lack of data concerning the corrosion of materials under these conditions constitutes a point of interest in current researches [69]. Corrosion has a negative impact on the mechanical properties particularly on the allowable stress. Therefore it is very important to have a perfect understanding of the behaviour of the materials in their working environment. Thus results of future and current work are fundamental for the choice of the appropriate materials for building the reactor core as well as thermal hydraulic circuits.

5.3.1 Pressure channel

Current pressure channel in CANDU-6 reactor has an inside diameter of 103.38 mm. Calculations of wall thickness, using equations 5-4 and 5-5, are performed for Hastelloy and Inconel-625 under an operating pressure of 25 MPa. In addition, the thickness calculations were

also carried for the 120 mm-pressure tube proposed by Chow *et al.* [70]. The wall thickness is calculated for two temperatures close to 625°C: 621.1°C and 648.9°C as given by ASME [68] table. The coefficient Y is taken equal to 0.4 according to ASME code and the tolerance for corrosion is assumed to be 0.5 mm as expressed for cases where no specifications are given. Allowable stress given by ASME is summarized in Table 5-4 along with the calculated thickness.

Table 5-4: Thickness of pressure tubes.

Materials	**Inside diameter (mm)**	**Temperature (°C)**	***S*** **(MPa)**	t_m **(mm)**
Hastelloy	103.38	621.1	97.22	16.37
	103.38	648.9	77.91	21.24
	120	621.1	97.22	18.90
	120	648.9	77.91	24.54
Inconel-625	103.38	621.1	144.80	10.55
	103.38	648.9	91.01	17.66
	120	621.1	144.80	12.15
	120	648.9	91.01	20.40

As expected, Inconel-625 offers the lowest thickness for each case; however, these calculations are performed without a precise consideration of corrosion effects. It is a good estimation of wall thickness for pressure channels but more complex and detailed calculations are still necessary. The impact of the temperature increase on the wall thickness is also clearly shown in Table 5-4, e.g., for a temperature increase from 621 to up to 649°C the wall thickness increases by 7 mm. Moreover, it is shown that both Hastelloy and Inconel-625 are suitable for manufacturing SCWR pressure tubes. For example the thickness required for a 316L stainless steel pipe with an inside diameter of 120 mm, at 621.1°C is 28.94mm. This thickness is 2.3 times the thickness required for Inconel-625 pipes and 1.5 times for Hastelloy ones.

It is obvious, however, that from a nuclear view point the mechanical calculation is not enough. In fact, the composition of these alloys may largely contribute in absorbing neutrons, which may require using enriched uranium for the fuel. Furthermore, it is apparent that mechanical properties

can strongly be affected by the absorption of neutrons; this constitutes another important subject of study that should be addressed.

5.3.2 Inlet / outlet flow collectors and feeder pipes

A second series of calculations are performed to evaluate the wall thickness required for the feeder pipes as well as for the inlet and outlet flow collectors. The actual inside diameter of CANDU reactors inlet and outlet flow collectors are 370 mm and 406 mm, respectively. For a SCWR, the outlet flow collectors should withstand critical conditions of 625°C and 25 MPa. CANDU feeder pipes have an inside diameter of 5 cm. The wall thicknesses obtained for these components by ASME code are summarized in Table 5-5.

Table 5-5: Wall thickness of inlet/outlet flow collectors and feeder pipes.

Materials	**Inside diameter (mm)**	**Temperature (°C)**	***S*** **(MPa)**	t_m **(mm)**
Hastelloy	370	621.1	97.22	56.90
	370	648.9	77.91	74.21
	406	621.1	97.22	62.38
	406	648.9	77.91	81.36
	50	621.1	97.22	7.75
	50	648.9	77.91	10.13
Inconel-625	370	621.1	144.80	36.23
	370	648.9	91.01	61.51
	406	621.1	144.80	39.70
	406	648.9	91.01	67.43
	50	621.1	144.80	4.91
	50	648.9	91.01	8.39

Khartabil *et al.* [71] proposed to terminate the outlet feeders in a single feeder block. One or two outlet connection could transport the coolant from this feeder block to the header as shown in Figure 5-11. This solution overcomes the mechanical challenges of pipes wall thickness imposed by high pressure and temperature. Other concepts are also being evaluated.

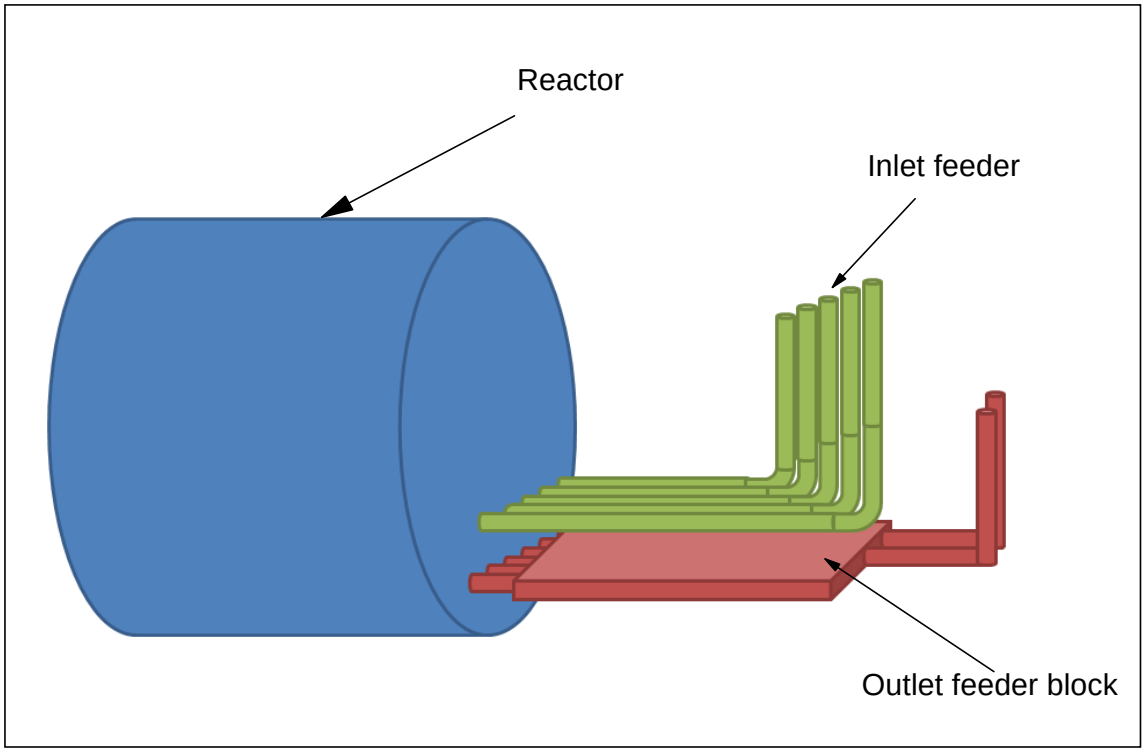

Figure 5-11: Scheme of feeder pipes option with one block at the outlet [71].

5.3.3 Distribution of temperatures in the channel

The conceptual design for the SCWR channel is shown in Figure 5-12. It consists of a pressure tube in contact with the moderator which operates at a temperature of about 80°C. The material envisaged for the pressure tube is a high strength, creep resistant zirconium alloy Excel (ZR-3.5% SN- 0.8%NB-0.8% MO-1130ppm O) developed by AECL in the 1970s [70]. The pressure tube is thermally insulated by an insulator which is porous Yttria Stabilizied Zirconia (YSZ). This material must have an excellent corrosion resistance and provide an effective thermal barrier that can withstand thermal stresses. A perforated metal liner is added to protect the insulator from the fuel bundles damages and from erosion by coolant flow. The fuel bundle consists of 43 elements with an outside diameter around 11.5 mm. The cladding is directly in contact with the fuel pellets.

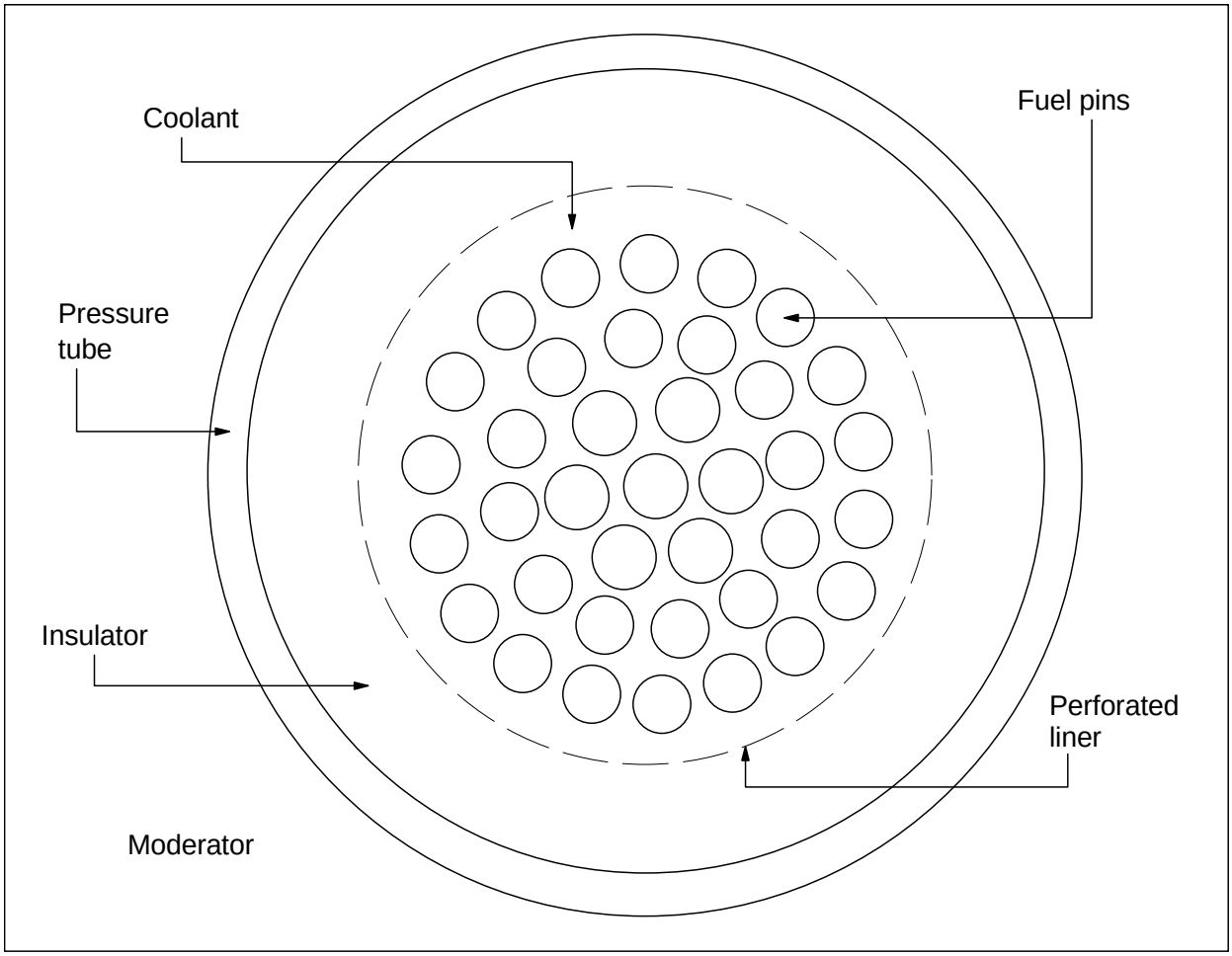

Figure 5-12: An insulated pressure tube design of the CANDU-SCWR fuel channel.

Simple calculations have been performed to establish the radial temperature distribution between the coolant and the moderator as well as the temperature distribution between the center of a pin and the coolant (see Figure 5-12). To perform these calculations the thermal conductivity of each material is necessary.

The thermal conductivity for a pressure tube made in Zr-2.5% Nb is expressed by the following equation [61] (5-7).

$$k_{PT} = 16.85 - 2.186 \times 10^{-3}T + 8.899 \times 10^{-6}T^2 \text{ , W·m}^{-1}\text{·K}^{-1}, \quad (5\text{-}7)$$

where T is the temperature in Kelvin.

The insulator proposed for this fuel channel is a ceramic with a porosity of 70% to reduce the heat loss from the coolant to the moderator. Chow *et al.* [70] have proposed that the thermal conductivity can be estimated by:

$$k_{in} = 0.3 \times k_{Zr0_2} + 0.7 \times k_{H_2O} \text{ , W·m}^{-1}\text{·K}^{-1} \quad (5\text{-}8)$$

where $k_{Zr0_2} = 2.7$ W/m.K and it is assumed to be a constant in the temperature range of interest; k_{H_2O} as a function of the temperature obtained from XSteam library [31] is shown in Figure 5-13.

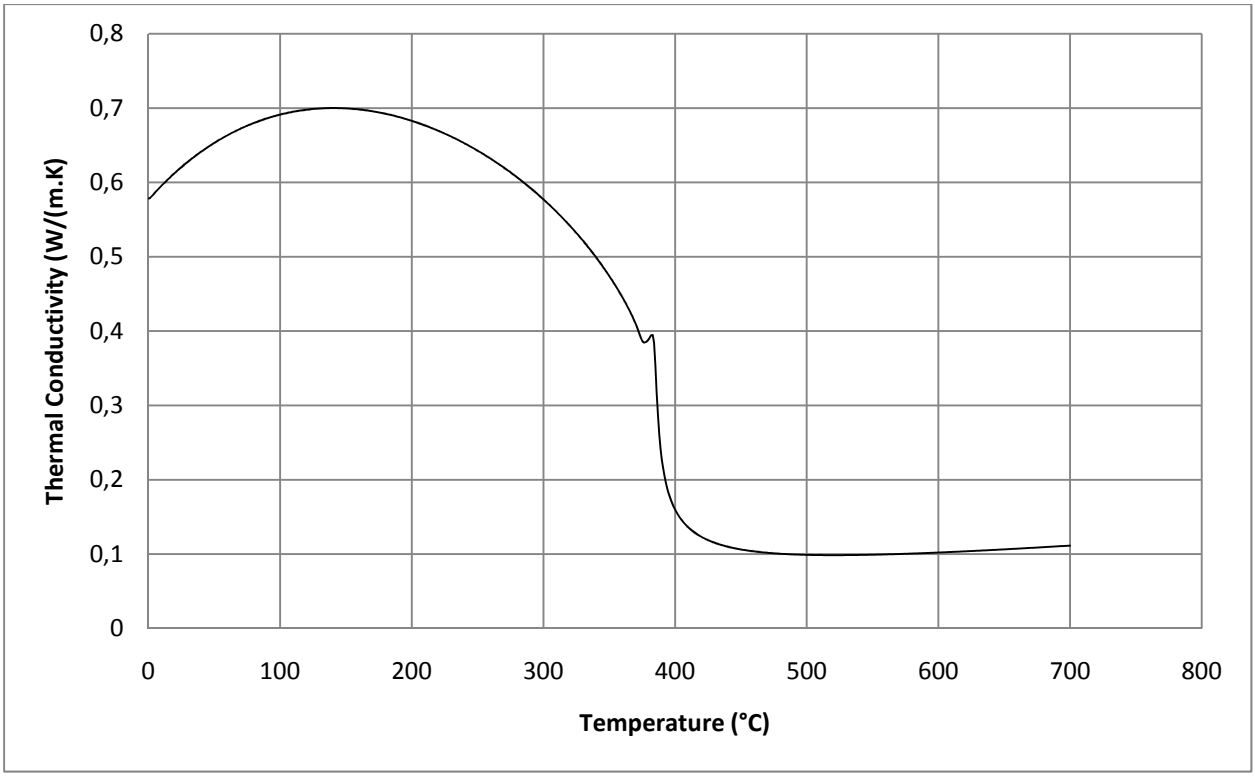

Figure 5-13: Thermal conductivity of water as a function of temperature at 25MPa.

The heat transfer coefficient for the coolant varies from 8527 W/m^2.K at the inlet of the reactor to up to 3228 W/m^2.K at the outlet [70].The thermal conductivity of the fuel cladding selected by EACL, as a function of the temperature in Kelvin, is given by [72]:

$$k_{cl} = a + b\,T + cT^2 \text{ , W·m}^{-1}\text{·K}^{-1} \quad (5\text{-}9)$$

The evaluation of temperature at the pin center has been estimated by using the conductivity integral method of the fuel. The conductivity is given with Kang [73] correlation: it is the conductivity of fuel with dissolved fission products.

$$k_{fuel} = \frac{1}{0.126+0.226 \times 10^{-3}\, T}\ , \mathrm{W \cdot m^{-1} \cdot K^{-1}} \qquad (5\text{-}10)$$

According to the author this value is higher than that of UO_2.

Heat transfer calculations are performed to evaluate the radial temperatures profile of the channel (see Figure 5-14). The average temperature of the coolant (t_4) is taken to be 625°C, which is the temperature at the outlet of the channel. The moderator is assumed to run at a constant temperature of 80 °C, thus it is supposed that t_1=80°C.

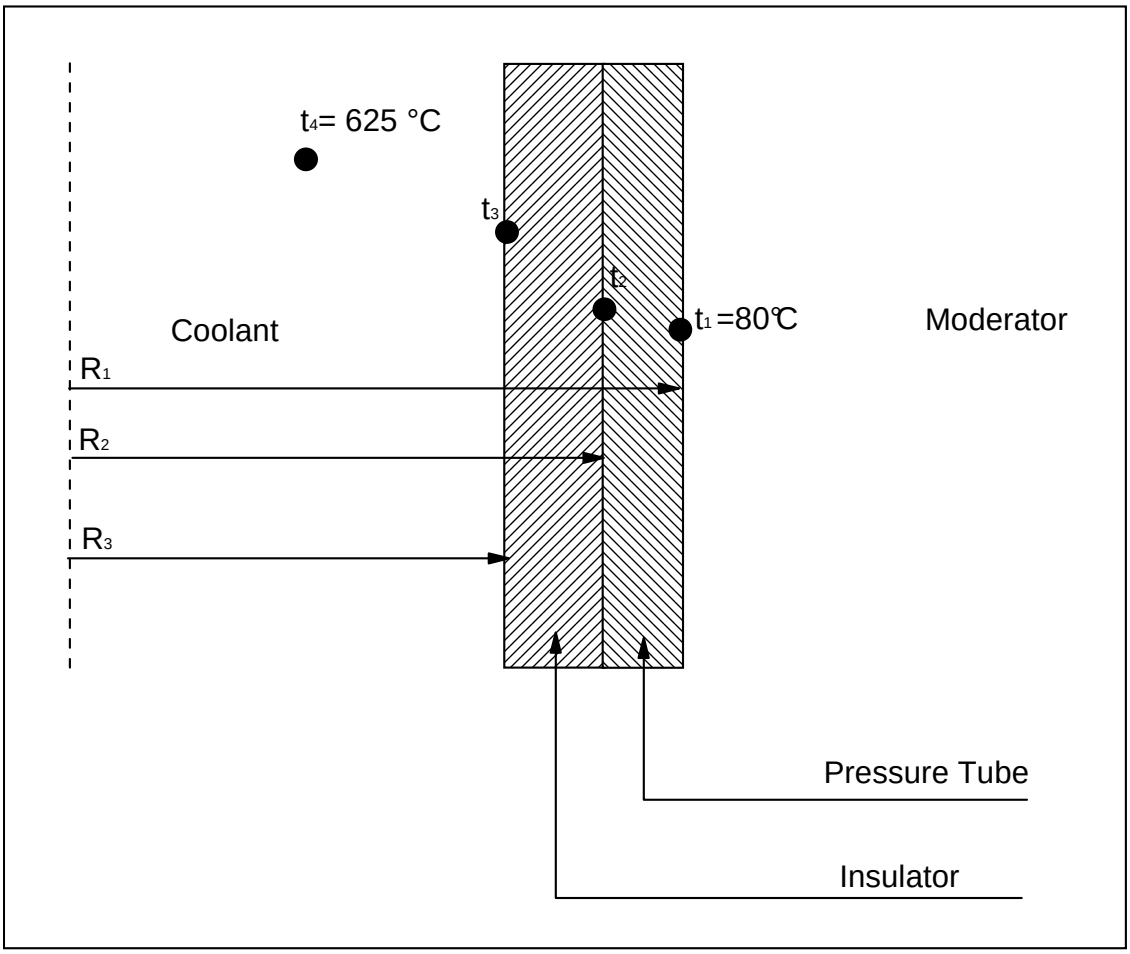

Figure 5-14: Transversal view of the pressure tube with insulator.

The heat transfers by conduction inside the pressure tube as well as inside the insulator are expressed as follows [74]:

$$t_2 = t_1 + \frac{\phi_l}{2\pi k_{PT}} \ln\left(\frac{R_1}{R_2}\right) \tag{5-11}$$

$$t_3 = t_2 + \frac{\phi_l}{2\pi k_{in}} \ln\left(\frac{R_2}{R_3}\right) \tag{5-12}$$

The heat transfer coefficient used in performing the calculation is equal to 3228 $W \cdot m^{-2} \cdot K^{-1}$ [70]. The expression of the temperature for the coolant is expressed by the equation (5-12) by using the same nomenclature shown in Figure 5-14 [74]:

$$t_4 = t_3 + \frac{\phi_l}{2\pi R_3 h} \tag{5-13}$$

Thus, after solving the equations (5-10), (5-11) and (5-12), the linear heat flux ϕ_l, which satisfies a coolant temperature (t_4) of 625°C, is about 28 kW/m. The calculated temperatures indicated in the Figure 5-14 are summarized in Table 5-6.

The second part of these temperature calculations consists of the evaluation of the temperature between the center of a fuel pin and the coolant (Figure 5-15). It assumed that the fuel pin is surrounded by a coolant with a uniform temperature of 625°C. Note, that we have also neglected the conductance between the fuel and the cladding. To perform heat transfer calculations, a uniform heat flux is considered along the fuel pin. It is obvious that it constitutes an approximation, but it provides a good idea on radial temperatures distributions. In literature, the thermal power of a supercritical channel is about 8.5 MW [61]. There are 43 fuel-elements with a length of 5.772 m in one channel. Thus, the average linear heat flux of one pin is about 34 kW/m.

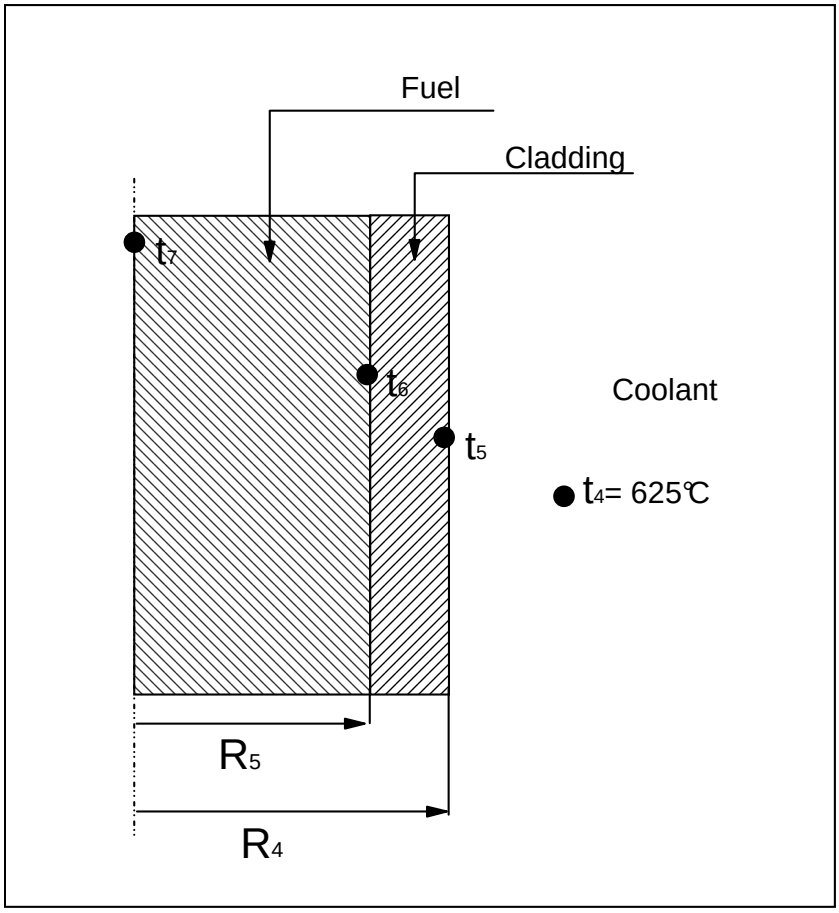

Figure 5-15: Transversal view of the fuel pin.

The temperature at the cladding outer surface (t_5) is given by:

$$t_5 = t_4 + \frac{\phi_l}{2\pi R_4 h}, \tag{5-14}$$

where $\phi_l = 34\ kW/m$ and h= 3228 W·m^{-2}·K^{-1}. Note that this value of h is 2.5 times lower than the value of the heat transfer coefficient of a Candu-6, indeed according to Chow *et al*. [70] h=8114 W·m^{-2}·K^{-1}.

The conduction inside the cladding is expressed as follows [74]:

$$t_6 = t_5 + \frac{\phi_l}{2\pi k_{Cl}} \ln\left(\frac{R_5}{R_6}\right) \tag{5-15}$$

The temperature at the center of the fuel pin (t_7) is determined by using the integral of conductivity expressed as:

$$\int_{t_6}^{t_7} k_{fuel} = \frac{\phi_l}{4\pi} \tag{5-16}$$

The calculated temperatures are summarized in Table 5-6. Note that these calculations are quite basics and are supposed to give an idea of the likely distribution of radial temperature in the channel.

Table 5-6: Radial temperatures in the channel.

Location	**Temperature (°C)**
t_1	80
t_2	108
t_3	607
t_4	625
t_5	920
t_6	931
t_7	2431

As shown in Table 5-6, the temperatures of the cladding (t_5 and t_6) are quite high. As discussed in previous sections, the temperature has a significant impact on the tensile strength of materials (see Figure 5-10). Nevertheless, these tubes are not under the pressure of the coolant of 25 MPa, however, the gas emitted by the fission products may have an impact on the structure of the pipes. In addition, the typical melting point of stainless steels is about 1400°C, thus the temperatures reached are lower by 470°C. Some pilot runs should be carried out, to be confident with the strength level of the cladding.

The temperature obtained at the center of a pin (t_7) seems to be quite high, on the other hand, the melting point of UO_2 measured by Kang *et al.* [75] is about 2815 ±20 °C. Thus, the temperature

calculated at the center of the fuel pin is lower than the melting point; however a higher range between the real temperature of the fuel and the melting point is required for safety concerns. Moreover, these calculations are performed with the highest values of the temperature of the coolant (625°C), and certainly, the linear heat flux at the outlet of the channel is lower than the 34 kW/m considered in these calculations. Nevertheless, it is quite interesting to see the order of magnitudes of these temperatures and it clearly shows the critical issue of the selection of the materials as well as the wall thickness of the pipes. On the other hand, the ceramic insulator allows low temperatures to be achieved in the pressure tube (t_1 and t_2), which means lower stress and thus lower wall thickness for these pipes.

Peiman *et al*. [61] carried out heat loss calculations along the pressure-channel of SCWRs. The calculations were performed for two fuel channel options: one with a ceramic insulator as seen in Figure 5-16 and the other with a gaseous insulator similar to that of current CANDU-6 as seen in Figure 5-17.

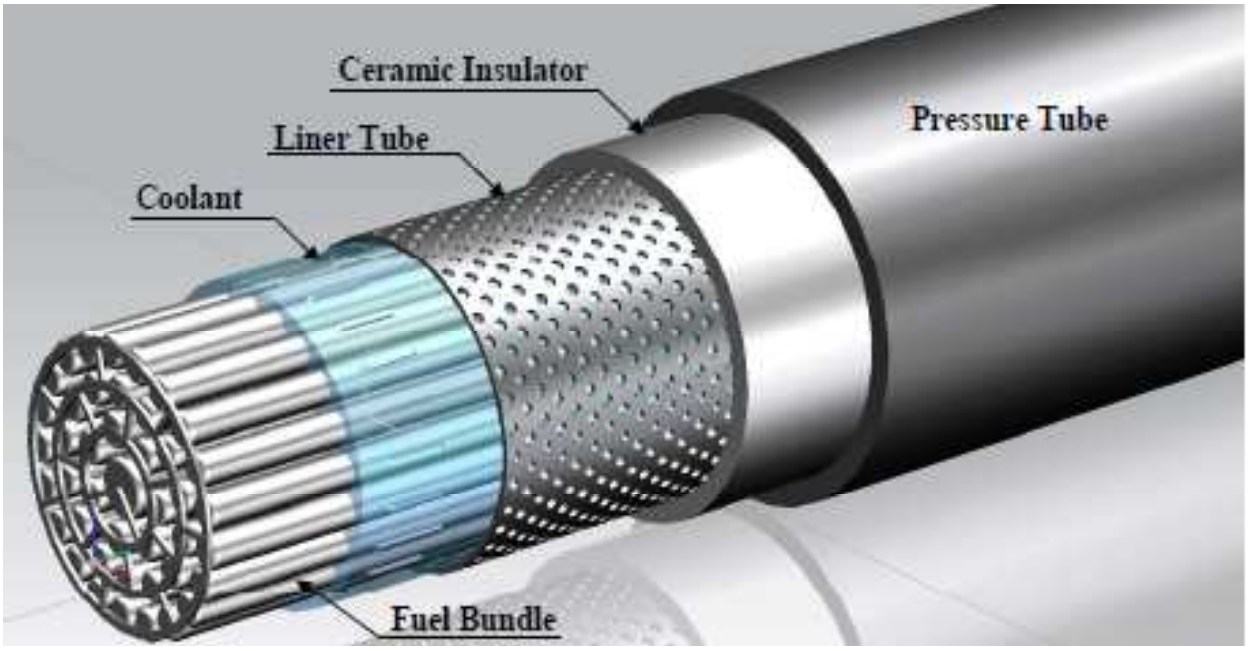

Figure 5-16: View of ceramic-insulated fuel-channel [61]

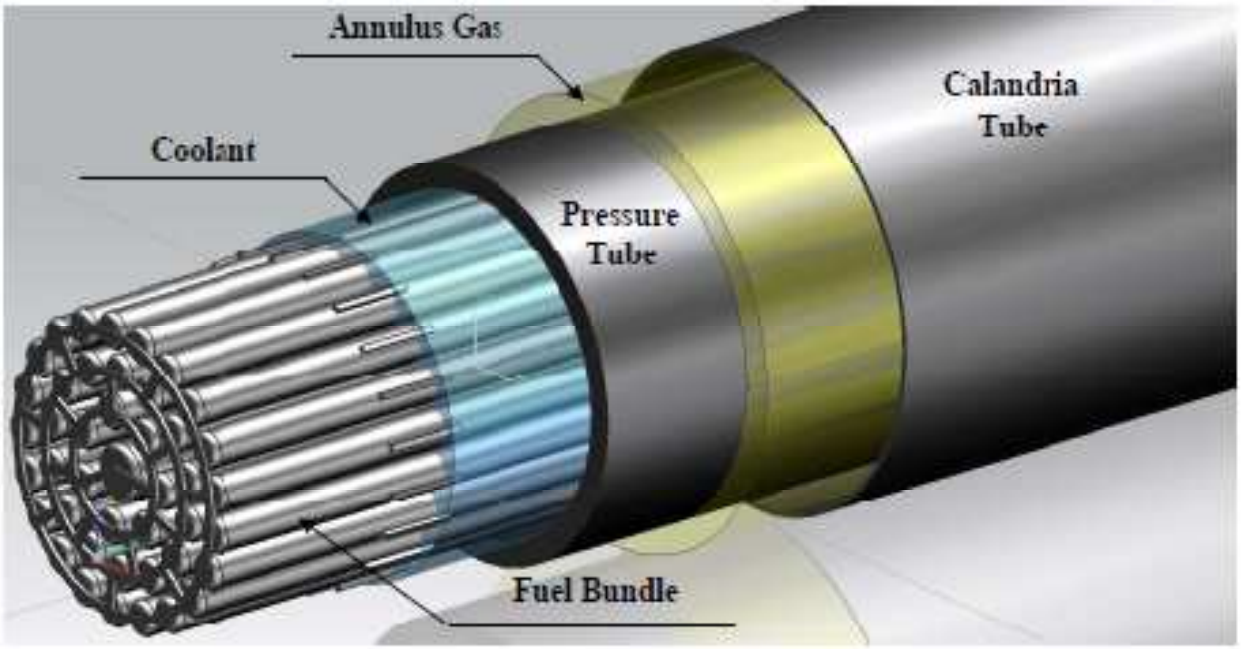

Figure 5-17: View of CANDU-6-type fuel-channel [61]

Each thermal resistance has been calculated and the heat loss is estimated as:

$$Q = \frac{T_{coolant} - T_{moderator}}{R_{total}} \tag{5-17}$$

Where R_{total} is the total thermal resistance of the fuel channel components. SCW channels and steam-reheat (SR) channels have been treated separately. The operating parameters are summarized in Table 5-7 [62] and they have been used to estimate the heat losses. The variation of the temperature along the channel is presented in Figure 5-18 [62] for a CANDU-6-type fuel-channel.

The result of this study shows that the heat losses for the CANDU-6-type fuel channel with ceramic insulation are 3 times higher than those for gas insulated channel. On the other hand, YSZ insulator has a lower neutron absorption cross-section. The same remark can be also made for the material used for the pressure tube. The material envisaged such as Zr-2.5%Nb has a good corrosion resistance and high creep strength. Some compromise has to be made between heat losses and physical or mechanical properties of materials for the next generation of SCWR's fuel-channels.

Table 5-7: Operating parameters [61].

Parameter	**Unit**	**SCWR**	
Electric Power	MW	1220	
Thermal Power	MW	2540	
Thermal Efficiency	%	52	
Coolant		H_2O	
Moderator		D_2O	
Pressure of SCW at Inlet / Outlet	MPa	25.8	25
Pressure of SHS at Inlet / Outlet	MPa	6.1	5.7
T_{in}/T_{out} Coolant (SCW)	°C	350	625
T_{in}/T_{out} Coolant (SR)	°C	400	625
Mass flow rate per SCW/SR Channel	kg/s	4.37	10
Thermal Power per SCW/SR Channel	MW	8.5	5.5
# of SCW/SR Channels		220	80
Heat flux in SCW/SR Channel	kW/m^2	970	628
Fuel Bundle		Variant-18 (42 elements with outside diameter of 11.5mm and one element with an OD of 18 mm)	

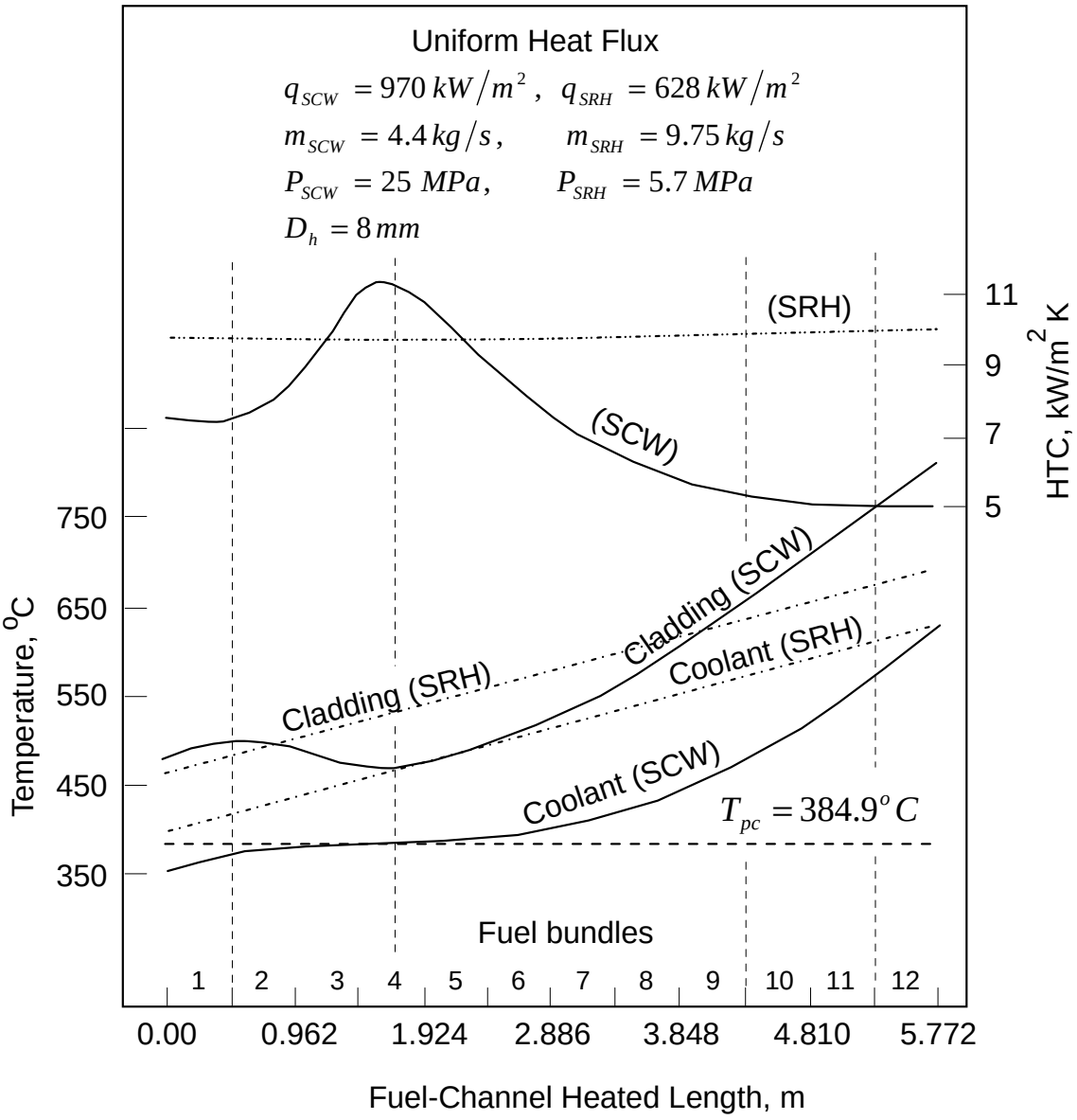

Figure 5-18: Coolant and cladding temperatures and heat transfer coefficient profiles [61].

CONCLUSION

In this work an innovative optimization technique is applied to thermodynamic cycles proposed to run future SuperCritical Water-cooled Reactors. The proposed methodology is based on coupled calculations implemented around a genetic algorithm and a series of thermodynamic plant models. To this aim, the in house optimization software "Boundary Exploration Search Technique" (BEST) developed at the institute of Nuclear energy by Dipama *et al*.[52] is linked to a Matlab plant simulator via a "Dynamic Data Exchange" (DDE*) protocol. To run the optimization software, several optimization variables, objectives function, as well as constraints for each problem treated in this work have been selected and implemented in BEST to obtain a the front of Pareto.

The simulations are performed by randomly changing key thermodynamic variables while the optimizer evaluates competing objectives until the whole process converges toward a convenient Pareto's front. A metric is introduced to control the entire iterative procedure. This optimization technique achieves a set of trade-off operating conditions and not a single configuration as in the case of a conventional thermal optimization method.

In the first part of this work, the optimization strategy has been largely described and validated against numerical benchmark cases given for steam power plants. Several possibilities to run power plants have been given by the front of Pareto. The steam extractions as well as the thermal efficiencies predicted are quite close to reference cases. However the front of Pareto offers the possibility to increase the thermal efficiency by decreasing the net mechanical power or vice versa.

Once the methodology was validated, few simple thermal cycles have been simulated and optimized. This step clearly shows the benefit of using water at supercritical conditions mainly for the high thermal efficiency offered by using high temperature and pressure water conditions. Furthermore, this work has permitted us to demonstrate that the proposed cycles given in the open literature still have plenty of possibilities to increase both efficiency and output power. The results obtained are clearly useful for future plant design engineers. Indeed, in some cases the Pareto's front was clearly controlled only by few key parameters. However, essential design features in particular for turbines, as the irreversibilities and limitations on both local pressure

* Trademark of Microsoft

and amount of extracted steam, are not considered. This will require a series of simulation-optimization by using more realistic cycle parameters.

In addition, two thermodynamic cycles which only differ by the reheat inside the reactor core have been presented and optimized. As expected, the cycle with single-reheat permits a higher thermal efficiency to be achieved, although the design complexity of the reactor core is also increased. In the optimization of both cycles, the concept of pressure ratio across turbine stages has also been introduced. This definition of the pressures, as the decision variables, has been carried out to better approach the design of real steam turbines. The range of solutions obtained by this process is lower than for a random selection of the pressure inside given bounds, nevertheless the Pareto's front reaches more than a single solution. The concept of pressure ratio across turbine stages is a very important aspect in the design of turbines. Additional work in this field should be carried out; the lack of data from manufacturers is still a hindrance to improvement.

A projected supercritical fossil-fuelled power plant has been adapted to a 1200-MW SCWR power plant and optimized. Two options are presented, the first one is a single 1200-MW unit and the second one consists of two 600-MW units running in parallel. In both cases the optimization shows a Pareto's landscape that offers quite large spectra of possible operating conditions. These two options mainly differ from a mechanical point of view. The configuration of two 600-MW units will necessitate doubling the mechanical and nuclear components which will increase both investment and operating cost. On the other hand a single 1200-MW unit will require much higher mass flow rates, which implies different dimensioning of major thermal components such as turbines, heat exchangers, etc.

These last cycles raise the question of the dimensioning, thus some basic calculations have been performed to evaluate the wall thickness required for pipes that must work under high temperature and pressure conditions. The main goal for current and future work in this subject is to establish the behavior of materials in this critical environment as well as the development of new materials with high mechanical resistance at high temperature. The calculations clearly show the impact of the design temperature on the wall thickness of pipes. Furthermore the corrosion process in such environment poses a major difficulty in the design and dimensioning of thermal components. Therefore in order to be able to solve these problems, a great amount of work must

be still carried out. Few calculations on the radial distribution of temperatures between the moderator and a fuel pin have been performed. The temperature at the center of the pin obtained by these simple calculations is lower than the melting point of the UO_2 given in literature. Furthermore the coolant and the cladding temperature along the pressure tube have also been presented. As mentioned on several occasions throughout this work, one of the major goals in this project is the design of a reheat loop inside the reactor core. A simplified thermo hydraulic circuit is proposed to show how it is possible to lay out this option. Therefore, along this thesis it was possible to show that a lot of work is on SCW's is still required, in particular in fields such as neutronic, mechanics, materials, thermo hydraulics, etc.

The main goal of the work, which proposes several thermodynamic cycles with their optimization, consisted to use the Pareto front as an optimization tool. We have shown that even though thermal efficiency and mechanical power are competing objective functions, the Pareto's fronts obtained indicate that it is still possible to improve both of them simultaneously. The results obtained in this work may be very useful for future plant design engineers; especially in a world in which population and energy demand are continuously rising, it is imperative to reach the maximum performance by using all the technologies available.

REFERENCES

[1] IEA, "World Energy Outlook 2010," Iternational Energy Agency, 2010.

[2] AREVA, "Renewed interest in nuclear power generation around the world," 2006.

[3] IAEA, "Nuclear Technology Review," International Atomic Energy Agency, 2010.

[4] IAEA, "Energy, electricity and nuclear power: developments and projections — 25 years past and futur," International Atomic Energy Agency, Vienne, 2007.

[5] "The Generation IV International Forum (GIF)," , 2010. Available: http://www.gen-4.org/index.html.

[6] T. Abram et S. Ion, "Generation-IV nuclear power: A review of the state of the science," *Energy Policy*, vol. 36, no. 12, pp. 4323-4330, 2008.

[7] I. Pioro, M. Naidin, S. Mokry, E. saltanov, W. Peiman, K. King, A. Farah, and H. Thind, "General Layouts of Supercritical-Water NPPS," in *18th International Conference On Nuclear Engineering, Xi'an, China*, vol. Paper #29993, 2010, pp. 9.

[8] M. Naidin, I. Pioro, U. Zirn, and K. Chophla, "SuperCritical Water Reactor NPP Concept: No-Reheat Cycle Option," in *17th International Conference On Nuclear Engineering, Brussels, Belgium*, vol. Paper #75989, 2009, pp. 9.

[9] M. Naidin, R. Monichan, U. Zirn, K. Gabriel, and I. Pioro, "Thermodynamic Considerations For a Single-Reheat Cycle SCWR," in *17th International Conference On Nuclear Engineering, Brussels, Belgium*, vol. Paper #75984, 2009, pp. 8.

[10] M. Naidin, S. Mokry, F. Baig, Y. Gospodinov, U. Zirn, I. Pioro, and G. Naterer, "Thermal-Design Options for Pressure-Channel SCWRS With Cogeneration of Hydrogen," *Journal of Engineering for Gas Turbines and Power*, vol. 131, no. 1, pp. 012901-8, 2009.

[11] M. Edwards and W. G. Cook, "Thermodynamic analysis of a supercritical water reactor," *Saint John, N.B., Canada*, vol. 2, 2007, pp. 1159-1170.

[12] M. Naidin, S. Mokry, and I. Pioro, "SCW NPPs: Layouts and Thermodynamic Cycles," in *International Conference Nuclear Energy for New Europe, Bled, Slovenia*, 2009.

[13] W. Hounkonnou, "Modélisation et optimisation des systèmes énergétiques à l'aide d'algorithmes évolutifs," M.Sc.A , École Polytechnique de Montréal, Montréal, 2010.

[14] J. Dipama, W. Hounkonnou, A. Teyssedou, and F. Aubé, "A Simulation-Based Optimization of the Secondary Loop of Gentilly-2 Nuclear Power Plant," in CNS/CAN Annual Int. Conf., Calgary, 2009,

[15] A. Teyssedou, J. Dipama, W. Hounkonnou, and F. Aube, "Modeling and optimization of a nuclear power plant secondary loop," *Nuclear Engineering and Design*, vol. 240, no. 6, pp. 1403-1416, 2010.

[16] L. Lizon-A-Lugrin, A. Teyssedou, and I. Pioro, "Optimization of Power-Cycle Arrangements for Supercritical Water Cooled Reactors (SCWRs)," *Proceedings of the 31st Annual Conference of Canadian Nuclear Society and 34th CNS/CNA Student Conference, Montreal, QC, Canada*, 2010, pp. 17.

[17] P. A. Kruglikov, Y. V. Smolkin, and K. V. Sokolov, "Development of Engineering Solutions for Thermal Scheme of Power Unit of Thermal Power Plant with Supercritical Parameters of Steam, (In Russian)," in *Workshop "Supercritical Water and Steam in Nuclear Power Engineering: Problems and Solutions", Moscow, Russia*, 2009, pp. 6.

[18] L. Lizon-A-Lugrin, Teyssedou, A. and I. Pioro, "Appropriate Thermodynamic Cycles to Be Used in Future Pressure-Channel Supercritical Water-Cooled Nuclear Power Plants," *International Conference "Nuclear Energy for New Europe", Portorož, Slovenia*, 2010.

[19] I. Pioro and R. B. Duffey, *Heat transfer and hydraulic resistance at supercritical pressures in power-engineering applications*, New York: ASME Press, 2007.

[20] A. S. Leyzerovich, *Steam Turbines for Modern Fossil-Fuel Power Plants*: Fairmont Press, Inc., 2008.

[21] A. S. Leyzerovich, *Large Power Steam Turbines : Design and Operation*, vol. 2, Tulsa, Oklahoma: PennWell Books, 1997.

[22] I. Obara, T. Yamamoto, and Y. Tanaka, "Design of 600 C Class 1 000 MW Steam Turbine," *Mitsubishi Heavy Industries, Technical Review*, vol. 32, no. 3, 1995.

[23] "Schwarze Pumpe: A new era in lignite fired power generation.," *Modern Power Systems*, vol. 17, no. 9, pp. 27-36, 1997.

[24] U. Hoffstadt, "Boxberg achieves world record for efficiency," *Modern Power Systems*, vol. 21, no. 10, pp. 21-23, 2001.

[25] Y. Tanaka, Y. Kadoya, T. Nakano, Y. Tarutani, and K. Tanaka, "Excellent Experience of the 1050MW Steam Turbine with Highest Temperatures 600/610°C and Further Application Technology Up to 630°C," in *Proceedings of the International Conference on Power Engineering : ICOPE, Kobe, Japan*, 2003.

[26] A. S. Leyzerovich, "New benchmarks for steam turbine efficiency," *Power Engineering*, vol. 106, no. 8, 2002.

[27] R. B. Duffey and I. L. Pioro, "Advanced high temperature concepts for pressure-tube reactors, including co-generation," in *3rd International Topical Meeting on High Temperature Reactor Technology, Johannesburg, South Africa*, 2006. http://htr2006.co.za/downloads/final_download_papers/D00000167.pdf.

[28] S. Mokry, M. Naidin, F. Baig, Y. Gospodinov, U. Zirn, K. Bakan, I. Pioro, and G. Naterer, "Conceptual Thermal-Design Options for Pressure-Tube SCWRS with Thermochemical Co-Generation of hydrogen," in *16th International Conference on Nuclear Enginneering, Orlando, Florida, USA*, vol. ICONE16-48319, 2008.

[29] M. A. B. Yunus A. Cengel, *Thermodynamics: An Engineering Approach, 6th Edition*, McGraw-Hill, 2008.

[30] MATHWORKS, "Matlab Operation Manual," 2008. Available: www.mathworks.com.

[31] M. Holmgren, "X Steam for Matlab,", 2006.

[32] S. Mokry, Gospodinov, Ye., Pioro, I. and Kirillov, P.L.,, "Supercritical Water Heat-Transfer Correlation for Vertical Bare Tubes," in *17th International Conference On Nuclear Engineering (ICONE-17), Brussels, Belgium*, 2010.

[33] I. L. Pioro and R. B. Duffey, "Experimental heat transfer in supercritical water flowing inside channels (survey)," *Nuclear Engineering and Design*, vol. 235, no. 22, pp. 2407-2430, 2005.

[34] S. Mokry, I. Pioro, A. Farah, K. King, S. Gupta, W. Peiman, and P. Kirillov, "Development of supercritical water heat-transfer correlation for vertical bare tubes," *Nuclear Engineering and Design*, vol. In Press, Corrected Proof.

[35] H.-J. Kretzschmar and W. Wagner, *International steam tables: properties of water and steam based on the industrial formulation IAPWS-IF97 : tables, algorithms, diagrams, and CD-ROM electronic steam tables : all of the equations of IAPWS-IF97 including a complete set of supplementary backward equations for fast calculations of heat cycles, boilers, and steam turbines* B. Springer, 2008.

[36] E. Schmidt, *Properties of Water and Steam in SI-Units*, 3rd ^{e} éd., Berlin, 1982.

[37] L. F. Drbal, P. G. Boston, K. L. Westra, and Black&Veatch, *Power plant engineering*, New York, NY, USA: Springer Science+Business Media, 1996.

[38] F. Aschner, *Planning fundamentals of thermal power plants*, New York: John Wiley & Sons, inc., 1978.

[39] M. Beychok, "Deaerator,", 2007. Available: http://en.wikipedia.org/

[40] M. Beychok, "Spray-type deaerator,", 2008. Available: http://en.wikipedia.org/

[41] A. Bejan, G. Tsatsaronis, and M. Moran, *Thermal Design & Optimization*: John Wiley & Sons, inc., 1996.

[42] B. Linnhoff and A. R. Eastwood, "Overall site optimisation by Pinch Technology," *Chemical Engineering Research and Design*, vol. 75, no. Supplement 1, pp. S138-S144, 1997.

[43] B. Linnhoff and E. Hindmarsh, "The pinch design method for heat exchanger networks," *Chemical Engineering Science*, vol. 38, no. 5, pp. 745-763, 1983.

[44] B. Linnhoff and D. R. Vredeveld, "PINCH TECHNOLOGY HAS COME OF AGE," *Chemical Engineering Progress*, vol. 80, no. Compendex, pp. 33-40, 1984.

[45] J. Manninen and X. X. Zhu, "Thermodynamic analysis and mathematical optimisation of power plants," *Computers & Chemical Engineering*, vol. 22, no. Supplement 1, pp. S537-S544, 1998.

[46] B. Linnhoff and V. R. Dhole, "Shaftwork targets for low-temperature process design," *Chemical Engineering Science*, vol. 47, no. 8, pp. 2081-2091, 1992.

[47] K. Deb, *Multi-Objective Optimization Using Evolutionary Algorithms*, Chichetser: John Willey & Sons, 2001.

[48] V. Pareto, *Cours d'économie politique*, Lausanne, 1896.

[49] D. A. V. Veldhuizen and G. B. Lamont, "Multiobjective Evolutionary Algorithms: Analyzing the State-of-the-Art," *Evol. Comput.*, vol. 8, no. 2, pp. 125-147, 2000.

[50] Coello C. A. C, Veldhuizen D. V., and G. B. Lamont, *Evolutionary algorithms for solving multi-objective problems*: Kluwer Academic Publishers, 2002.

[51] D. E. Goldberg and J. Richardson, "Genetic algorithms with sharing for multimodal function optimization," in Proceedings of the Second International Conference on Genetic Algorithms on Genetic algorithms and their application. Cambridge, Massachusetts, United States: L. Erlbaum Associates Inc., 1987, pp. 41-49.

[52] J. Dipama, "Optimisation multi-objectif des systèmes énergétiques ", Ph.D., École Polytechnique de Montréal, 2010.

[53] D. F. Torgerson, B. A. Shalaby, and S. Pang, "CANDU technology for Generation III+ and IV reactors," *Nuclear Engineering and Design*, vol. 236, no. 14-16, pp. 1565-1572, 2006.

[54] J. Dipama, A. Teyssedou, and M. Sorin, "Synthesis of heat exchanger networks using genetic algorithms," *Applied Thermal Engineering*, vol. 28, no. 14-15, pp. 1763-1773, 2008.

[55] D. E. Goldberg, *Genetic Algorithms in Search, Optimization and Machine Learning*: Addison-Wesley Longman Publishing Co., Inc. , 1989.

[56] J. Dipama, A. Teyssedou, F. Aubé, and L. Lizon-A-Lugrin, "A Grid Based Multi-Objective Evolutionary Algorithm for the Optimization of Energy Systems," *App. Thermal Eng*, vol. 30, pp. 807-816, 2010.

[57] F. Herrera, M. Lozano, and J. L. Verdegay, "Tackling real-coded genetic algorithms: Operators and tools for behavioural analysis," *Artificial Intelligence Review*, vol. 12, no. 4, pp. 265-319, 1998.

[58] A. Sefidi and A. Arashi, "Optimization of steam extractions mass flowrate in advanced steam power plant with using combined pinch and exergy analysis (CPEA)," in *PWR2006, Atlanta, GA, USA*, May 2-4, 2006.

[59] Canteach, "Principes fondamentaux des réacteurs CANDU," Rapport technique, 2005. http://canteach.candu.org/library/20060300.pdf

[60] W. Snook, "CANDU6 Reactor Assembly,", 2001. Available: http://canteach.candu.org

[61] W. Peiman, K. Gabriel, and I. Pioro, "Heat-loss calculations for pressure-chanel SCWRS," in The 2nd Canda-China Joint Workshop on Supercritical Water-Cooled Reactors (CCSC-2010), ed. Toronto, Ontario, Canada, 2010.

[62] E. Saltanov, Peiman, W., Farah, A., King, K., Naidin, M.andPioro, I., , "Steam-Reheat Options for Pressure-Tube SCWRs," in *18thInternational Conference On Nuclear Engineering (ICONE-18), Xi'an, China*, 2010, pp. 12.

[63] N. A. Dollezhal, P. I. Aleshchenkov, Y. V. Evdokimov, I. Y. Emel'yanov, B. G. Ivanov, L. A. Kochetkov, M. E. Minashin, Y. I. Mityaev, V. P. Nevskii, G. A. Shasharin, V. N. Sharapov, and K. K. Orlov, "Operating experience with the beloyarsk nuclear power station," *Atomic Energy*, vol. 27, no. 5, pp. 1153-1161, 1969.

[64] N. A. Dollezhal, A. K. Krasin, P. I. Aleshchenkov, A. N. Galanin, A. N. Grigor'iants, I. I. Emel'ianov, N. M. Kugushev, M. E. Minashin, I. I. Mitiaev, B. V. Florinskii, and B. N. Sharapov, "Uranium-graphite reactor with superheated high pressure steam," *Atomic Energy*, vol. 5, no. 3, pp. 1085-1106, 1958.

[65] N. A. Dollezhal, I. Y. Emel'yanov, P. I. Aleshchenkov, A. D. Zhirnov, G. A. Zvereva, N. G. Morgunov, Y. I. Mityaev, G. D. Knyazeva, K. A. Kryukov, V. N. Smolin, L. I. Lunina, V. I. Kononov, and V. A. Petrov, "Development of superheating power reactors of the beloyarsk nuclear power station type," *Atomic Energy*, vol. 17, no. 5, pp. 1078-1087, 1964.

[66] A. G. Samoilov, A. V. Pozdnyakova, and V. S. Volkov, "Steam-superheating fuel elements of the reactors in the I. V. Kurchatov Beloyarsk nuclear power station," *Atomic Energy*, vol. 40, no. 5, pp. 451-457, 1976.

[67] Novick. M, Rice. R.E, Graham C.B, Imhoff. D.H, and West. J.M, "Developments in Nuclear Reheat," in *3rd International Conference Geneva*, vol. 6, 1965, pp. 225-233.

[68] The American Society of Mechanical Engineers, *Process piping- ASME code for pressure piping, B31*, New York,USA, 2002.

[69] P. Kritzer, "Corrosion in high-temperature and supercritical water and aqueous solutions: a review," *The Journal of Supercritical Fluids*, vol. 29, no. 1-2, pp. 1-29, 2004.

[70] C. K. Chow and H. F. Khartabil, "Conceptual fuel channel designs for CANDU-SCWR," *Nuclear Engenneering and technology*, vol. 40, no. 2, pp. 139, 2007.

[71] H.F. Khartabil, R.B. Duffey, N. Spinks, and W. Diamond, "The Pressure-Tube Concept of Generation IV Supercritical Water-Cooled Reactor (SCWR): Overview and Status," in *International Congress on Advances in Nuclear Power Plants 2005 (ICAPP05) Seoul, Korea*, 2005.

[72] J. Sweet, E. Roth, and M. Moss, "Thermal conductivity of Inconel 718 and 304 stainless steel," *International Journal of Thermophysics*, vol. 8, no. 5, pp. 593-606, 1987.

[73] K. Kang, H. Moon, K. Song, M. Yang, S. Lee, and S. Kim, "Thermal Conductivity of a Simulated Fuel with Dissolved Fission Products," *International Journal of Thermophysics*, vol. 28, no. 5, pp. 1595-1606, 2007.

[74] Frank P. Incropera and D. P. DeWitt, *Fundamentals of heat and mass transfer*, New York: John Wiley, 2007.

[75] K. W. Kang, J. H. Yang, J. H. Kim, Y. W. Rhee, D. J. Kim, K. S. Kim, and K. W. Song, "The solidus and liquidus temperatures of UO2-Gd2O3 and UO2-Er2O3 fuels," *Thermochimica Acta*, vol. 455, no. 1-2, pp. 134-137, 2007.